LASS-ICP-MS collection of trace element and $^{87}Sr/^{86}Sr$ isotope data using a novel uneven distribution of sample material for otolith microchemistry

by

Ivan Patrick Edgeworth

A thesis

presented to the University of Waterloo

in fulfillment of the

thesis requirement for the degree of

Master of Science

in

Earth Sciences

Waterloo, Ontario, Canada, 2022

© Ivan Edgeworth 2022

Author's Declaration

I hereby declare that I am the sole author of this thesis. This is a true copy of the thesis, including any required final revisions, as accepted by my examiners.

I understand that my thesis may be made electronically available to the public.

Abstract

Understanding the behaviour and movement of fish populations is crucial to developing plans to properly manage fisheries, and to predict effects of ongoing environmental change. In northern regions, physically tracking fish populations is difficult and expensive for researchers to accomplish at spatial scales that are relevant for populations. Otoliths (fish ear bones) are comprised of metabolically inert aragonite that stores elemental and isotopic data throughout the lifetime of a fish in seasonal growth bands centered around a nucleus.

Previous LA-ICP-MS studies have utilized trace element and isotopic data gathered from otoliths to investigate fish migration patterns, discriminate stocks, spawning and rearing sites, and reconstruct characteristics of habitats used, such as relative temperature or pH. Otolith structures can be small and fragile, depending on the species of fish, and may only have room for a single laser transect. Most previous LA-ICP-MS studies have measured isotopic or trace element data across a single transect, limiting the amount of information that can be acquired from a single otolith.

This thesis focuses on the development of a new analytical technique that simultaneously quantifies trace element and strontium isotope ratios from a single line transect. A novel, uneven distribution of material in a split-stream configuration couples the laser ablation system with two mass spectrometers diverting more material towards isotopic analyses. Long-term accuracy assessments of trace element concentrations indicate that measured values are within 5 – 10% of accepted/preferred values of standard reference and in-house reference materials. Isotopic precision increased with increased laser diameters and requires evaluation of whether the technique is suitable for most otolith studies.

The utility of this innovative split stream technique is demonstrated by analyzing three transects on otoliths from two species of fish (lake trout (*Salvelinus namaycush*) and arctic char (*Salvelinus alpinus*)). Transects of lake trout and arctic char (25µm and 40µm laser diameter, respectively) were analyzed and assessed, and results indicated that larger laser diameters yield more accurate and precise data without sacrificing significant spatial resolution with the 40µm spot size.

Acknowledgements

I would like to thank my supervisors Dr. Chris Yakymchuk and Dr. Heidi Swanson for giving me the opportunity and resources to work on a project as interesting and dynamic as this one. I am incredibly grateful for the time and effort Chris has taken over the years to teach me laser ablation practices, as well as improve my writing and several other aspects of geology and geochemistry. I am lucky to have gotten the chance to work with Heidi Swanson and for her patience with my ineptitude to grasp some of the simpler primary uses of otoliths and our difficulties keeping a clear head after a full long week in the lab. I am also in debt to Dr. Brian Kendall for his support, maintenance, and general level headedness through what has been just a truly tough and stressful pandemic.

Assistance and collection of the laboratory data wouldn't have been possible without the significant amount of support from Jillian Kendrick coming in throughout the early days of the pandemic, assisting me in the development of the technique and collection of data. Thank you especially to Carson Kinney, Holden Little, Natasha Bell, Sarah Turner, Quinn Worthington, Phillip Wright, and the rest of the geology graduate department for discussions and assistance.

As part of an interdisciplinary trailblazer program the collaboration between the Swanson otolith research graduate students has been insightful, informative and an absolute pleasure, and I look forward to working and developing the technique with the group. Special thanks to Rosie Smith and Taylor Luu for putting up with my questions and overall grumpiness on long otolith analysis days.

I absolutely could not have done this without the love and support of my family and friends. Thank you to John Edgeworth, Imelda Edgeworth, Max Edgeworth, and Nick Edgeworth for supporting my academic ventures albeit a difficult to understand topic. An incredible amount of gratitude goes out to the boys; JC Robertson, Mac Valiant, and Jim Brooks for the late-night drinks and keeping me sane throughout the pandemic with our "Tims" picks, fantasy hockey, and online boardgames. A very special thank you to my partner Amanda Jarvis for everything she does for me and puts up with daily. I would have mentally broken down a long-long time ago if it weren't for her love and support.

Last but not least, I would like to thank the NuPlasma II and Agilent for working with me and not actively against me, although somedays it was tough to tell the difference.

Table of Contents

List of Figures

List of Tables

List of Abbreviations

DRS – data reduction scheme
EIL – Environmental Isotope Laboratory
EPMA – Electron probe microanalysis
ICP-MS - inductively-coupled plasma mass spectrometry
LA-ICP-MS – Laser ablation inductively-coupled plasma mass spectrometry
LA-MC-ICP-MS – Laser ablation multi-collector inductively-coupled plasma mass spectrometry
LASS-ICP-MS – Laser ablation split-stream inductively-coupled plasma mass spectrometry
LOD – limit of detection
LOQ – limit of quantification
MC-ICP-MS – multi-collector inductively-coupled plasma mass spectrometry
MFC – mass flow controller
MIG – Metal Isotope and Geochemistry
MMC – modern marine carbonate
NIST – National Institute of Standards and Testing
NP2 – NuPlasma II
PIXE – proton induced x-ray emission
QQQ-ICP-MS – Triple Quadrupole inductively-coupled plasma mass spectrometry
RM – reference material
RSD – relative standard deviation
SD – standard deviation
SE – standard error
SIMS – secondary ion mass spectrometry
SRM – standard reference material
TIMS – Thermal Ionization Mass Spectrometry
USGS – United States Geological Survey

1. INTRODUCTION

1.1. Introduction to Otoliths

1.1.1. *Otolith Structure and Composition*

Otoliths are bio-mineral structures located within the inner ear of fish and consist of three pairs of structures referred to as the *sagittae*, *lapilli*, and *asterisci* (Fig. 1; Thomas & Swearer, 2019). Composed of calcium carbonate in the form of aragonite, otoliths accrete layers throughout the lifetime of a fish and can be utilized as natural chronometers (e.g., Wright et al., 2002). These layers begin accretion around a central nucleus and continue to form throughout the fish's life, storing chemical information about habitats used (e.g., Arslan & Secor, 2005; Tzadik et al., 2017). The daily formation of these bands/layers alternate between mineral-rich and protein-rich bands that are referred to as the "incremental zone" and "discontinuous zone," respectively (Thomas & Swearer, 2019). Protein-rich bands do not dominate the crystal structure and elemental incorporation and are typically a very minor component of overall otolith structure. In temperate fishes, annual growth bands are characterized by two distinct seasonal variations due to fast growth in the warm summer months and slow growth in the cold winter months (e.g., Halden et al., 2000). Mineral-rich and protein-rich bands develop at different rates depending on the species of fish and the environment in which they reside (see Campana, 1999).

The sagittae is the primary otolith structure used in microchemistry due to its size and mineral composition (Wright et al., 2002). In teleost (bony) fishes, sagittae are typically ~1–2mm in length along the long axis, but sizes and width of annular increments vary with age and among species (Campana, 1999) (Fig. 2). Generally, wider growth bands allow for the collection of higher-precision data using spatially resolved microchemical techniques. Therefore, width of the growth bands can affect which research questions can be effectively answered. Growth bands can be <5μm wide, but are typically ~ 10–20μm wide in some migratory fish (Campana, 1999; Wright et al., 2002) (Fig. 2). Since the sagittae is the largest of the three otolith structures, the growth bands are inherently larger and allow for the best spatial resolution in microchemical analyses.

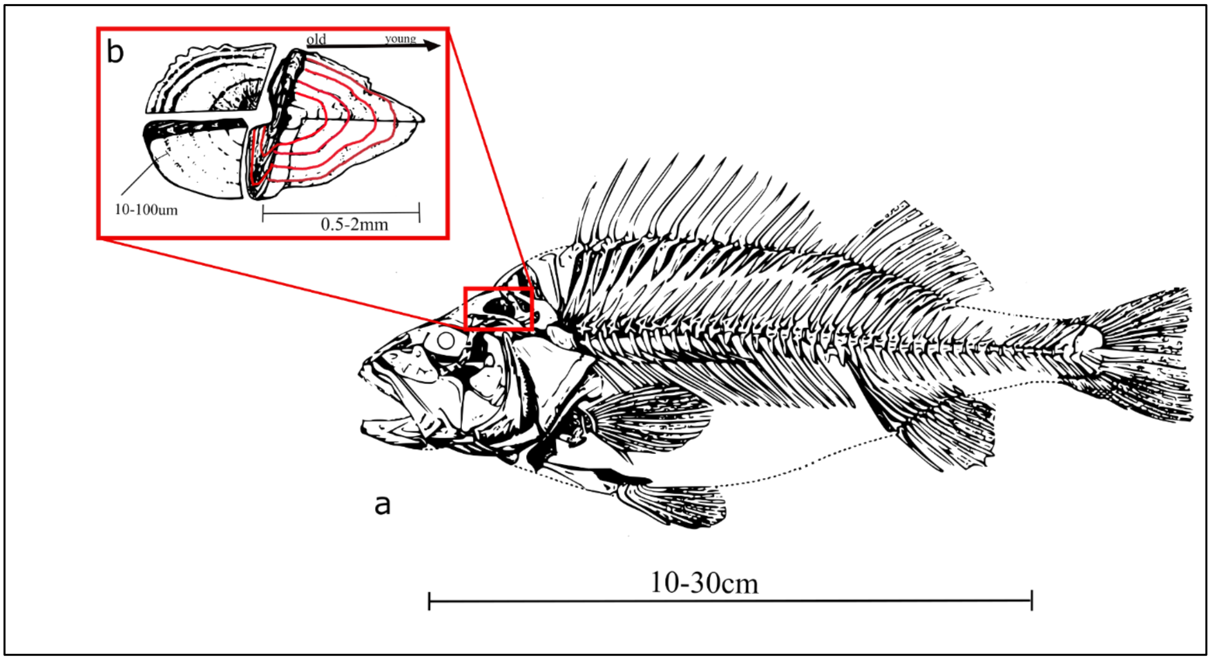

Figure 1: a. Skeleton of the common perch showing location of otolith structures (modified from Tzadik et al., 2017) b. *Sagitta* otolith structure showing annual growth rings in red (modified from Wright et al., 2002)

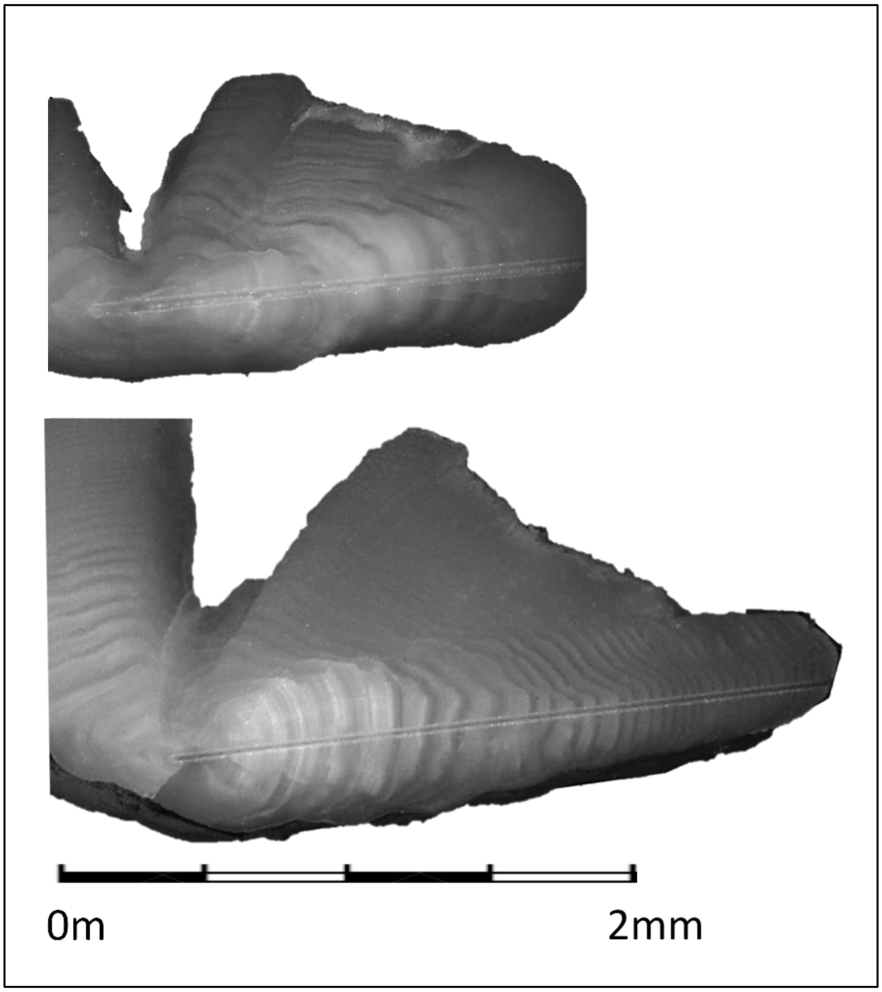

Figure 2: Transmitted light images of *sagittae* otoliths from two different species of fish: Arctic char (top) and lake trout (bottom) collected in Nunavut. The Arctic char otolith pictured reflects ~9 years of growth whereas the lake trout otolith pictured reflects ~27 years of growth (images from Heidi Swanson). The lines that cross-cut the growth bands are trenches from laser ablation.

1.1.2. *Otolith Growth and Element Incorporation*

Otoliths are chemically stable, very resistant to external stresses, and do not undergo any chemical change upon deposition, making them an ideal structure for age estimation and microchemistry techniques (Outridge et al., 2002). The microchemistry of otoliths reflects chemical conditions that the fish experienced at the time the material was accreting, and different elements reflect patterns in fish growth and migration. Incorporation of elements into the otolith structure occurs through substitution of various trace elements for calcium in the aragonite structure. Vaterite inclusions within the calcite structure can also occur, impacting the lattice's ability to incorporate elements. This can be simple cation substitution (e.g., Sr^{2+} for Ca^{2+}) or coupled substitution to maintain charge balance (e.g. Li^{+} + X <–> 2 x Ca^{2+}) (see Yoshimura et al., 2017; Füger et al., 2018). Within the protein-rich bands, substitution occurs with different major elements, and trace element concentrations within this protein matrix are usually lower than those in the crystalline component (see Thomas & Swearer, 2019). Although resistant to post-crystallization modification, incorporation of trace elements into the crystalline structure can be significantly affected by environmental conditions and result in relatively higher or lower concentrations throughout the otolith. Environmental factors that affect trace element concentrations, which can then be analyzed to reconstruct growth and migration patterns, are discussed in detail in Section 1.3.

1.1.3. *Elemental Signatures in Otoliths*

Elements incorporated into otoliths during the lifetime of the fish can be influenced by environmental conditions such as temperature, pH, salinity, and elemental concentrations in water (see Gauldie & Nelson, 1990; Chen et al., 2008; Fukuda et al., 2009; Landaeta et al., 2018; Thomas & Swearer, 2019; Fey & Greszkiewicz, 2021). Each of these variables affect otolith growth that is represented through elemental (and/or isotopic) uptake during that period of growth. In-situ analytical line transects that are run perpendicular to otolith growth rings can be used to trace annular or other patterns of trace elements throughout the lifetime of a fish, and provide time-resolved data that can be used to reconstruct environmental conditions. Elements used to reconstruct life history events (e.g., migrations) or environmental conditions (e.g., temperature) can exist within the otolith structure in concentrations that vary from trace (<1 mg/kg) to minor (~100 mg/kg) to major (>100 mg/kg) (e.g., Campana, 1999).

Temperature and salinity are often the focus of otolith microchemistry investigations. Water temperature during otolith growth has been extensively investigated using Sr:Ca and Ba:Ca ratios as indicators (see Fowler et al. 1995; Elsdon & Gillanders 2004; Dimaria et al. 2010). The effects of temperature on trace element concentrations are not as straight-forward as a single element trend and can be affected by salinity due to changing solubility with temperature (e.g., Fukuda et al., 2009). Previous authors have determined that Sr:Ca ratios can be used to reconstruct fish use of environments that vary in salinity (e.g., Tabouret et al., 2010; Walther & Limburg, 2012). Estimates of salinity from otolith microchemistry can be used to assess fish migration from freshwater to saltwater, or the relative salinity of freshwater regions that vary due to background geology (e.g., Farrel & Campana, 1996; Arai et al., 2004). Finally, fish populations can be traced back to rearing locations with increased concentrations of non-toxic trace elements if the geology contains high concentrations of these elements (e.g., Mn) (see Friedrich & Halden, 2008).

Age estimation is an important aspect of otolith investigations and multiple elemental markers have been used as indicators of seasonal changes and as a result, yearly growth. Zinc is used as a chemical indicator of yearly growth as it is typically well above the detection limits on many instruments and follows a regular cyclical change (annual) in concentration in otoliths that is relatively unaffected by changes in fish habitats. Oscillations in zinc can be compared to patterns in other chemical markers to reconstruct fish life history events, such as age at first migration to sea; life history characteristics are used to characterize populations and properly manage conservation (e.g., Walther & Limburg, 2012; Tzadik et al., 2017; Serre et al., 2018).

Impacts on otolith growth can include ambient concentrations and the pH of the water. Ambient concentrations of trace elements in various aquatic systems are also reflected proportionately in the otoliths; this can be particularly useful when investigating metals mobilized by anthropogenic activities such as mining (e.g., Halden & Friedrich, 2008). The pH of the surrounding environment can also affect the growth of otolith structures by inhibiting the formation of aragonite in high acidity environments by dissolving carbonate material.

The incorporation of such a wide range of environmentally sensitive elements and metabolically inert properties provide researchers with many technical options to quantify incorporated elements. As instrumentation improves and more data can be retrieved with a single analysis, recently collected, and preserved archived otoliths that previously yielded unsatisfactory results can be re-evaluated and provide previously unavailable insights into the habitats used by fish, fish migratory patterns, and indicators of anthropogenic pollution.

1.1.4. *Strontium isotopic signatures in otoliths*

Determining rearing environments and discriminating fish stocks is critical for the conservation and management of fish stocks (see Zitek et al., 2010). Unfortunately, tracking mass populations of migratory fish is often inefficient, costly, and unfeasible. Geochemical markers preserved within calcified tissues during growth provide an opportunity to investigate geographical information about fish populations. Strontium isotopic signatures in otoliths were first investigated by Kennedy & Folt (1997) as a potential method to distinguish among salmon populations with different natal origins. Natural variations in strontium isotope signatures among freshwater streams, combined with relatively high strontium uptake in calcified tissues yields a method to extract geographical information from calcified tissues such as otoliths - if the Sr isotope values of the different environments of fish growth are distinct (e.g., Kennedy et al., 2002; Avigliano et al. 2020). Strontium isotopes do not show evidence of biological fractionation during uptake, indicating that isotopic signatures within the calcified tissues are directly comparable to variations in water systems (e.g., Kennedy et al., 2000).

As otoliths accumulate aragonite rings throughout the life of the fish, strontium (Sr) from the surrounding environment substitutes readily into the otolith structure for calcium due to its similar ionic radius and charge (see Yoshimura et al., 2017). Sr can accumulate in otoliths in concentrations of up to thousands of mg/kg depending on the environment; more Sr is incorporated when Sr:Ca ratios in water are relatively high. Sr has four stable naturally occurring isotopes: ^{84}Sr, ^{86}Sr, ^{87}Sr, and ^{88}Sr, one of which is radiogenic (^{87}Sr). $^{87}Sr/^{86}Sr$ ratios are traditionally used as isotopic geochemical markers due to the radioactive decay of ^{87}Rb to ^{87}Sr (see Wiederhold, 2015). The erosion of geologic material introduces the isotopic signature of the eroded rock into the water system for ultimate incorporation by growing fish. Natural variations of $^{87}Sr/^{86}Sr$ ratios in bedrock are caused by variable concentrations of Rb and the accumulation of radiogenic ^{87}Sr. Generally, older 'evolved' crustal rocks will have higher $^{87}Sr/^{86}Sr$ signature than younger continental crust due to a longer time to permit radioactive decay of ^{87}Rb and ingrowth of radiogenic ^{87}Sr, as well as felsic rocks with a higher % of Ca rich minerals such as feldspars, and biotite (Avigliano et al., 2020). The long residence time of Sr within the ocean produces a current stable homogeneous $^{87}Sr/^{86}Sr$ signature of ~0.70918 – 0.709202 through the erosion of continental crust and volcanic rocks (Kuznetsov et al., 2012; Mokadem et al., 2015).

$^{87}Sr/^{86}Sr$ isotopic signatures in studies of otolith chemistry were initially investigated using solution-based ICP-MS, where otolith material was dissolved and analyzed; this effectively averaged the isotopic signatures acquired across a fish's lifetime (e.g., Kennedy et al., 2002; Kennedy et al., 2000; Barnett-Johnson et al., 2005). While this method can provide data that is useful for assigning provenance of non-migratory fish in freshwater systems, it becomes ineffective and inaccurate when dealing with migratory fish that transit between environments with different $^{87}Sr/^{86}Sr$ ratios over their lifetime (e.g., Kennedy et al., 2000). In-situ spatially resolved $^{87}Sr/^{86}Sr$ ratio data can, however, be used to reconstruct migration history of fish when the isotope data are overlain on data that reflect age and season.

Diadromous describes fish that spend portions of their life cycles partially in freshwater and partially in salt water (ocean). A crucial question for researchers is the time of fish migration to seawater, which uses both the Sr concentrations and Sr isotope ratios on removed otolith sections to identify the juvenile (freshwater) and adult (migratory) periods of their lifetime. Counting individual growth rings originating from the center of the otolith and cross-referencing them with increased concentrations of Sr, the age of the first migration can be estimated. Researchers use this info to assist in sustaining fish populations and tracking long-term changes in fish behavior (Swanson et al., 2010).

In addition to elucidating fish migration patterns, there are other important biological applications of in-situ analysis of otolith $^{87}Sr/^{86}Sr$ ratios, and these are listed in Table 1. Sr isotope signatures can be utilized for a wide range of fish research questions, including natal source identification, discrimination between stocks, and maternal run-times (e.g., time of year fish returns to natal sources). Natal source investigations involve comparing the $^{87}Sr/^{86}Sr$ isotopic signatures in waters of natal rearing areas with isotope signatures in the nucleus (point of origin) of fish (e.g., Barnett-Johnson et al., 2010; Zimmerman et al., 2013). Individual species of fish can also exhibit different behavioral and migration patterns and provide a method for the discrimination of stocks through isotopic signatures (e.g., Loewen, et al., 2015). Strontium isotope ratios provide a powerful and relatively inexpensive tool to discriminate stocks, determine natal origins, and track migration patterns of fish populations in areas where direct observation is difficult.

Table 1: Applications of Sr isotope ratios in otoliths.

Publication	*$^{87}Sr/^{86}Sr$ ratio application*
Miller & Kent (2009)	Discrimination of maternal run-times
Barnett-Johnson et al. (2010)	Natal sources of chinook salmon
Zimmerman et al. (2013)	Natal fish origins
Loewen et al. (2015)	Discrimination of char stocks in Canada
Brennan et al. (2015)	Natal and provenance implications
Crook et al. (2015)	Migration across salinity gradients
Willmes et al. (2016)	Nonlethal isotope alternatives (fins/scales)
Crook et al. (2017)	Migration in tropical rivers

1.2. Otolith Microchemistry Analytical Methods

Otolith microchemistry can be determined through either bulk analytical techniques—where each otolith yields a single datum that represents an average of the whole—or through in situ techniques that are spatially resolved at the microscale, and which can target specific areas of an otolith. A major advantage of bulk analytical techniques is the significantly higher accuracy and precision, at the expense of greater destruction of material and lack of spatial resolution. In-situ analyses provide a (generally) low-cost technique that provides spatial resolution, at the expense of accuracy and precision. These advantages and disadvantages vary with respect to technique and instrumentation.

1.2.1. *Bulk Analytical Techniques*

1.2.1.1. *TIMS*

Thermal ionization mass spectrometry (TIMS) is a high-sensitivity method for $^{87}Sr/^{86}Sr$ isotope analysis involving the dissolution of otolith samples. TIMS is one of the most accurate and precise measurement methods and is used primarily for high-precision isotope analysis. The method ionizes samples through the heating of a metal filament which evaporates the solution and releases electrons which are then accelerated and measured using an isotopic mass spectrometer (see Carlson, 2013). Otolith studies using TIMS can involve the dissolution of the entire otolith or the removal of material by microdrilling along a transect of the otolith (e.g., Barnett-Johnson et al., 2005; Gao & Bean, 2008; Shao et al., 2018; Kennedy et al., 2002). This method has limited biological applications due to the dissolution of the entire otolith or limitations in drilling a small enough area without infringing on adjacent growth zones. Laboratories routinely use TIMS as an external analysis method to produce matrix matched in-house standards for in-situ analysis methods, due to its unmatched accuracy and precision. Routinely measured $^{87}Sr/^{86}Sr$ isotope ratios usually have a precision of 0.1–1 ppm (e.g., 0.000001 – 0.0000001) using TIMS (e.g., Carlson, 2013).

1.2.2. *In-situ analytical techniques*

1.2.2.1. *Proton Microprobe*

Proton induced x-ray emission (PIXE) allows for spatially resolved analysis of otoliths at the micrometer scale (~5μm). A proton microprobe uses a very fine, focused beam of protons to induce electromagnetic radiation in the form of X-rays that are specific to a given element (Stroud, 2013). An early study using PIXE was successful at resolving concentrations of trace elements in otoliths but employed a broad proton beam, which effectively eliminated spatial resolution (Gauldie et al., 1986). Micro-PIXE utilizes a smaller proton beam to preserve spatial resolution and was first used by Coote et al. (1991). However, the authors of this study found it difficult to match concentrations to physical features in the otolith. Later studies utilized the in-situ micro-PIXE technique to match trace element concentrations to environmental transitions, such as seasonal changes and migration patterns (e.g., Halden et al., 1995; Halden et al., 1996; Babaluk et al., 1997; Radtke et al., 1997; Halden et al., 2000; Howland et al., 2009). The micro-PIXE method can routinely analyze trace element concentrations for Sr, Ba, Zn, Mn, and Fe down to the 2–5 mg/kg range (e.g., Halden et al., 2000).

1.2.2.2. *Electron Microprobe*

Electron probe microanalysis (EPMA) utilizes a high-energy focused beam of electrons at the surface of samples to induce electromagnetic radiation like micro-PIXE (Stroud, 2013). This method utilizes a beam typically <10µm in diameter and can routinely analyze elemental concentrations of 100 mg/kg or higher (e.g., Campana et al., 1997; McFadden et al., 2016). Electron microprobe studies are widely used in otolith microchemistry, primarily focused on Sr, Ca, and other primary elements for the purposes of tracking migration patterns on individual fish (e.g., Kalish, 1989; Severin et al., 1995; Arai et al., 2004). A particular advantage of EPMA is that it is a non-destructive technique and samples are mostly unaffected by the analysis. However, EPMA cannot easily resolve concentrations <100 mg/kg, which is a limitation for trace elements such as Zn and Li in most otoliths.

1.2.2.3. *SIMS*

Secondary ion mass spectrometry (SIMS) uses a targeted ion beam to sputter the surface of a sample and generates secondary ions (from the sample) that are measured with a mass spectrometer (Henkel and Gilmour, 2014). SIMS allows for high-precision isotope analysis with surface spatial resolution and is currently the most sensitive surface analysis technique available. It is minimally destructive but requires extensive sample preparation. Otolith studies have primary utilized the technique for carbon and oxygen isotope analysis (e.g., Thorrold et al., 1998; Weidman & Millner, 2000; Hanson et al., 2010; Matta et al., 2013; Helser et al., 2018). These isotope ratios are used to investigate migration, diets, and habitat characteristics, such as experienced temperature (e.g., Campana, 1999; Matta et al., 2013). Results of SIMS analyses (e.g., O and C isotope ratios) are commonly coupled with information from other techniques.

1.2.2.4. *LA-ICP-MS*

Laser ablation inductively coupled plasma mass spectrometry (LA-ICP-MS) is an evolving technique that can analyze both elemental and isotopic signatures through in-situ analysis of otoliths. Initially used in the Earth Sciences to measure trace elements in-situ, further advancements allowed for the analysis of in-situ isotopic signatures (Longerich, 2008; Jakubowski, 2011). An LA-ICP-MS system contains three separate components: the laser ablation cell, the coupled plasma (ion source), and the mass spectrometer. The laser ablation (LA) component consists of a shortwave laser (usually 213 or 193 nm) being focused onto a solid sample within an ablation chamber that collects the ablated material and transports it through tubing as an aerosol towards the mass spectrometer. The inductively coupled plasma (ICP) component is a high temperature (~5000ºC) plasma that atomizes and ionizes 80-95% of the ablated material (Longerich, 2008). The ionized constituents can be distinguished based on mass to charge ratios. This can be applied to trace elements or isotope ratios depending on the nature of the coupled ICP-MS instrument.

Elemental analysis of otoliths using LA-ICP-MS began in the mid 1990's as a potentially cheaper and faster alternative to microprobe techniques (Campana et al., 1994; Fowler et al., 1995). Early analyses had issues with sample transport, spatial resolution, and sensitivity that limited the applications of LA-ICP-MS to studies of materials with relatively high concentrations of trace elements. However, advancements in these areas has led to the rapid widespread use of LA-ICP-MS in otolith microchemistry studies. LA-ICP-MS trace element analyses are routinely used to track migrations in diadromous and anadromous fish (e.g., Palace et al., 2007; Tabouret et al., 2010; Swanson et al., 2010; D'Avignon et al., 2013; Morrison et al., 2019; Harris et al., 2020). Isotopic analyses using LA-ICP-MS have been used to discriminate between various fish populations and proven to be an invaluable tool in otolith microchemistry studies (e.g., Kennedy et al., 2002; Miller & Kent, 2009; Zitek et al., 2010, Barnett-Johnson et al., 2010; Loewen et al., 2015; Crook et al., 2017).

1.2.2.5. *Split-stream LA-ICP-MS*

Individually, trace element and isotopic analyses provide invaluable information about fish populations. However, obtaining both sets of data from a single otolith normally requires two separate analytical sessions with ablation of different parts on the same otolith. This leads to the isotope data being spatially decoupled from the elemental data; considering the narrow (<10μm) zoning of otoliths, even slight deviations can affect the researchers' ability to generate inferences. A relatively recent advancement in LA-ICP-MS is the simultaneous collection of isotopic and trace element data from the same ablated material using a ‘split stream’ configuration, where two mass spectrometers are used simultaneously. Laser ablation split stream (LASS) was developed in the late 2000s (Yuan et al., 2008) and is now routinely applied in Earth Science studies (Kylander-Clark et al., 2013). Originally developed to simultaneous acquire U–Pb ages and Hf isotopes in zircon, the split stream technique has since been the focus of several novel research studies and two technical papers in otolith microchemistry (Prohaska et al., 2016; Hegg et al., 2020).

A split stream configuration involves physical separation of an ablated aerosol to two different mass spectrometers; the total amount of material going to any one mass spectrometer is less than if a single stream configuration is used. Therefore, split stream analysis usually requires analysis using a larger laser beam size, which reduces spatial resolution. There is an analytical trade-off between laser spot size and spatial resolution and this needs to be considered in the context of the scientific question that is the focus of the analysis. Two previous studies applied LASS to otoliths. Prohaska et al. (2016) required a spot size of 150µm to resolve both elemental and isotopic data, sacrificing the spatial resolution desired by most otolith researchers (usually <20 µm). Hegg et al. (2020) was able to achieve spot sizes ranging from 15 – 35µm, resulting in similar accuracy and precision of $^{87}Sr/^{86}Sr$ ratios in collected otoliths compared to single stream analysis. However, trace element data were routinely below LOD. The comparison study was deemed successful and innovative with room for improvement in precision and the collection of trace element data. For most otolith research questions that are routinely addressed, the spatial resolution required is 15–40 µm, $^{87}Sr/^{86}Sr$ isotope ratios need to be resolved to the third or fourth decimal place, and trace elements need to be detectable to ~10 mg/kg (see Panfili et al., 2002; Loewen et al., 2015). Neither of the previous LASS studies on otoliths (Prohaska et al., 2016; Hegg et al., 2020) could meet these analytical requirements. This thesis presents a technique for meeting these analytical requirements using the novel approach of splitting the ablated aerosol unevenly between the mass spectrometers.

2. OBJECTIVES

The main objective of my MSc research was to develop a LA-ICP-MS split-stream method for otolith microchemistry at the University of Waterloo's MIG laboratory that allows quantification of trace element concentrations of ~10 mg/kg and $^{87}Sr/^{86}Sr$ data to the third decimal place while achieving a spatial resolution of 15-25 µm. As part of this method development, I aimed to:

1. Establish the long-term reproducibility of $^{87}Sr/^{86}Sr$ isotope data and trace element data by assessing accuracy and precision on standard reference materials.
2. Evaluate how laser diameter affects accuracy and precision of trace element data and $^{87}Sr/^{86}Sr$ ratio data
3. Apply and evaluate the developed technique on a small number (2) of otolith samples
4. Assess the limitations of the technique with respect to possible research questions

These objectives are addressed using data collected from a variety of independent and collaborative sessions throughout a period of roughly 12 months.

3. METHODS

3.1. Thermal Ionization Mass Spectrometry (TIMS)

The $^{87}Sr/^{86}Sr$ signature of deep-sea gastropod samples (lab name: HSSr) were analyzed at the Environment Isotope Laboratory (EIL) to support use of an in-house matrix-matched reference material. This reference material was then used to evaluate accuracy of $^{87}Sr/^{86}Sr$ isotope ratios measured during LA-MC-ICP-MS and, if necessary, to correct for instrumental mass fractionation of $^{87}Sr/^{86}Sr$ ratios. The EIL TIMS laboratory instrumentation consists of a Thermo Finnigan Triton Thermal Ionization Mass Spectrometer (TIMS) measuring isotopes of Sr using multi-collector Faraday cups. 5 solid samples were digested using 5% acetic acid, which was prepared from OMNI trace stock reagent and milli-Q water. Strontium was extracted from the digested material using Eichrom Sr-specific ion exchange resin. A rhenium double filament method was used to ionize Sr, with 1 μg of analyte loaded for each sample. Results are reported with respect to NIST SRM 987 (accounting for mass bias with $^{86}Sr/^{88}Sr = 0.1194$, and normalization to $^{87}Sr/^{86}Sr = 0.71025$), a strontium carbonate standard reference material (NIST, 2007).

3.2. Laser ablation inductively-coupled plasma mass spectrometry (LA-ICP-MS)

3.2.1. *Sample preparation*

Otolith collection and preparation was conducted by Heidi Swanson and Rosie Smith at the University of Waterloo. Detail on otolith sample preparation methods can be found in Swanson et al. (2010). Briefly, otoliths were embedded in ColdCureTM epoxy and sectioned transversely through the core with a low-speed saw (Buehler Isomet, Buehler Ltd., Lake Bluff, Illinois). Sections were re-embedded in epoxy in 25 mm leuite ring mounts and polished with 30 μm lapping film, 9 μm lapping film, 1 μm lapping film, and finally on a Buehler MetaServ grinder polisher with a microcloth and 0.01 μm diamond paste. When scratches through the otolith were not visible under coaxial light at 5 x magnification, rings were ultrasonically cleaned, dried, and photographed prior to analysis. Modern deep-sea gastropod shells (*Megayoldia thraciaeformis)* from Nunavut (provided by Tracey Loewen, Department of Fisheries and Oceans, Natural Resources Canada) that were developed as in-house reference materials for $^{87}Sr/^{86}Sr$ isotope ratios (see Section 2.1) were broken into smaller pieces and embedded in a 25mm plastic ring form using epoxy. Shells were then polished with diamond grit paper, ultrasonically cleaned, and dried prior to analysis. Other fragments of the same shells were ground in an agate mortar and pestle for TIMS analysis (Section 2.1).

3.2.2. *Instrumentation and Parameters*

LA-ICP-MS analyses were conducted using either laser ablation split-stream (LASS) (e.g., Kylander-Clark et al., 2013) or a traditional single stream configuration using a Photon Machines Analyte G2 laser ablation system connected in series to the QQQ-ICP-MS or NuPlasma II MC-ICP-MS. Details and operating conditions are detailed below for these different analytical configurations.

3.2.2.1. *LASS-ICP-MS*

Otoliths and reference materials were analyzed using a laser ablation split-stream configuration in tandem with an Agilent 8800 QQQ-ICP-MS and a Nu Plasma II MC-ICP-MS in the MIG Lab at the University of Waterloo. Ablation was performed with an Analyte G2 laser ablation system using a laser scan speed of 2–3 μm s^{-1}, a frequency of 20 Hz, and a fluence of 4.5 J/cm^2 (measured at sample surface), with circular spot diameters of 8–40 μm. Ablated material was flushed from the laser sample chamber using He as a carrier gas (~ 0.4–1.0 L min^{-1}). Nitrogen was utilized to increase signal intensity and was introduced into the aerosol via a mixing bulb before the addition of argon gas through a Y-junction. The effects of N_2 are still being investigated; other laboratories routinely use N_2 in LASS-ICP-MS whereas others do not. Analyses were completed with and without nitrogen to determine effects on sensitivity, which have been observed for geological applications of LASS-ICP-MS in other laboratories (Kylander-Clark et al., 2013; Yuan et al., 2008; Viete et al, 2015; Hacker et al., 2015). The aerosol combined with the mixing gas (N_2) was then split with a novel "loop" junction to divert >50% of the aerosol to the MC-ICP-MS. The remaining aerosol was routed to the QQQ-ICP-MS. Sr isotope ratios were measured with the MC-ICP-MS and trace element concentrations were measured with QQQ-ICP-MS. Specific instrument operating parameters are shown in Table 2.

3.2.2.2. *LA-MC-ICP-MS*

Strontium isotope ratios on reference materials were analyzed using a LA-ICP-MS single-stream configuration for comparison with the split stream configuration. The single-stream configuration consists of an Analyte G2 laser ablation system and a Nu Plasma II MC-ICP-MS. Samples were ablated and analyzed using a scan speed of 2–3 μm s^{-1}, a frequency of 20 Hz, and a fluence of 4.5 J/cm^2 (measured at sample surface), with circular spot diameters of 8–40μm. Ablated material was flushed from the laser sample chamber using He as a carrier gas (~ 0.4–0.6 L min^{-1}). Nitrogen was introduced into the aerosol via a mixing bulb before the addition of argon gas (~1L min^{-1}) through a Y-junction prior to introduction to the ICP-MS. Specific instrument operating parameters are shown in Table 3. Although the single-stream results are not the focus of this thesis, the results are summarized in Appendix A.

3.2.2.3. *LA-QQQ-ICP-MS*

Trace elements on reference materials were analyzed using a single-stream LA-ICP-MS configuration consisting of an Analyte G2 laser ablation system and an Agilent 8800 QQQ-ICP-MS. Samples were ablated and analyzed using a scan speed of 2–3 μm s^{-1}, a frequency of 20 Hz, and a fluence of 4.5 J/cm^2 (measured at sample surface), with circular spot diameters varying from 8 to 40 μm. Ablated material was flushed from the laser sample chamber using He as a carrier gas (~ 0.4–0.6 L min^{-1}). Argon gas is introduced into the aerosol via a mixing bulb (~1L min^{-1}) prior to introduction to the ICP-MS. Nitrogen was not used in this configuration. Specific instrument operating parameters are shown in Table 4. Results for the single-stream analyses are reported in Appendix A.

Table 2: Instrument operating parameters for split-stream laser ablation analyses

Nu Plasma II MC-ICP-MS	
Carrier gas and flow rate	0.3 – 0.7 L min^{-1} (He-MFC1) + 0.1 – 0.3 L min^{-1} (He-MFC2) + 0 – 1 mL min^{-1} (N_2-MFC3) + 1.67 L min^{-1} (Ar). Nitrogen is added after the ablation chamber with a mixing bulb. Ar is added subsequently using a 'Y'-junction.
Auxillary gas flow rate	0.9 L min^{-1} (Ar)
Cool gas flow rate	13 L min^{-1} (Ar)
RF power	1300 W
Reflected power	< 1 W
Sample cone	Nickel (0.9mm Orifice)
Skimmer cone	Nickel (0.6mm Orifice)
Collector types	7 Faraday cups
Integration times	0.1–0.2 s
Masses measured (cup)	88 (H8), 87 (H6), 86 (H4), 85 (H2), 84 (Ax), 83 (L2), 82 (L4) amu
Reference Materials	Modern Marine Carbonate ($^{87}Sr/^{86}Sr$: 0.709176 $\pm$ 0.000008; in house- TIMS) USGS-MACS3 ($^{87}Sr/^{86}Sr$: 0.7075532 $\pm$ 0.000002; Jochum et al., 2019) NanoSr ($^{87}Sr/^{86}Sr$: 0.70756 $\pm$ 0.00003; Weber et al., 2020)
Photon Machines Analyte G2 193nm ArF excimer laser	
Cell	Two volume Helex cell (Eggins et al., 1998; Eggins et al., 2005)
Sample transport tubing	1 m length (to NP2), 1.5 m length (to Agilent), PTFE 2 mm x 4 mm
MFC 1	0.3 – 0.7 L min^{-1} (He)
MFC 2	0.1 – 0.3 L min^{-1} (He)
MFC 3	0 – 1 mL min^{-1} (N_2)
Wavelength	193 nm ArF
Fluence	4.5 J cm^{-2}
Spot size	8 – 40 µm diameter circle
Scan speed	2 –3 µm s^{-1}
Repetition rate	20 Hz
Agilent Technologies 8800 ICP-MS Triple Quadrupole	
RF power	1550 W
RF matching	1.80 V
Sample cone	Nickel (x-lens)
Skimmer cone	Nickel (x-lens)
Sample depth to cone	4.9 mm
Dilution gas	0.1 – 0.4 L min^{-1} (Ar)
Reflected power	12 W
Integration time	10 ms, 0.269 s/cycle
Masses measured	^{88}Sr, ^{66}Zn, ^{137}Ba, ^{7}Li, ^{56}Fe, ^{55}Mn, ^{24}Mg, ^{208}Pb, ^{43}Ca, ^{63}Cu, ^{23}Na, ^{29}Al, ^{28}Si, ^{31}P, ^{32}S, ^{39}K, ^{202}Hg, ^{89}Y, ^{90}Zr, ^{85}Rb
Scan type	Single Quadrupole mode

Table 3: Instrument operating parameters for single-stream isotope laser ablation analyses

Nu Plasma II MC-ICP-MS	
Carrier gas and flow rate	0.3 – 0.7 L min^{-1} (He-MFC1) + 0.1 – 0.3 L min^{-1} (He-MFC2) + 1 mL min^{-1} (N_2-MFC3) + 1.67 L min^{-1} (Ar). Nitrogen is added after the ablation chamber with a mixing bulb. Ar is added subsequently using a 'Y'-junction.
Auxillary gas flow rate	0.9 L min^{-1} (Ar)
Cool gas flow rate	13 L min^{-1} (Ar)
RF power	1300 W
Reflected power	< 1 W
Sample cone	Nickel (0.9mm Orifice)
Skimmer cone	Nickel (0.6mm Orifice)
Collector types	7 Faraday cups
Integration times	0.1–0.2 s
Masses measured (cup)	88 (H8), 87 (H6), 86 (H4), 85 (H2), 84 (Ax), 83 (L2), 82 (L4) amu
Reference Materials	Modern Marine Carbonate ($^{87}Sr/^{86}Sr$: 0.709176 $\pm$ 0.000008; in-house – TIMS) USGS-MACS3 ($^{87}Sr/^{86}Sr$: 0.7075532 $\pm$ 0.000002; Jochum et al., 2019) NanoSr ($^{87}Sr/^{86}Sr$: 0.70756 $\pm$ 0.00003; Weber et al., 2020)
Photon Machines Analyte G2 193nm ArF excimer laser	
Cell	Two volume Helex cell (Eggins et al., 1998; Eggins et al., 2005)
Sample transport tubing	1 m length (to NP2), 1.5 m length (to Agilent), PTFE 2 mm x 4 mm
MFC 1	0.3 – 0.7 L min^{-1} (He)
MFC 2	0.1 – 0.3 L min^{-1} (He)
MFC 3	1 mL min^{-1} (N_2)
Wavelength	193 nm ArF
Fluence	4–4.5 J cm^{-2}
Spot size	8 – 40 µm diameter circle
Scan speed	2 –3 µm s^{-1}
Repetition rate	20 Hz

Table 4: Instrument operating parameters for single-stream trace elements laser ablation analyses

Photon Machines Analyte G2 193nm ArF excimer laser	
Cell	Two volume Helex cell (Eggins et al., 1998; Eggins et al., 2005)
Sample transport tubing	1 m length (to NP2), 1.5 m length (to Agilent), PTFE 2 mm x 4 mm
MFC 1	0.3 – 0.7 L min^{-1} (He)
MFC 2	0.1 – 0.3 L min^{-1} (He)
MFC 3	1 mL min^{-1} (N_2)
Wavelength	193 nm ArF
Fluence	4–4.5 J cm^{-2}
Spot size	8 – 40 µm diameter circle
Scan speed	2 –3 µm s^{-1}
Repetition rate	20 Hz
Agilent Technologies 8800 ICP-MS Triple Quadrupole	
RF power	1550 W
RF matching	1.80 V
Sample cone	Nickel (x-lens)
Skimmer cone	Nickel (x-lens)
Sample depth to cone	4.9 mm
Dilution gas	0.1 – 0.4 L min^{-1} (Ar)
Reflected power	12 W
Integration time	10 ms, 0.269 s/cycle
Masses measured	^{88}Sr, ^{66}Zn, ^{137}Ba, ^{7}Li, ^{56}Fe, ^{55}Mn, ^{24}Mg, ^{208}Pb, ^{43}Ca, ^{63}Cu, ^{23}Na, ^{29}Al, ^{28}Si, ^{31}P, ^{32}S, ^{39}K, ^{202}Hg, ^{89}Y, ^{90}Zr, ^{85}Rb
Scan type	Single Quadrupole mode

3.2.3. *Configuration and aerosol plumbing*

3.2.3.1. *LASS-ICP-MS*

A schematic diagram of the novel split-stream plumbing developed in this thesis is illustrated in Figure 3A. The split method was developed to allow for the reduction of spot sizes during otolith analysis, preserving material and spatial resolution. Ablated sample material travels downstream to where N_2 is introduced with a glass mixing bulb. Ar is then added using a Y-junction. The total flow prior to entering the "loop" junction is ~2 L/min. The material is then split using a "loop" junction that provides an uneven distribution of sample material between the two mass spectrometers. After the split, Ar-dilution gas is introduced at the torch for QQQ-ICP-MS before sample introduction to the plasma. No additional Ar is added to the Nu Plasma II prior to sample introduction.

The "loop" junction is a unique design intended to divert 2/3 of the ablated material towards one mass spectrometer, with the goal of improving $^{87}Sr/^{86}Sr$ data quality. Ibanez-Mejia et al. (2015) described a set-up where an uneven distribution of sample material was created using a needle valve to limit the flow of material for hafnium isotopes. This design was tested (i.e., needle valve), but yielded no significant improvement in the amount of signal and an inconsistent split of material. The "loop" junction that was thus developed consists of a T-connector that splits material from the sample chamber, circles around, and reconnects to a manifold connector with 3 output lines (Fig. 3A). This maintains forward flow within the lines and ensures a consistent redirection of material. The low backgrounds and high sensitivity of the Agilent 8800 QQQ-ICP-MS allow the user to maintain the necessary signal intensity on trace elements, even with a 2/3 diversion of sample material to the MC-ICP-MS.

3.2.3.2. *LA-MC-ICP-MS*

A schematic diagram of single-stream MC-ICP-MS plumbing is illustrated in Figure 3B. The ablated sample material travels downstream to where optional N_2 is introduced with a glass mixing bulb (based on sensitivity requirements/possible interferences). Ar is then added using a Y-junction. The total flow prior before entering the ICP-MS at this point is approximately 1.8–2 L min^{-1} (Fig. 3B).

3.2.3.3. *LA-QQQ-ICP-MS*

A schematic diagram of single-stream QQQ-ICP-MS plumbing is illustrated in Figure 3C. The ablated sample material travels downstream to where Ar is introduced with a glass mixing bulb at a rate of ~1 L min^{-1}. Nitrogen is currently not used in this configuration but can be accommodated using a modified single-stream configuration not described in this thesis. Additional Ar gas can be added directly before the torch to increase signal strength with an approximate flow rate of 0.2–0.3 L min^{-1}. The total flow prior before entering the ICP-MS is approximately 1.8–2 L min^{-1} (Fig. 3C).

3.3. Data Collection and Processing

Standard–sample bracketing (reference materials analyzed every ~ 3 unknowns) was conducted using an in-house deep sea gastropod (HSSr; $^{87}Sr/^{86}Sr$ of 0.709176 ± 0.000008; value from Thermal Ionization Mass Spectrometry) as the primary reference material for Sr isotopes. HSSr has a Sr mass fraction of ~2500–5500 mg/kg. USGS-MACS3 (0.7075532 ± 0.000002; Jochum et al., 2019) and NanoSr (0.70756 ± 0.00003; Weber et al., 2020) were analyzed as secondary reference materials and have Sr mass fractions of ~6000–8000 and 500 mg/kg, respectively. For trace elements, NIST SRM 610 (preferred values in Appendix B) was used as a primary reference material and NIST SRM 612 (preferred values in Appendix B) was monitored as a secondary reference material (NIST, 2012; Jochum et al., 2011). ^{43}Ca was used as an internal standard for analyses of otoliths with an assumed concentration of 40.04 wt.% Ca, which is the stoichiometric amount of Ca in calcite and aragonite. While NIST glasses are not matrix-matched to otoliths, a homogenous trace element carbonate standard has yet to exist or be made readily available; this is a primary limitation of trace element analyses of carbonate matrices in all laser ablation laboratories. Since trace element concentration data are generally treated semi-quantitatively in otolith microchemistry studies, matrix-matching is not crucial for data analysis. Data were processed using the Iolite (v4.4.5) trace element internal standard data reduction scheme (Paton et al., 2011; Longerich et al. 1996). Strontium isotope data were processed using the strontium isotopes data reduction scheme (Woodhead et al., 2005) within Iolite (v4.4.5), which accounts for mass bias as well as indirect and direct interference on specific strontium isotope masses.

The Sr isotope data reduction of Woodhead et al. (2005) requires collection of seven masses; 82, 83, 84, 85, 86, 87, and 88. Initially, ^{86}Kr is background-subtracted from baseline measurements of mass 86 and are selected prior to running the data reduction scheme (DRS). A preliminary mass fractionation factor that corrects for the mass bias from the laser and multi-collector is calculated using an exponential correction to the $^{86}Sr/^{88}Sr$ ratio of 0.1194. Interferences on ^{86}Sr and ^{88}Sr masses from $^{48}Ca^{40}Ar$ and $^{46}Ca^{40}Ar$ are corrected for using the $^{42}Ca^{40}Ar$ (82) mass with an exponential preliminary fractionation factor to strip CaAr from collected masses. A refined fractionation factor is then calculated from those CaAr stripped Sr masses. Using the refined fractionation factor, the Rb fractionation factor is calculated, which is usually the same as the Sr fractionation factor. Using the previously calculated values above, ^{87}Rb, ^{87}Sr, ^{84}Sr, ^{88}Sr, and ^{86}Sr signals are calculated using mass bias values and known stable isotopic ratios. An additional correction to a ‘primary standard’ can be done to account for consistent variation from the accepted value.

In general, only a mass bias correction was needed to reproduce the accepted Sr isotope values of the standard reference materials; additional corrections for interferences were generally not needed and this is discussed in detail in Section 4.2. Sampling periods and integration times for each mass spectrometer can be found in Tables 2, 3 and 4.

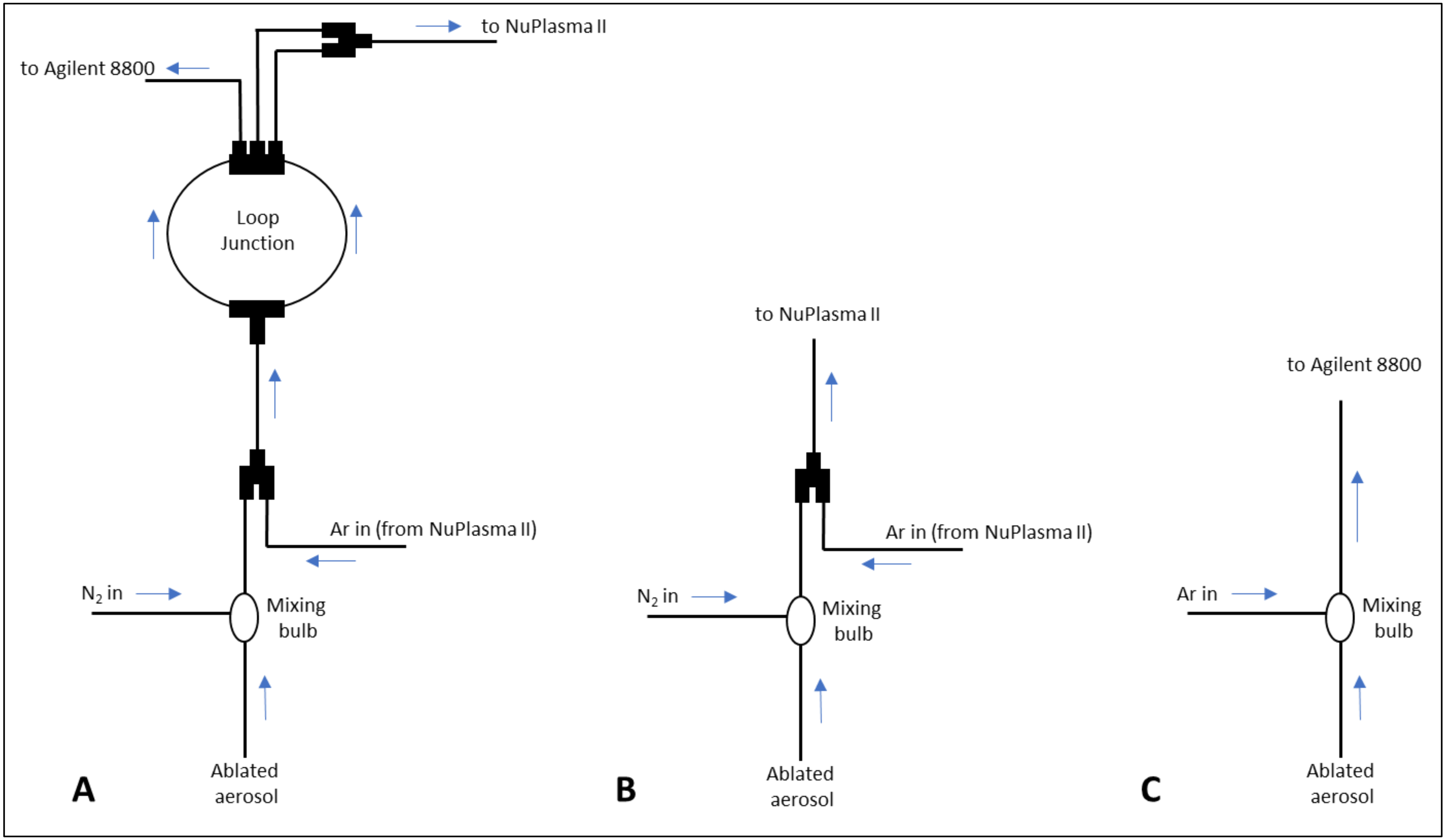

Figure 3: Schematic diagram of ICP-MS transport tubing for split-stream (A) and single stream configurations for the NuPlasma II (B) and Agilent (C)

4. RESULTS

4.1. TIMS results on HSSr

The deep-sea gastropod shell (HSSr) was analyzed via TIMS (see Section 2.1) for $^{87}Sr/^{86}Sr$ isotope ratios. This analysis supported use of HSSr as an in-house matrix-matched reference material that was then used to evaluate accuracy of $^{87}Sr/^{86}Sr$ ratios on LA-ICP-MS analyses of otoliths. The $^{87}Sr/^{86}Sr$ ratio of HSSr was determined to be 0.709176 $\pm$ 0.000002 (SD) and falls within the range of modern seawater (0.70890 – 0.70920; Kuznetsov et al., 2012; Mokadem et al., 2015).

4.2. LASS-ICP-MS data from reference materials

Measured strontium isotopic ratios and concentrations of USGS-MACS3, HSSr, NanoSr, and NIST SRM 612 were analyzed to evaluate the long-term reproducibility of strontium isotope data from the LASS-ICP-MS technique, as well as the effect of laser spot diameters on accuracy and precision. Although accuracy and precision were improved at smaller spot diameters, there were no obvious trends that demonstrate a systematic issue with instrumentation or the technique (i.e., consistent inaccuracies/inconsistent signal intensity)(Figs. 4 – 7).

$^{87}Sr/^{86}Sr$ ratios were used to assess accuracy and precision within analytical sessions, whereas $^{84}Sr/^{86}Sr$ ratios are used as a secondary ratio to evaluate the DRS corrections being used to calculate the $^{87}Sr/^{86}Sr$ ratios (Vroon et al., 2008). The $^{84}Sr/^{86}Sr$ ratio is a stable ratio due to both isotopes of Sr being non-radiogenic with a natural abundance ratio of 0.0568 and experimental value of 0.056493 $\pm$ 0.000034 (2SE) determined using TIMS analysis on NIST SRM 987 (Thirlwall, 1991).

4.2.1. *USGS-MACS3 (n=214)*

Strontium isotope ratios of USGS-MACS3 were recorded over a 9-month period (August 2020 – May 2021) and are reported here to assess long-term accuracy and precision of analytical sessions (Fig. 4). Analyses of USGS-MACS3 are reported as a secondary reference material; the in-house deep-sea marine gastropod shell (HSSr) or NanoSr were used as the primary reference material(s) in all analytical sessions.

The calculated mean for $^{87}Sr/^{86}Sr$ instrumental corrected isotope ratios for the USGS-MACS3 pressed pellet standard reference material was 0.707585 $\pm$ 0.000055 (2SE, n=214) (Fig. 4a) with a 2RSD (Relative Standard Deviation) of 0.11%, which is slightly higher than the accepted value of 0.7075532 $\pm$ 0.0000176 (2SD) but within analytical uncertainty. Note that ‘instrumental corrected’ isotope ratios do not include the minor additional correction described in section 3.3 for standard corrected ratios. Standard corrected isotope ratios (corrected with HSSr) yielded mean values of 0.707632 ± 0.000054 (2SE) with a 2RSD of 0.11%. $^{84}Sr/^{86}Sr$ uncorrected ratios yielded a mean value of 0.05697 ± 0.000092 (2SE) and instrumental corrected ratios a value of 0.05573 ± 0.00012 (2SE) (Fig. 4c). Note that corrected $^{84}Sr/^{86}Sr$ ratios are calculated using correction factors on masses 84 and 86 to mitigate interferences on Ca dimers and Ca argides (Vroon et al., 2008) and deviate slightly from the natural $^{84}Sr/^{86}Sr$ ratio of ~0.0568 (calculated based on natural Sr isotope abundance). These deviations can be due to Ca dimer (e.g., $^{42}Ca^{42}Ca$) or argide interferences. (e.g., $^{44}Ca^{40}Ar$).

4.2.2. *HSSr (n = 197)*

Strontium isotope ratios of HSSr were recorded over a 4-month period (October 2020 – January 2021) and are reported here to assess long-term accuracy and precision of analytical sessions (Fig. 5). Analyses of HSSr are reported as a secondary reference material; USGS-MACS3 was used as the primary reference material in all analytical sessions.

The calculated mean for $^{87}Sr/^{86}Sr$ instrumental-corrected isotope ratios for the HSSr deep sea gastropod shell is 0.709136 ± 0.0000436 (2SE) (Fig. 5a) with a 2RSD (Relative Standard Deviation) of 0.08%. The calculated mean is slightly lower than the value of 0.709176 ± 0.000002 (2SD) obtained from TIMS analysis (possibly due to depth fractionation, interferences, and differences in reference material and sample matrix material). Standard-corrected isotope ratios (corrected with USGS_MACS3) yielded mean values of 0.709174 ± 0.0000436 (2SE) with a 2RSD of 0.08%. $^{84}Sr/^{86}Sr$ uncorrected ratios yielded a mean value of 0.05698 ± 0.000088 (2SE) and corrected ratios a value of 0.05638 ± 0.00020 (2SE) (Fig. 5c).

4.2.3. *NanoSr (n = 77)*

Strontium isotope ratios of NanoSr were recorded over a 4-month period (February 2021 – May 2021) and are reported here to assess long-term accuracy and precision of analytical sessions (Fig. 6). Analyses of NanoSr are reported as a secondary reference material; the in-house deep-sea marine gastropod or USGS-MACS3 were used as the primary reference material in all analytical sessions.

The calculated mean for $^{87}Sr/^{86}Sr$ instrumental corrected isotope ratios for the NanoSr pressed pellet standard is 0.70722 ± 0.00099 (2SE) (Fig. 6a) with a 2RSD (Relative Standard Deviation) of 1.23%. The calculated mean is slightly lower than the accepted value of 0.70756 ± 0.00002 (2SD).

Standard corrected isotope ratios (corrected with USGS-MACS3) yielded mean values of 0.70719 ± 0.00099 (2SE) with a 2RSD of 1.23%. $^{84}Sr/^{86}Sr$ uncorrected ratios yielded a mean value of 0.06075 ± 0.0016 (2SE) and corrected ratios a value of 0.05834 ± 0.0108 (2SE) (Fig. 6c).

4.2.4. *NIST612 (n = 174)*

Trace element analyses of NIST SRM 612 that were conducted over a 7-month period (October 2020 – May 2021) are reported here to illustrate the long-term accuracy of the method (Fig. 7a-c). Analyses of NIST SRM 612 are reported as a secondary reference material; NIST SRM 610 was used as the primary reference material for all analytical sessions. Sr, Ba, and Zn were used as index trace elements to assess accuracy of the secondary reference material accuracy, because of the significance of these elements in otolith research studies, and similarity to concentrations found in otolith structures (refer to Section 1). Measured trace element concentrations and standard errors can be found in Appendix A.

Zn, Sr, and Ba yielded mean concentrations of 40.88 mg/kg ± 0.33 (2SE), 79.15 mg/kg ± 0.38 (2SE), and 39.84 mg/kg ± 0.24 (2SE) with RSDs of 10.7%, 6.28%, 7.89% respectively. Deviation from the preferred values increased as laser spot size decreased due to lower volume of ablated material (Fig. 7a-c). Trace element concentrations at smaller laser spot sizes were ~ 1–2 mg/kg higher than the preferred values, whereas trace element concentrations were within ~ 1mg/kg of preferred values at larger laser spot sizes. The accuracy of individual results for Sr, Ba, and Zn concentrations in NIST 612 are discussed in detail below.

Concentrations of Ba were within 10% of the accepted value for ~96% of all analyses and within 5% of the accepted value for ~85% of all analyses (Fig. 7a). Deviation from the accepted value were predominantly positive, with 70% of all analyses being above the accepted value. Some analyses at smaller laser diameters (8 – 15µm) were just outside analytical uncertainty, whereas analyses at larger laser diameters (20 – 40µm) were within analytical uncertainty. Sr concentrations fell within 10% of the accepted value for ~98% of all analyses and within 5% for ~92% of all analyses. (Fig. 7b). Deviations from the accepted value were predominantly positive, with < 20% yielding concentrations below the accepted value. Zn shows more variation from the accepted values than both Sr and Ba with only 83% of all analyses being within 10% of the accepted value and 50% of all analyses being within 5%. Deviations from the accepted value were predominantly positive, with 78% of the total analyses being above the accepted value (Fig. 7c).

There are several ways to calculate the limit of detection (LOD) for trace element analyses using LA-ICP-MS. I used the LOD formulation defined by Pettke et al. (2012) for use on ICP-MS instruments with low backgrounds, such as the Agilent 8800 QQQ-ICP-MS. Since calculated LOD values fluctuate depending on signal sensitivity and standard deviation of the background signal, laser spot diameter and signal intensity influence the calculated LOD values. Because signal sensitivity varies day-to-day (e.g., humidity, temperature, cone degradation), the calculated LOD varies between analytical sessions. Regardless, larger laser spot diameters result in increased signals that lead to a decrease in the calculated average LOD; the negative relationship between laser spot diameter and LOD is approximately exponential (Fig. 8). While LODs are used to determine the lowest concentration of an element that can be detected, the limit of quantification (LOQ) is used as a measurement of the lowest concentration that is acceptable for a specific use (Armbruster & Pry, 2008). LOQ has various definitions and methods of calculation, with the most common described as three times the LOD. Average LOD values for Sr, Ba, and Zn can be found in Table 5 and individual analyses in Appendix A.

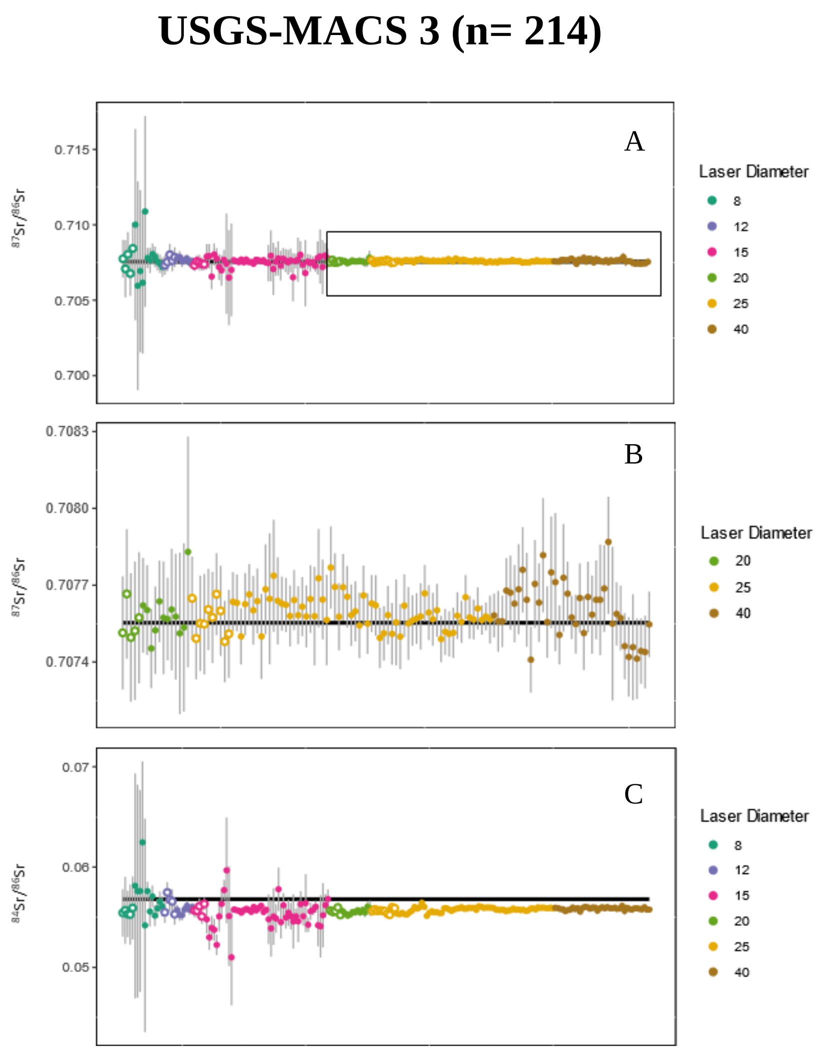

Figure 4: Split-stream collected USGS-MACS3 mean instrumental corrected $^{87}Sr/^{86}Sr$ results (A) are arranged in order of increasing laser diameter. An inset of $^{87}Sr/^{86}Sr$ instrumental corrected results (black box) shows results for laser diameters >20µm (B). The accepted $^{87}Sr/^{86}Sr$ ratio for USGS-MACS3 is represented by a black bar. $^{84}Sr/^{86}Sr$ results (C) are in order of increasing laser diameter then date collected with the natural $^{84}Sr/^{86}Sr$ ratio (~0.0568; calculated based on natural abundances) represented by a black bar.

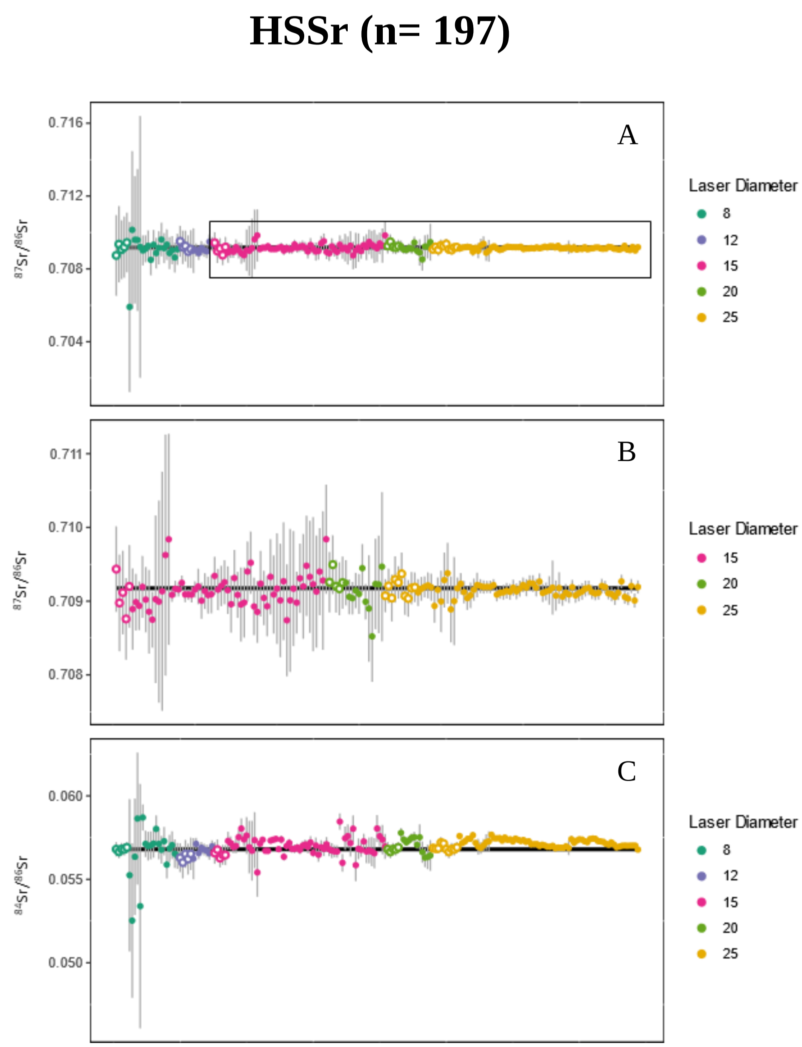

Figure 5: Split-stream collected HSSr mean instrumental corrected $^{87}Sr/^{86}Sr$ results (A) are arranged in order of increasing laser diameter. An inset of $^{87}Sr/^{86}Sr$ instrumental corrected results (black box) shows results for laser diameters >15µm (B). HSSr has a TIMS $^{87}Sr/^{86}Sr$ value of 0.709176 and is represented by a black bar. $^{84}Sr/^{86}Sr$ results (C) are in order of increasing laser diameter then date collected with the natural $^{84}Sr/^{86}Sr$ ratio (~0.0568; calculated based on natural abundances) represented by a black bar.

NanoSr (n= 77)

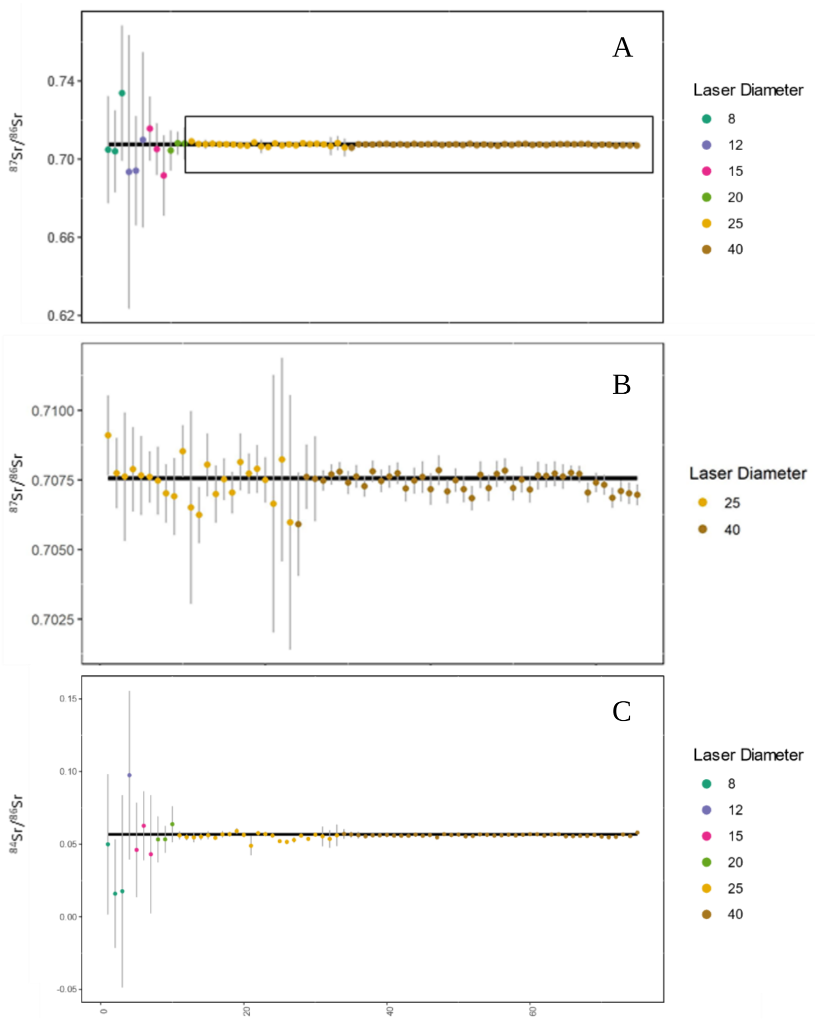

Figure 6: Split-stream collected NanoSr mean instrumental corrected $^{87}Sr/^{86}Sr$ results (A) are arranged in order of increasing laser diameter. An inset of $^{87}Sr/^{86}Sr$ instrumental corrected results (black box) shows results for laser diameters >25µm (B). NanoSr has a determined value for $^{87}Sr/^{86}Sr$ of (0.70756: Weber et al., 2020) is represented by a black bar. $^{84}Sr/^{86}Sr$ results (C) are in order of increasing laser diameter then date collected with the natural $^{84}Sr/^{86}Sr$ ratio (~0.0568; calculated based on natural abundances) represented by a black bar.

NIST SRM 612 (n= 174)

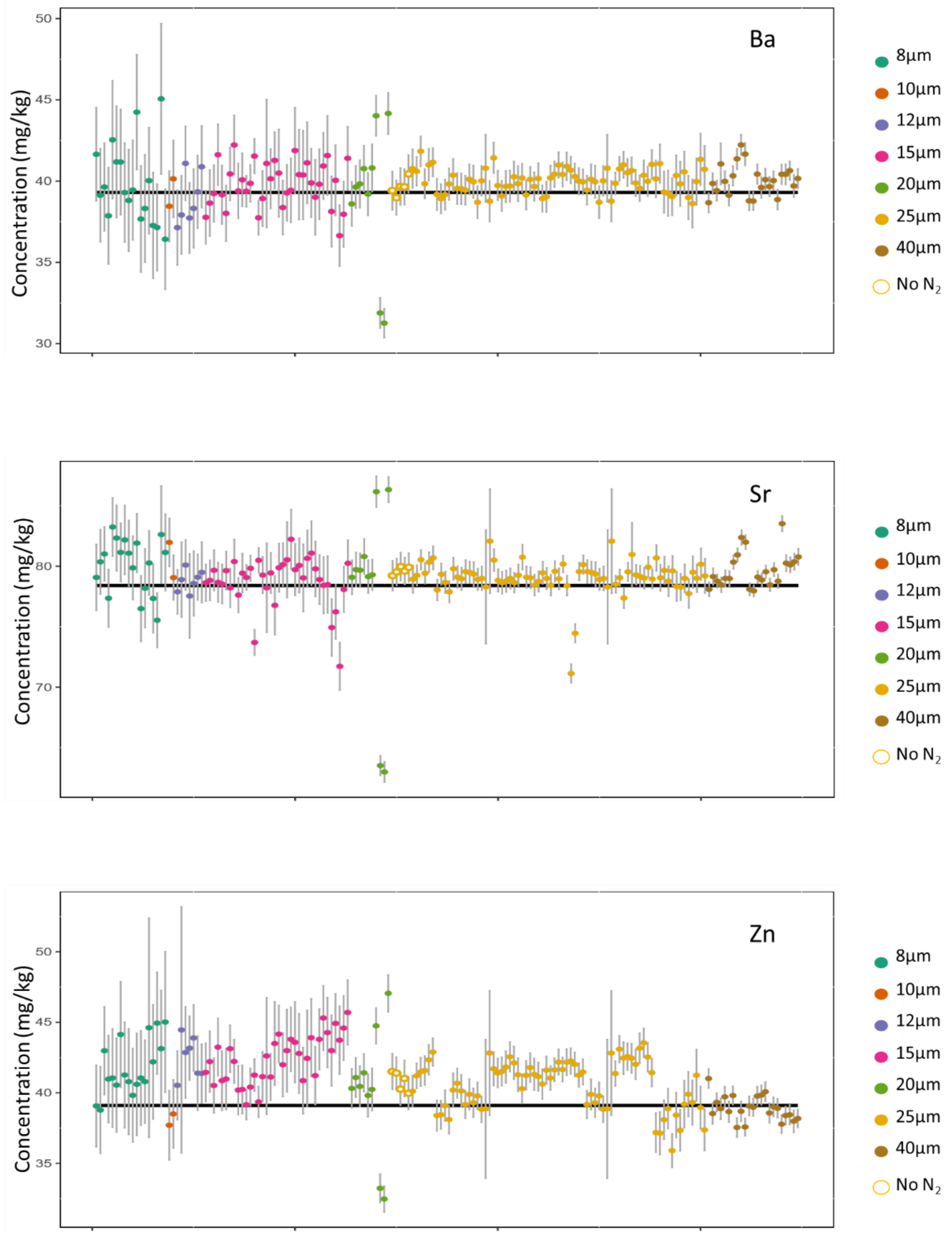

Figure 7: Split stream collected NIST SRM 612 mean concentrations of Ba (top), Sr (middle), and Zn (bottom) are arranged in order of increasing laser diameters then date collected, and error bars represent 2xSE of individual analyses. Preferred concentrations of Sr, Ba and Zn are represented by black bars in each plot (Jochum et al., 2011).

NIST612 – Limit of Detection (LOD)

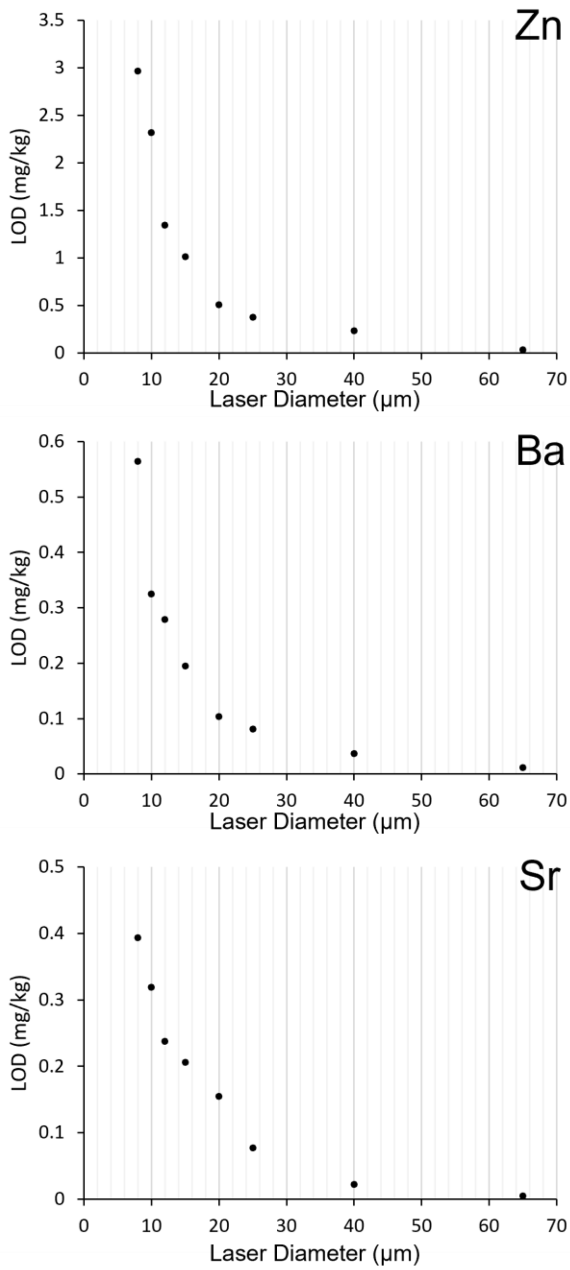

Figure 8: Mean limit of detection values for Sr, Ba and Zn at various laser diameters between 8 and 65μm. LOD values calculated using the Pettke et al. (2012) method on NIST SRM 612.

4.3. Laser diameter influence

4.3.1. *Effects of laser diameter on $^{87}Sr/^{86}Sr$ ratios*

Seven laser diameter spot sizes (8µm, 10µm, 12µm, 15µm, 20µm, 25µm, and 40µm) were analyzed and assessed for accuracy based on deviation from accepted $^{87}Sr/^{86}Sr$ ratios on HSSr, USGS-MACS3 and NanoSr. Some analyses on reference materials HSSr, USGS-MACS3 and NanoSr were not possible due to issues in ablation consistency (e.g., 8µm, 10µm) and restrictions to reference material spot sizes in collaborative sessions (i.e., HSSr reference material not used for Heidi Swanson analyses at 40µm) (see Table 5).

Precision of measured $^{87}Sr/^{86}Sr$ ratios improved with larger spot diameters and with increased Sr mass fractions; these results are illustrated in Figures 9-11. This pattern is consistent across all reference materials and laser diameters (Figs. 9-11). USGS-MACS3 showed significantly higher 2SE at spot diameters of 8µm, 12µm, and 15µm; at laser spot diameter >15µm, precision was similar(Fig. 9). Uncertainty on HSSr decreased with increasing laser diameter following an identical trend as USGS-MACS3 with respect to precision at higher spot sizes 20µm and 25µm (Fig. 10). However, analyses of HSSr at laser diameters of 20µm had a larger range of 2SE values than USGS-MACS3 (Fig. 10). NanoSr analyses were conducted primarily at laser diameters of 25µm and 40µm due to use required session parameters, and only 3 analyses of all other laser diameters were conducted (10µm, 12µm, 15µm, 20µm). Analyses that were conducted on NanoSr yielded decreasing 2SE with increasing laser diameters. Uncertainty on laser diameters <25µm were an order of magnitude higher than uncertainty on laser diameters 25µm and 40µm (Fig. 11).

Mean calculated instrumental corrected $^{87}Sr/^{86}Sr$ ratios on USGS-MACS3 had less than <0.3‰ variation from the accepted value across all laser diameters. HSSr and NanoSr had <0.2‰ and <12‰ variation on each reference material, respectively. Variation from the accepted values decreased with increasing laser diameters and Sr mass fractions (Table 5).

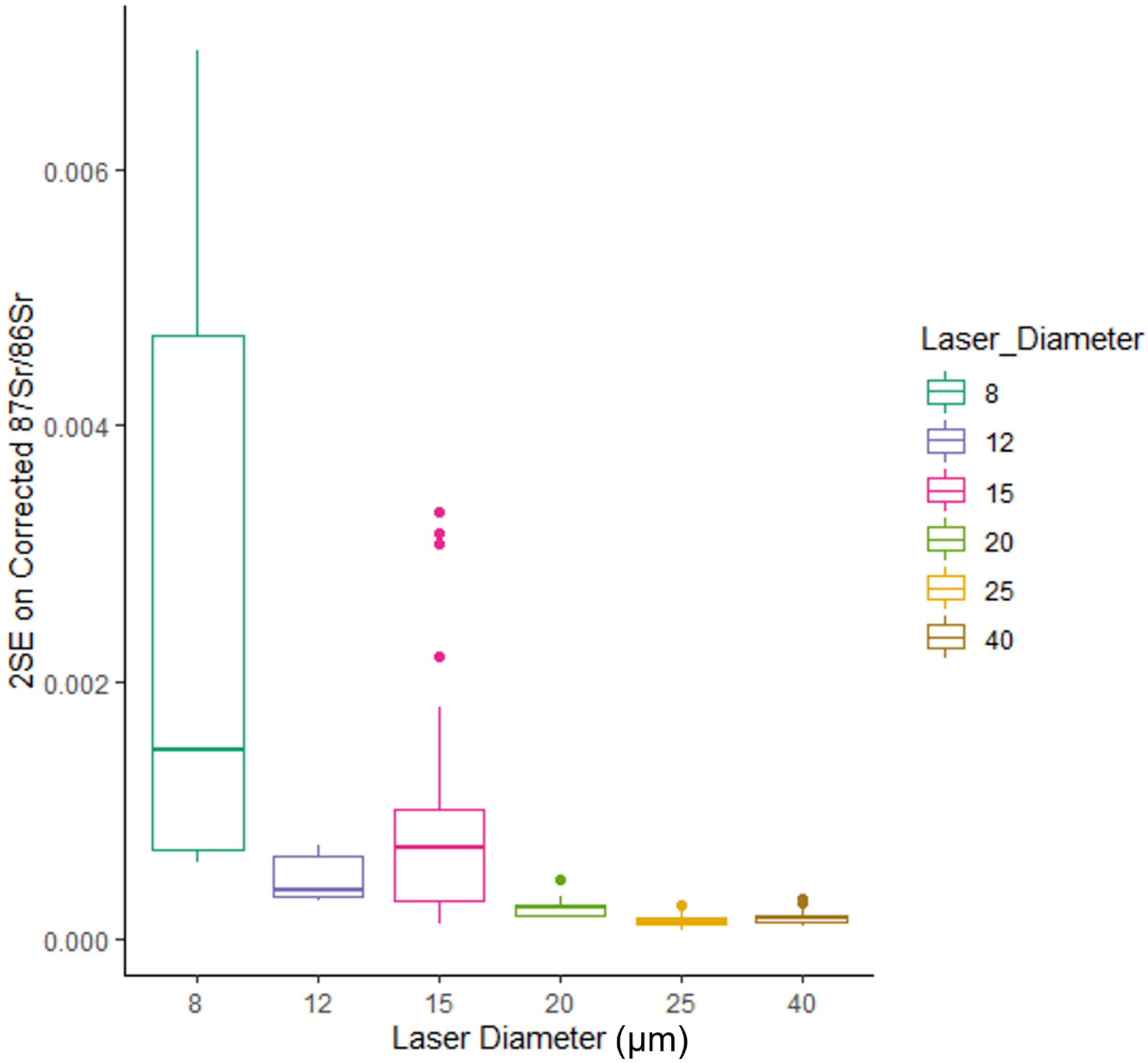

Figure 9: 2SE uncertainty on USGS-MACS3 instrumental corrected $^{87}Sr/^{86}Sr$ values across laser diameters.

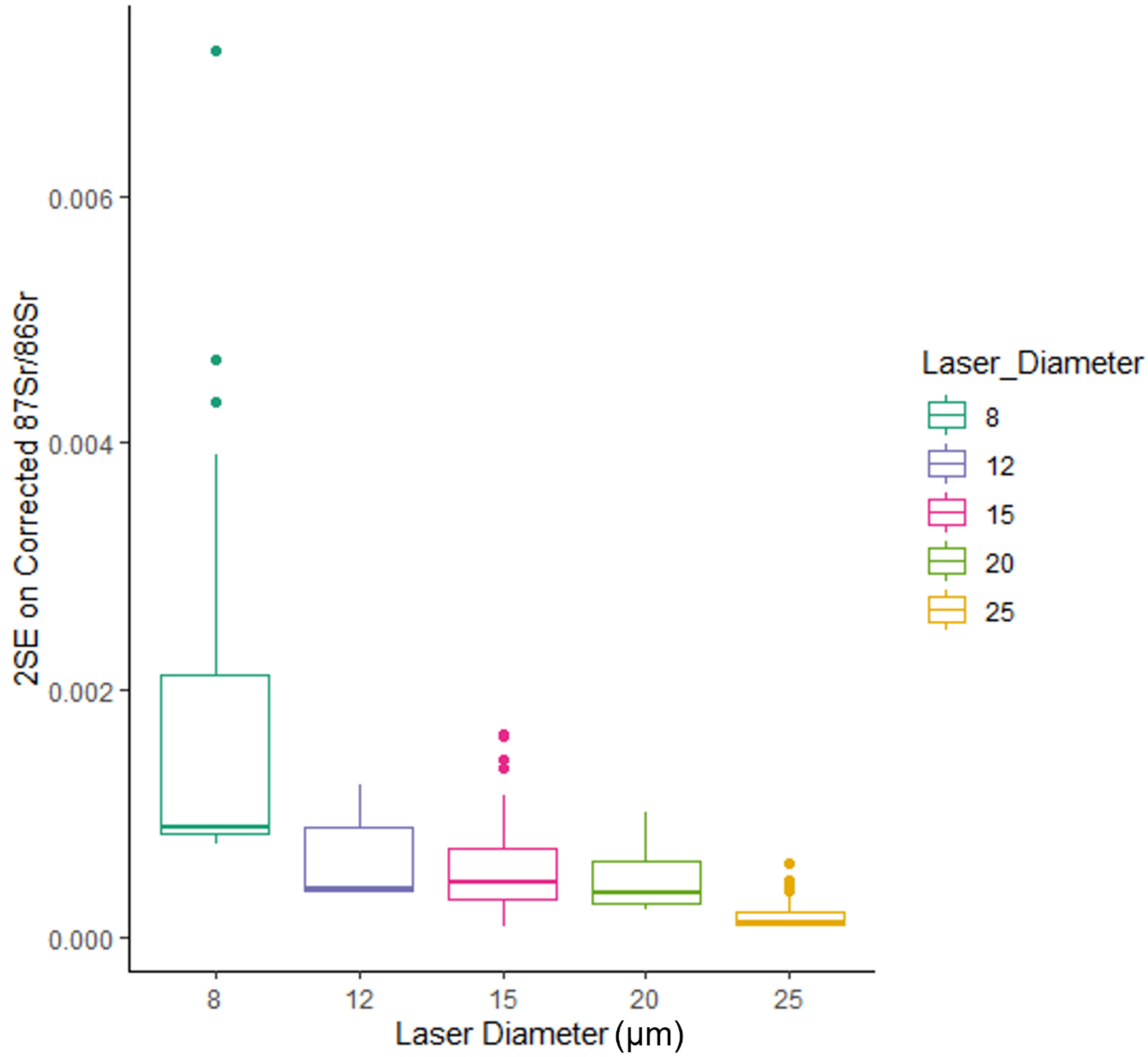

Figure 10: 2SE uncertainty on HSSr instrumental corrected $^{87}Sr/^{86}Sr$ values across laser diameters.

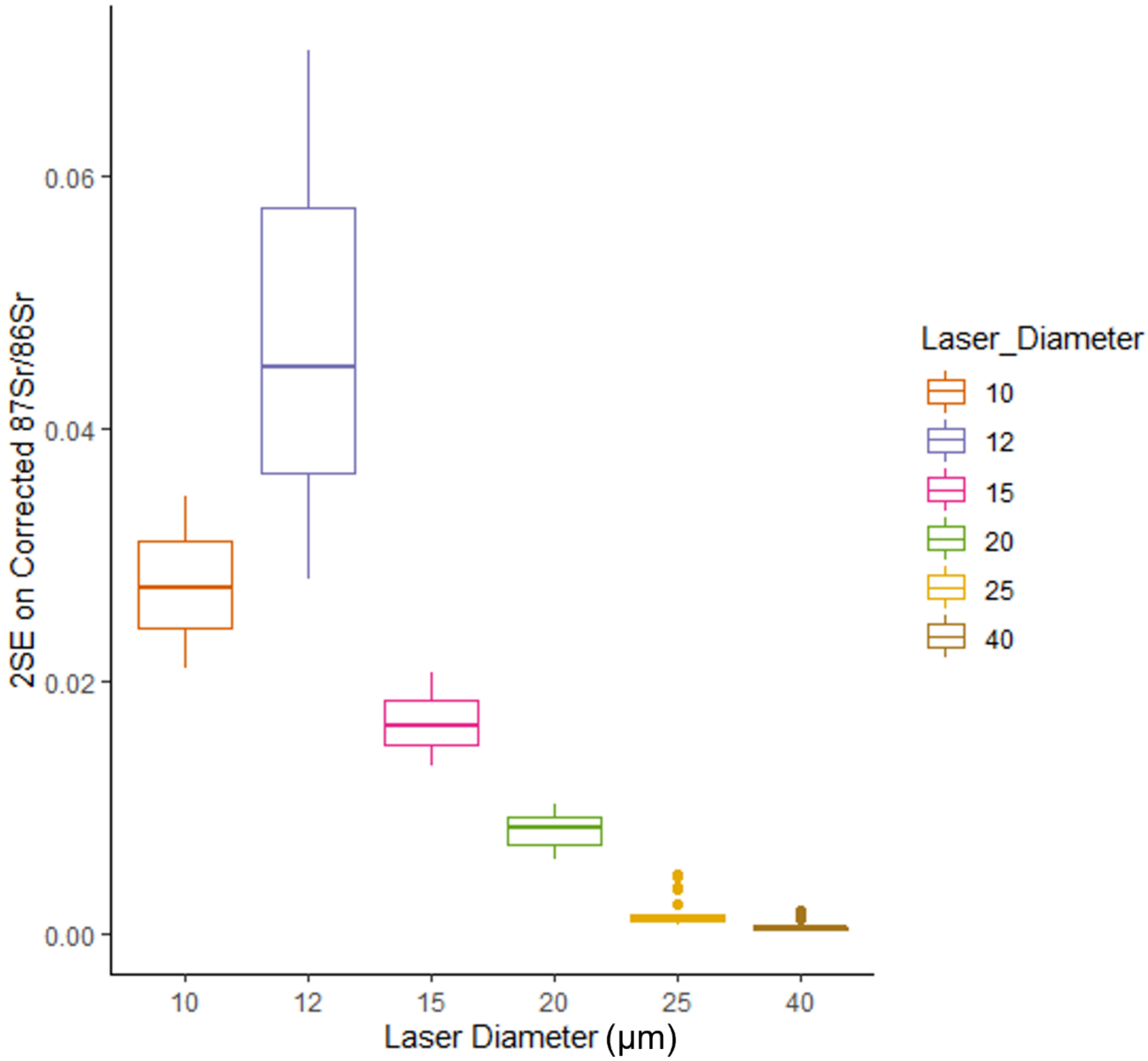

Figure 11: 2SE uncertainty on NanoSr instrumental corrected $^{87}Sr/^{86}Sr$ values across laser diameters.

Table 5: Calculated 2 standard deviation on instrumental corrected $^{87}Sr/^{86}Sr$ for individual laser diameters on HSSr, NanoSr, and USGS-MACS3.

	HSSr			NanoSr			USGS-MACS3		
Laser Diameter (µm)	**n**	**Corrected $^{87}Sr/^{86}Sr$**	**2SD**	**n**	**Corrected $^{87}Sr/^{86}Sr$**	**2SD**	**n**	**Corrected $^{87}Sr/^{86}Sr$**	**2SD**
8	24	0.709048	0.000755	0	na	na	17	0.707739	0.001223
10	0	na	na	3	0.714208	0.016946	0	na	na
12	13	0.709147	0.000208	3	0.699146	0.009305	12	0.707671	0.000194
15	65	0.709148	0.000219	3	0.704128	0.012038	55	0.707498	0.000348
20	17	0.709162	0.000232	3	0.706870	0.002104	17	0.707577	0.000085
25	78	0.709147	0.000086	23	0.707477	0.000738	74	0.707593	0.000062
40	0	na	na	42	0.707403	0.000370	39	0.707603	0.000112

4.3.2. *Effects of laser diameter on trace element analyses*

Seven laser diameter spot sizes (8µm, 10µm, 12µm, 15µm, 20µm, 25µm, and 40µm) were analyzed and assessed with respect to NIST SRM 612 accepted values on Sr, Ba and Zn. Smaller laser diameters decreased the amount of ablated material delivered to the ICP-MS, and caused increased deviation from accepted values. Mean concentrations and 2SD for Sr, Zn, and Ba on each laser diameter can be found in Table 6. Analyses across laser diameters for all reference materials were collected over several months and as a result, sensitivity, cone degradation, and environmental factors such as temperature and humidity, as well as improvement of the technique cause the precision of analyses to differ from expected ranges. Due to time restraints and an ongoing pandemic, very poor results were removed, but certain laser diameters (e.g., 20µm) were limited in the number of analyses collected. While this may compromise the comparison of the results the overall justifications on precision can still be made, especially at larger laser diameters.

Table 6: Calculated mean concentrations and 2SD of Sr, Ba, and Zn on NIST612 for spot sizes between 8 and 40µm

Laser Diameter (µm)	Number of Analyses (n)	^{88}Sr Mean (ppm)	^{88}Sr 2SD (ppm)	^{66}Zn Mean (ppm)	^{66}Zn 2SD (ppm)	^{137}Ba Mean (ppm)	^{137}Ba 2SD (ppm)
8	18	80.06	4.52	41.76	3.90	39.83	4.84
10	2	80.51	4.12	38.10	1.13	39.29	2.38
12	7	78.79	1.78	42.52	2.91	38.92	3.13

15	36	78.79	4.08	42.40	3.39	39.81	2.72
20	10	81.27	6.23	40.08	5.20	39.02	4.23
25	78	79.13	2.71	40.58	3.37	39.99	1.47
40	23	79.72	2.90	38.90	1.72	40.06	1.87

Increasing precision of trace element concentration measurements with larger laser diameters is due to counting statistics associated with an increased signal. This is consistent across all elements of interest (Sr, Ba, Zn) signifying that larger laser diameters provide higher precision data for otolith research (Fig. 12). Precision of analyses are consistently <5% (2SE) for diameters >15µm for all elements (Fig. 12). Sr (~78 mg/kg) consistently yielded the lowest 2SE (%) across all laser diameters with Zn and Ba (~ 40 mg/kg) both yielding similar precision to each other within each laser diameter.

Variation from the preferred values for NIST SRM 612 was used to assess accuracy of the split-stream technique on various trace elements (Sr, Ba, Zn). Variation >10% of the accepted values is considered inaccurate while variation between 5 – 10% is considered acceptable. These zones are used to indicate inaccurate data across laser diameters and are illustrated in Figure 13.

There were only 3 and 6 analyses for Sr and Ba, respectively, that were considered inaccurate (>10%) when considering all laser diameters (n=174). There was more than a 10% difference for Sr on 3 analyses at a 20µm spot diameter (Fig. 13b). Measurements of Sr and Ba can be considered within an acceptable range of accuracy for otolith research at spot sizes from 8 – 40µm.

There were a total of 29 inaccurate results for Zn across all laser diameters (n = 174) which is significantly higher when compared to Sr and Ba (Fig. 13b). Accurate Zn analyses fall within a 5 – 10% range of variation from the accepted values. Most of the inaccurate results were from analyses with 15µm and 25µm laser diameters. These analyses were conducted in sessions very close to the beginning of recorded data prior to refinement of the tuning parameters on the ICP-MS. Precision and accuracy of Zn analyses improved significantly at spot sizes >20µm (Table 6).

In summary, laser diameters have a direct effect on precision where increasing laser diameter improved the precision on trace element concentration measurements. This effect however was less consistent when considering the accuracy of the individual analyses where no direct correlation can be made comparing measured elements (Sr, Ba, Zn) across laser diameters perhaps due to differences in behavior, interferences, or concentration values between NIST SRM 610 and 612. Zn analyses while considered to be more inaccurate when compared to Zn and Ba, are still ~80% within an acceptable range with that number improving to 96% when adjusting the criteria for ‘accurate data’ to be within 15% of the accepted value.

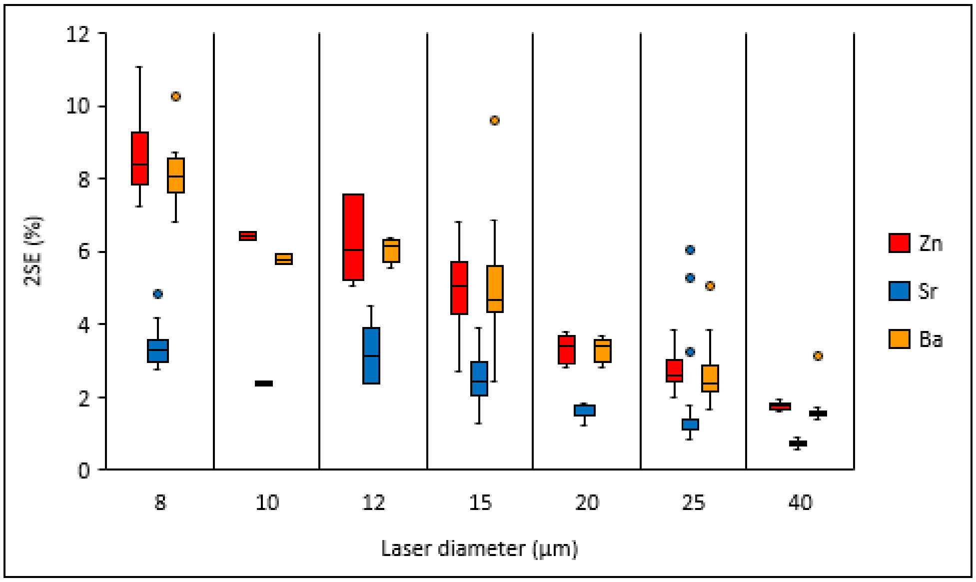

Figure 12: 2SE (%) of Sr, Zn, and Ba across laser diameters from 8 – 40µm for analyses measured via LASS-ICP-MS

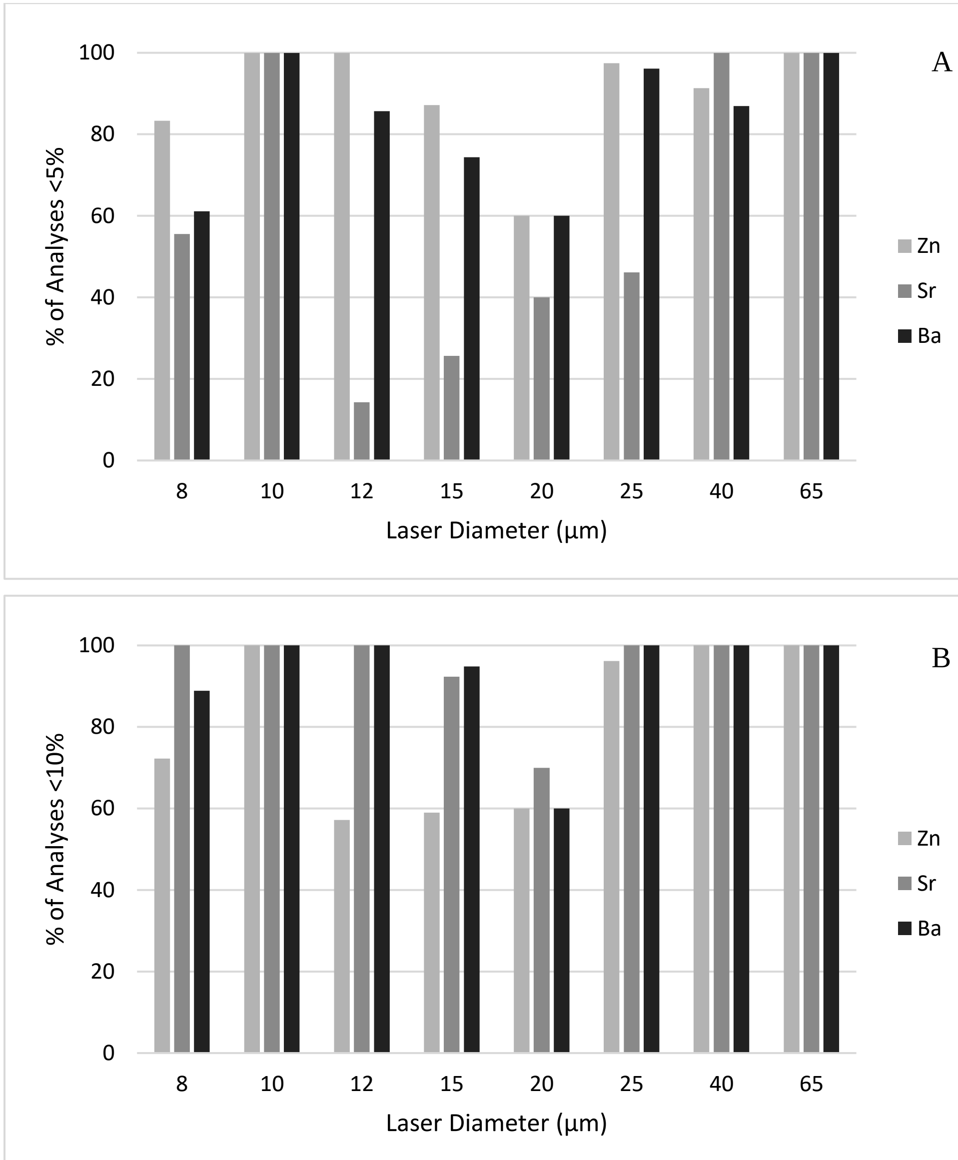

Figure 13: Number of analyses of NIST612 which have <10% (A) and <5% (B) difference from the preferred value for Sr, Ba, and Zn.

4.4. LASS-ICP-MS Data from otoliths

Strontium isotope ratios and trace element concentrations were measured using LASS-ICP-MS to investigate the spatial resolution and applications of the technique. Older lake trout (~20 years old), which have otoliths with small annular growth zones (often less than 10 µm) were chosen to evaluate achieved spatial resolution of trace elements such as Zn, Sr, and Ba for growth zones < 10µm. Strontium isotope ratios and trace element concentrations were measured in younger arctic char (~10 years old) during different life history stages, emphasizing natal, rearing, and migration growth zones. I report the results from two otolith samples below that include a lake trout (LAU3-5) and arctic char (KUG-1-1a and KUG1-1b). The char otolith was large enough that I analyzed two parallel transects with different spot sizes to investigate the role of spot size on trace element and Sr isotope resolution.

4.4.1. *Lake trout – Salvelinus namaycush (LAU3-5)*

Analyses were carried out using LASS-ICP-MS (see Section 2.3) with a laser spot diameter of 25µm, fluence of 4.5 J cm^{-2}, a scan speed of 2 µm s^{-1}, and a frequency of 20Hz. Data were reduced using data reduction procedures described in section 2.3. A transect was analyzed from the core (oldest growth zone) of the otolith to the distal edge (youngest). Spatially resolved concentrations and $^{87}Sr/^{86}Sr$ values were overlain on transmitted light images of the post-ablated otoliths to visualize spatial resolution of trace element concentrations relative to growth zone thickness (Fig. 14). Raw trace element and Sr-isotope ratio data were separated into zones of interest based on elevated strontium concentrations and changes in isotopic signature. Results were divided into three zones based on the trace element and isotope zoning (Fig. 14a-c): zone 1 (0–0.2mm along the transect), zone 2 (0.2–1.6mm), and zone 3 (1.6–2.3mm).

4.4.1.1. *Trace Elements*

Zone 1, which represents an elemental signature from fish birth to 1 year, is the core of the otolith and has relatively stable concentrations of most trace elements (Appendix D), low concentrations of Sr, and a single oscillation of Zn (Fig. 14b). The transition from zone 1 to zone 2 occurs at ~0.2mm along the transect where concentrations of Zn reach >80 mg/kg (Fig. 14b). Zone 2 has oscillation concentrations of Zn that vary from ~20 to 80 mg/kg; oscillations are separated by 150µm at the beginning of zone 2 and decrease to ~50 µm towards the boundary with zone 3 (Fig. 14b). Concentration of Sr in zone 2 are ~50 mg/kg and show minor oscillations with a gentle increase to higher value towards zone 3 (Fig. 14b). The transition from zone 2 to 3 occurs at ~1.6mm along the transect and found at a rapid increase in the concentration of Sr. In zone 3, the Sr concentrations contains regular oscillations with spikes separated by ~50µm with maximum peaks around 350 mg/kg and minima around 125 – 150 mg/kg (Fig. 14b).

4.4.1.2. *Strontium Isotope Ratios*

$^{87}Sr/^{86}Sr$ ratios vary along the transect (Fig. 14c). In general, regions with low concentrations of Sr (i.e., zones 1 and 2) have lower precision on isotope ratios whereas areas with high concentrations of Sr (e.g., zone 3) have more precise ratios; the low Sr concentrations results in erratic signal intensity (Fig. 14c). An average value for $^{87}Sr/^{86}Sr$ across all three zones yields a mean value of 0.7190 $\pm$ 0.0012 (2SE); however, this value has limited use as there are systematic changes in $^{87}Sr/^{86}Sr$ along the transect. Individual zones yield slightly different mean values and uncertainties. Zone 1 yielded a mean ratio of 0.7240 $\pm$ 0.0067 (2SE) (Fig. 14c). This growth corresponds to a Sr concentration of ~50mg/kg as identified in the trace element analysis. Zone 2 yielded a mean $^{87}Sr/^{86}Sr$ ratio of 0.7204 $\pm$ 0.0015 (2SE) and a slightly higher Sr mass fraction (~80 mg/kg) before leading into zone 3 which is dominated by oscillations in Sr signal (Fig. 14c). Zone 3 yielded a mean $^{87}Sr/^{86}Sr$ ratio of 0.7134 $\pm$ 0.0014 (2SE) and oscillate between ~ 0.709 and ~ 0.718 (Fig. 14c).

4.4.2. *Arctic char – Salvelinus alpinus (KUG1-1a – 40µm)*

Analyses were carried out using the LASS-ICP-MS setup (see Section 3.2) with a laser spot diameter of 40µm, fluence of 4.5 J cm^{-2}, a scan speed of 2 µm s^{-1}, and a frequency of 20Hz. Similar to otolith LAU3-5, results are separated into visually assessed zones based on elevated strontium concentrations and isotopic signatures. Three zones are identified: zone 1 (0–0.3mm), zone 2 (0.3–0.85mm), and zone 3 (0.85–1.64 mm). Spatially resolved data are plotted next to a reflected light image of the otolith in Figure 15.

4.4.2.1. *Trace Elements*

Concentrations of trace elements other than Zn, Sr, Mg, Mn, Ba remain relatively stable outside of the transition from the core (zone 1) to regular growth zones (zone 2) with most to all elements with significant concentrations above LOD (Appendix D). Sr concentrations in zone 1 reside around 400 mg/kg until around 0.2mm where concentrations decrease to around 250 mg/kg with minor oscillations (~100μm in duration) and continue until around 0.85mm where concentrations spike (Fig. 15b). After 0.85mm the Sr concentrations contains regular oscillations with spikes being around 50 – 75μm in duration with maximum peaks around 3000 mg/kg and minima around 1000 – 1500 mg/kg (Fig. 15b). Zn concentrations linearly decrease and maintain regular highly accentuated oscillations throughout the entire duration of the transect with the peak maxima concentrations decreasing from 100 mg/kg to ~20-40 mg/kg and minima concentrations around 40 mg/kg in the core to ~10 – 20 mg/kg further in the transect (Fig. 15b). Zn maxima and minima appear to be around 150μm in duration at the beginning of the transect decreasing to ~50μm by the end of the transect (Fig. 15b).

4.4.2.2. *Strontium Isotope Ratios*

Strontium isotope ratios for KUG1-1a were calculated for the three zones (Figure 15c). While the $^{87}Sr/^{86}Sr$ ratio across all three zones yields a mean value of 0.7285 ± 0.0005 (2SE), individual zones yield slightly different mean values and uncertainties. Zone 1 yielded a mean ratio of 0.7327 ± 0.00047 (2SE) (Fig. 15c). This zone includes a Sr concentration of ~400mg/kg as identified in the trace element analysis. Zone 2 yielded a mean ratio of 0.7495 ± 0.00032 (2SE) and relatively lower Sr mass fraction (~250 mg/kg) before leading into zone 3 at 0.85mm (Fig. 15c). Zone 3 contains oscillations in Sr concentrations and isotope ratios yielding a mean $^{87}Sr/^{86}Sr$ ratio of 0.71099 ± 0.000084 (2SE) (Fig. 15c). Integrating only the peaks and the troughs of the maxima and minima, $^{87}Sr/^{86}Sr$ ratios of the maxima were around 0.7096 ± 0.00017 (2SE), while the minima yielded slightly higher ratios of ~ 0.7113 ± 0.0002 (2SE) (Fig. 15c).

4.4.3. *Arctic char – Salvelinus alpinus (KUG1-1b – 25μm)*

Analyses were carried out using the LASS-ICP-MS setup (see Section 3.3) with a laser spot diameter of 25μm, fluence of 4.5 J cm^{-2}, a scan speed of 2 μm s^{-1}, and a frequency of 20Hz. The transect was parallel to the transect conducted with a 40μm diameter laser spot (section 3.3.2). The results of the two parallel lines are generally similar, however we cannot rule out the possibility that some of the differences are due to the slightly different placement of the laser ablation lines. With that caveat in mind, I now report the results from the 25μm transect (Fig. 16) using the same zone boundaries as for the 40μm laser spot transect (Fig. 16).

4.4.3.1. *Trace Elements*

Concentrations of trace elements other than Zn, Sr, Mg, Mn, Ba remain relatively stable outside of the transition from the core to regular growth zones with most to all elements with significant concentrations above LOD (Appendix D). Sr concentrations in the core were approximately 400 mg/kg until ~ 0.2mm, where concentrations decrease to ~ 250 mg/kg with minor oscillations (~100µm in duration) and continue until around 0.85mm, where concentrations spike (Fig. 16b). After 0.85mm, the Sr concentrations regularly oscillate, with peaks being around 50 – 75µm in duration with maximum peaks around 3000 mg/kg and minima ~ 1000 – 1250 mg/kg (Fig. 16b). Zn concentrations linearly decrease and maintain regular highly accentuated oscillations throughout the entire duration of the transect with the peak maxima concentrations decreasing from 120 mg/kg to ~30 mg/kg and minima concentrations around 60 mg/kg to 10 – 20 mg/kg (Fig. 16b). Zn maxima and minima appear to be around 150µm in duration at the beginning of the transect decreasing to ~50µm by the end of the transect (Fig. 16b).

4.4.3.2. *Strontium Isotope Ratios*

Strontium isotope ratios for KUG1-1b (25µm) were calculated for the three zones. While the $^{87}Sr/^{86}Sr$ ratio across all three zones yields a mean value of 0.7305 $\pm$ 0.0005 (2SE), individual zones yield slightly different mean values and uncertainties. Early growth corresponding to zone 1 yielded a mean ratio of 0.7431 $\pm$ 0.001 (2SE) (Fig. 16c). This growth corresponds to a Sr concentration of 400mg/kg as identified in the trace element analysis. Zone 2 yielded a mean ratio of 0.7475 $\pm$ 0.00071 (2SE) and lower Sr mass fraction (~250 mg/kg) before leading into zone 3 (Fig. 16c). This zone is dominated by oscillations in Sr concentration yielding a mean ratio of 0.71083 $\pm$ 0.000084 (2SE) which is slightly higher than that of modern seawater (0.7092) (Fig. 16c). This is due to the averaging of the minima and maxima of the migration induced spikes. Integrating only the peaks and the troughs of the maxima and minima, $^{87}Sr/^{86}Sr$ ratios of the maxima were around 0.70923 $\pm$ 0.0005 (2SE), while the minima yielded slightly higher ratios of ~ 0.7115 $\pm$ 0.0008 (2SE) (Fig. 16c).

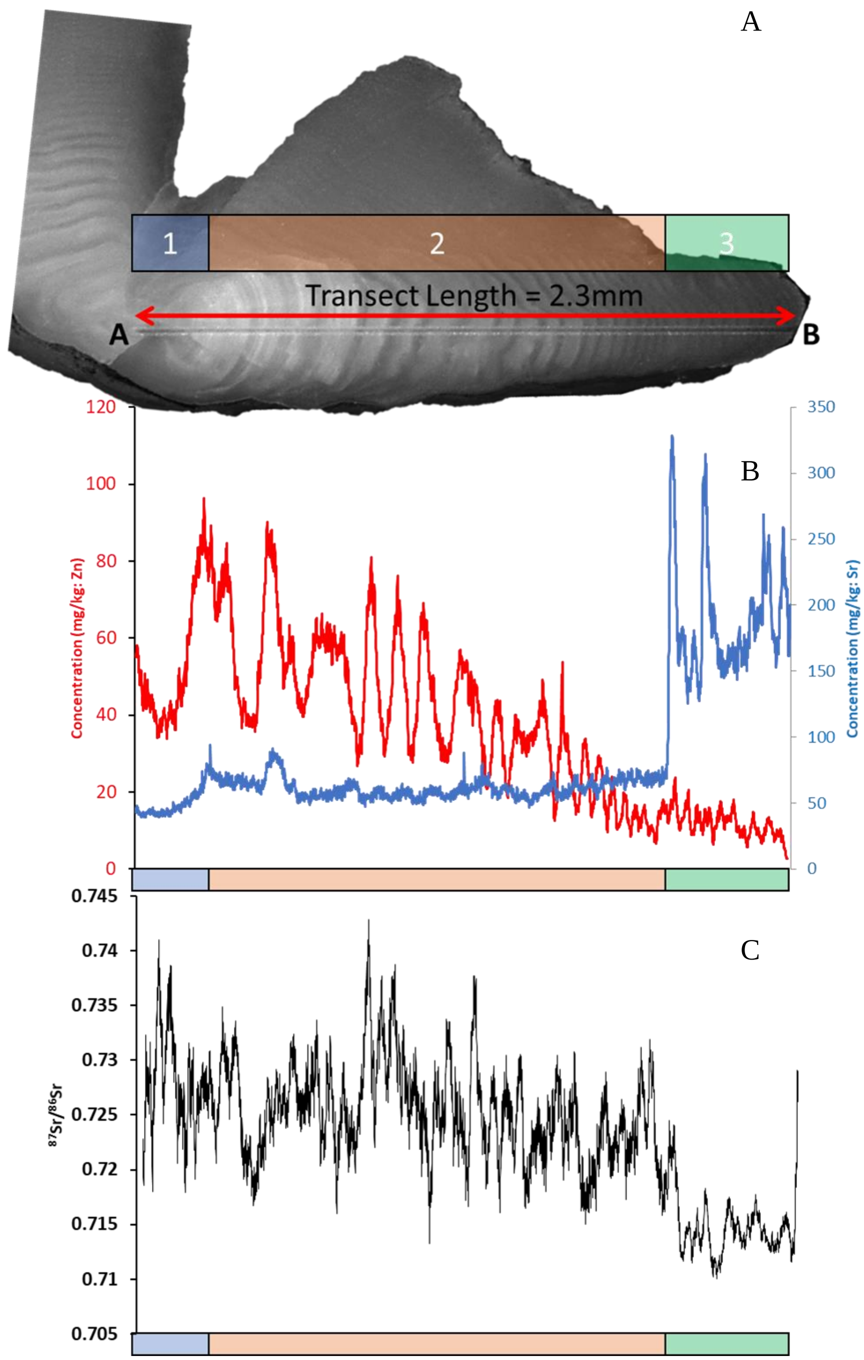

Figure 14: Strontium isotope ratios (C) and Sr (blue) and Zn (red) concentrations (B) of sample LAU3-5 are plotted with respect to the laser transect (A→B: 2.3mm). A transmitted light image of sample LAU3-5 (A) shows the laser transect with zone 1 (blue), 2 (orange), 3 (green) highlighted across plots.

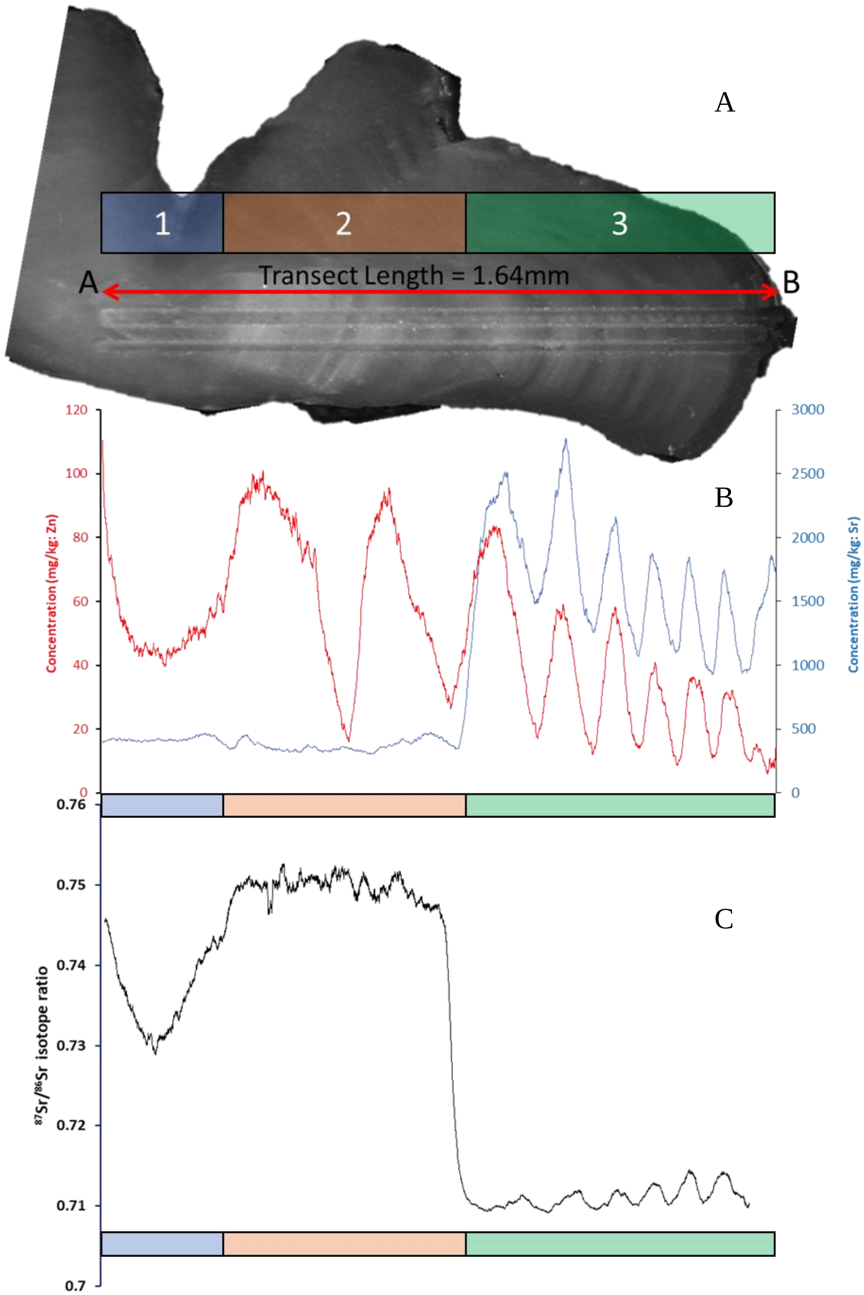

Figure 15: Strontium isotope ratios (C) and Sr (blue) and Zn (red) concentrations (B) of sample KUG1-1a (40µm) are plotted with respect to the laser transect (A→B: 1.63mm). A transmitted light image of sample KUG1-1a (A) shows the laser transect with zone 1 (blue), 2 (orange), 3 (green) highlighted across plots.

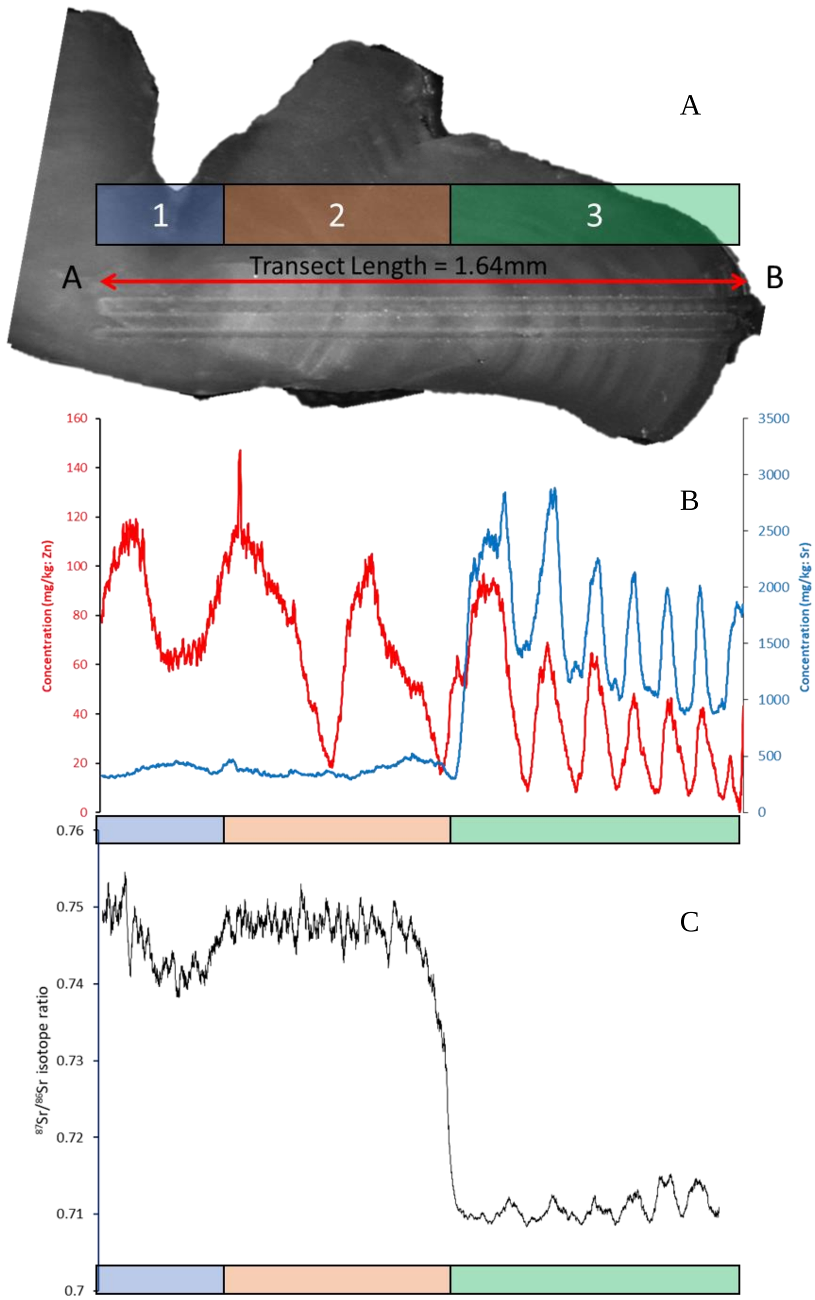

Figure 16: Strontium isotope ratios (C) and Sr (blue) and Zn (red) concentrations (B) of sample KUG1-1b (25µm) are plotted with respect to the laser transect (A→B: 1.63mm). A transmitted light image of sample KUG1-1b (A) shows the laser transect with zone 1 (blue), 2 (orange), 3 (green) highlighted across plots.

5. DISCUSSION

5.1. Reproducibility and Precision of Standard Reference Materials for Sr isotope analyses

Reproducibility of analyses across matrix-matched reference materials for analysis of otolith samples is important to the development of a technique as instruments and laboratory configurations are rarely the same. All analyses of Sr isotopes were done using the split-stream configuration for all assessments of reproducibility and precision. Reference materials here are assessed individually based on variation from accepted/measured values, and sample population uncertainties. The three reference materials used in this study for Sr isotope analyses (USGS-MACS3, HSSr, and NanoSr) are discussed below progressing from materials with high concentrations of Sr to those with low concentrations of Sr.

5.1.1. *USGS-MACS3*

The standard reference material USGS-MACS3 is the most widely used SRM for Sr isotope analyses across laboratories (e.g., Jochum et al., 2019). Long-term analyses of this material using the split-stream technique (n = 214) yielded ratios with instrumental (e.g., mass fractionation) corrected $^{87}Sr/^{86}Sr$ values within analytical uncertainty of the accepted value (Fig. 4). The widely used Iolite software package (Paton et al., 2011) applies an additional correction to $^{87}Sr/^{86}Sr$ ratios after instrumental fractionation is considered. This additional correction is used to account for fractionation due to factors outside instrumental mass fractionation, such as polyatomic interference on ^{86}Sr (e.g., Horstwood et al., 2008) and any laser-induced fractionation, which is considered negligible except in rare cases (c.f. Jackson and Günther, 2003). When an additional correction factor is applied to the $^{87}Sr/^{86}Sr$ ratio using our in-house HSSr reference material as the 'primary standard', the deviation from the accepted value is slightly higher than the instrumental fractionation corrected $^{87}Sr/^{86}Sr$ values but is still within analytical uncertainty of the accepted values (Fig. 4). Although the cause of this slight difference could be from many factors, it is probably due to differences in the matrix of the two reference materials. HSSr has values of ~3,000 mg/kg whereas USGS-MACS3 has significantly higher Sr concentrations of ~6,500 mg/kg. In addition, USGS-MACS3 is a pressed pellet of synthetic strontium carbonate powder that can ablate erratically whereas HSSr is crystalline calcite and ablates well (e.g., well-defined ablation craters, e.g., Kuhn et al., 2010). The precision of analyses of USGS-

MACS3 remains consistent in each spot size diameter and long-term analysis precision improves over time reflecting optimized tuning procedures (Fig. 4); the most recent set of analyses yielded values that are of a similar precision to other laser ablation laboratories that analyze otoliths using a single-stream system (e.g., Loewen et al., 2015).

The $^{84}Sr/^{86}Sr$ ratio of reference materials is an important monitor of the efficacy of instrumental mass fractionation corrections because the natural $^{84}Sr/^{86}Sr$ ratio shows little variation as both ^{84}Sr and ^{86}Sr are non-radiogenic stable isotopes of Sr. Natural values reported in the literature vary from 0.0555 – 0.0575 (Thirlwall, 1991) and deviation out of this range is usually attributed to problems correcting for instrumental-induced mass fractionation or Ca dimer or argides (Vroon et al., 2008). Analyses of USGS-MACS3 yield instrumental mass-fractionation corrected values that were within analytical uncertainty of the natural ratio (0.0568) (Fig. 4c). However, the standard-corrected value (as implemented in Iolite based on repeat analyses of a primary reference material) yielded values lower than the natural value (Appendix C). This indicates that the standard correction method employed during data reduction overcorrects that instrumental mass-fractionation corrected ratios of USGS-MACS3. Therefore, based on the corrected values of $^{87}Sr/^{86}Sr$ and $^{84}Sr/^{86}Sr$ of USGS-MACS3, only instrumental mass fractionation needs to be considered in materials with high Sr mass fractions using the instrumental setup developed in this thesis.

Although the USGS-MAC3 reference material is widely used in laser-ablation MC-ICP-MS analysis of Sr isotope ratios, it has a Sr mass fraction of ~6,500 mg/kg, which is significantly higher than most natural materials commonly investigated. For example, otoliths often have Sr concentrations <3000 mg/kg (e.g., Swanson et al., 2010). Our newly characterized in-house reference material HSSr has concentrations of ~1000–1500 mg/g Sr that are similar to those of concentrations found in otoliths that grew from seawater (~1000–3000 mg/kg Sr; Swanson et al., 2010). Although many aragonite/calcite shells are compositionally heterogeneous, our long-term analyses of HSSr suggests that it is isotopically homogeneous (Fig. 5) and, therefore, an appropriate material for assessing long-term accuracy and precision of Sr isotope values during analysis of otoliths.

5.1.2. *HSSr*

The reference material ‘HSSr’ is an in-house developed crystalline calcite deep sea gastropod shell with an $^{87}Sr/^{86}Sr$ signature which falls within the accepted range of seawater (Section 3.1; Kuznetsov et al., 2012; Mokadem et al., 2015). Long term analyses of this material using the split-stream technique (n=197) yielded ratios with instrumental corrected $^{87}Sr/^{86}Sr$ values within analytical uncertainty of the TIMS value (Fig. 5). An additional correction factor (Section 2.3) applied to $^{87}Sr/^{86}Sr$ ratios using USGS-MACS3 as the ‘primary standard’, yielded lower deviations from the accepted value than instrumental corrected values, and within analytical uncertainty of the accepted value (Appendix A). As discussed above, the differences between the instrumental and additional standard corrected values could be due to several factors including variable matrix compositions and strontium mass fractions. The sample population uncertainty (2SD) of analyses of HSSr shows consistency between laser spot diameters with long-term uncertainty decreasing over time and with increasing laser spot diameters (Fig. 5a). These recent analyses yield population uncertainties to a level of precision similar to other otolith laser ablation facilities that analyze an in-house marine carbonate standard using a single-stream setup (Loewen et al., 2015).

Analyses of HSSr yield instrumental mass-fractionation corrected $^{84}Sr/^{86}Sr$ values that were higher but within analytical uncertainty of the natural ratio (Fig. 5c). However, long-term instrumental corrected values and uncorrected values (raw 84/86 signals from ICP-MS) yielded $^{84}Sr/^{86}Sr$ ratios within analytical uncertainty (Fig. 5c) (Appendix C). Since both correction methods were within analytical uncertainty and showed little variability over time, both correction methods are suitable for calculating $^{84}Sr/^{86}Sr$ ratios of HSSr. Therefore, instrumental corrected values of $^{87}Sr/^{86}Sr$ and both uncorrected and corrected values of $^{84}Sr/^{86}Sr$ ratios should be reported for materials with moderate Sr mass fractions to generate more accurate and properly reduced isotope ratios.

Although heterogeneous in elemental concentrations, deep sea gastropod shells (HSSr) are widely used in otolith laboratories and tend to be isotopically homogeneous (Loewen et al., 2015; Miller & Kent, 2009). HSSr is an appropriate reference material in terms of matrix composition (crystalline calcite) and Sr mass fraction (~1000-3000 mg/kg Sr) when analyzing otolith isotopic signatures. Although a sufficient reference material for otoliths with comparable Sr mass fractions, many otoliths based in freshwater systems can routinely yield Sr concentrations < 500 mg/kg (e.g., Swanson et al., 2010).

5.1.3. *NanoSr*

The standard reference material ‘NanoSr’ is a pressed pellet calcite reference material created as a low Sr standard for Sr isotope ratios (Weber et al., 2020). Long-term analyses of NanoSr using the split-stream technique (n=77) yielded individual analyses ratios with instrumental corrected $^{87}Sr/^{86}Sr$

values within analytical uncertainty of the accepted value (Fig. 6). Additional correction factors (Section 2.3) are applied to $^{87}Sr/^{86}Sr$ values using USGS-MACS3 as the 'primary standard', and yielded lower $^{87}Sr/^{86}Sr$ ratios from the accepted value than instrumental corrected values, but within analytical uncertainty on most individual analyses (Fig. 6). Due to the low Sr mass fraction of NanoSr, laser spot diameters < 25μm have increased analytical uncertainties and larger deviation from the accepted value of 0.70756 $\pm$ 0.00003. Long-term analyses of data > 25μm (n=65) yielded ratios closer to the accepted value for both the instrumental (0.70743 $\pm$ 0.0009) and 'standard' corrected values (0.7074 $\pm$ 0.0009), with both slightly outside analytical uncertainty of the accepted value (Fig. 6a). At laser diameters > 25μm, 'standard' corrected values yielded lower $^{87}Sr/^{86}Sr$ ratios which deviated further from the accepted value than instrumental corrected values (Appendix A). These differences between the instrumental and additional standard corrected $^{87}Sr/^{86}Sr$ ratios are attributed to differences in strontium mass fractions between NanoSr (~500 mg/kg) and USGS-MACS3 (~6500 mg/kg). Sample population uncertainties of recent NanoSr analyses decreased with respect to laser diameter and continue to improve as the method is refined.

Analyses of NanoSr yielded instrumental corrected $^{84}Sr/^{86}Sr$ values that were higher, but within analytical uncertainty of the natural ratio (Fig. 6c). However, long-term uncorrected values yielded $^{84}Sr/^{86}Sr$ ratios that are lower than the instrumental corrected values and closer to the natural ratio (Appendix C). This indicated that the standard-correction method corrects the $^{84}Sr/^{86}Sr$ ratios of NanoSr but not enough to correct back to the natural ratio likely due to the lower concentration of Sr in the reference material being corrected with a higher reference material (USGS-MACS3). Therefore, based on the corrected values of $^{87}Sr/^{86}Sr$ and $^{84}Sr/^{86}Sr$, both standard-corrected and instrumental corrected methods can be used for $^{87}Sr/^{86}Sr$ ratios recognizing that low Sr materials should be corrected with a more comparable (in terms of concentration) reference material.

5.1.4. *Summary*

Based on repeat measurements of several reference materials, accuracy with respect to the newly developed LASS-ICP-MS vary based on the concentration of Sr. In general, concentrations of Sr >1000 mg/kg can be considered accurate to 10–100ppm level (e.g., 0.70901–0.709011) whereas lower concentrations of Sr (<500 mg/kg) can lead to accuracy only acceptable to the 100–1000ppm level (e.g., 0.709–0.7091). However, these values are also dependent on spot size which can cause variation in the uncertainty upwards of a magnitude between large and small laser diameters. In general, laser diameters of 15µm on USGS-MACS3 and HSSr were calculated with an analytical uncertainty of >100ppm, while laser diameters of 25µm and 40µm have regular analytical uncertainty on the 10ppm level. Currently, the LASS technique produces accurate results on samples >1000 mg/kg on the 10ppm level for spot sizes >25µm and 100ppm for the 15µm laser diameter, with samples <1000 mg/kg requiring laser diameters >25µm to provide accurate results with analytical uncertainties <1000ppm.

5.2. Reproducibility and Precision of SRMs for trace element analyses

The precision and accuracy of trace elements concentrations in the split-stream configuration were assessed by repeat analyses (n = 174) of the NIST SRM 612. Concentrations of Sr, Ba and Zn are of interest to otolith researchers (refer to Section 1). There are two main limitations to using this reference material to assess precision and accuracy in otolith samples: (1) the NIST SRM 600 series reference materials are synthetic silica glasses, which is not matrix-matched to otolith samples that are carbonate, and (2) concentrations of trace elements NIST SRM 600 series glasses are mostly different from those in otoliths; for example, concentrations of Sr in otoliths are often >500 mg/kg whereas NIST SRM 612 has 78 mg/kg Sr (Jochum et al., 2011). However, there are no known alternative reference materials that are compositionally homogeneous at the micron scale needed for laser ablation analysis. With these limitations in mind, I now discuss the results of repeat analysis of NIST SRM 612 and implications for the accuracy and precision of trace element analyses in otolith samples.

5.2.1. *NIST SRM 612*

Measurements of Sr, Ba and Zn on analyses of NIST SRM 612 via LASS-ICP-MS yielded mean concentrations higher than the preferred value (section 4.2.4). However, all mean concentrations across laser diameters from 8 – 40µm were within analytical uncertainty and <10% variation from the accepted values for Sr, Ba, and Zn is true for over 90% of the analyses other than analyses of Sr at a 20µm laser diameter (Fig. 7). While NIST SRM 612 is not comparable to otoliths in terms of concentration and matrix composition, maintaining accurate data at lower concentrations across multiple laser diameters is indicative of the developed LASS-ICP-MS technique producing long-term reproducible accurate data with respect to Sr, Ba, and Zn. Precision of measurements on Sr, Ba and Zn were assessed across laser diameters from 8 – 40µm with all uncertainties being < 12% (2SE) on all analyses (Fig. 7). Measurements of Sr yield significantly lower standard error values due to the increased elemental concentration of Sr compared to Zn and Ba (80 mg/kg to 40mg/kg) (Fig. 7). The lack of a matrix-matched reference material for otolith analyses with homogeneous trace element concentrations, NIST SRM 612 suffices as an appropriate indicator of accuracy and precision for the purposes of otolith research.

5.2.2. *LOD and LOQ*

A significant advantage of the technique is the low background counts on trace elements due to the use of a QQQ-ICP-MS (in single quad mode), allowing for lower LOD values. Hegg et al. (2020) developed a split-stream technique for otolith microchemistry which utilized a 50-50 split between instruments measuring both strontium isotopes and trace elements (section 1.2). In this method, trace elements were analyzed but were routinely below detection limits on a ThermoFisher Element2 sector field ICP-MS for TE's. Trace element concentrations should be routinely above LOD and ideally above LOQ when reporting values. Table 5 shows the LOD values associated with Sr, Zn, and Ba concentrations for various laser spot diameters on NIST SRM 612. these values Sr, Zn, and Ba on all analyses have trace element concentrations above calculated LOD values (Fig. 8).

Recognizing that Sr concentrations are regularly >100mg/kg and Zn concentrations are often ~40mg/kg in otoliths, these results demonstrate the ability for the novel split-stream technique to consistently produce accurate and precise data even with reduced sample material to the TE ICP-MS. Regardless of accuracy and precision, concentrations are routinely above LOD and commonly above LOQ using our analytical instrumentation which is an invaluable quality for research questions focusing on contamination or within freshwater ecosystems.

5.3. Effects of laser diameter on precision and accuracy of $^{87}Sr/^{86}Sr$ and trace element

Accuracy of analyses on trace element and $^{87}Sr/^{86}Sr$ were assessed based on the variation from the accepted values of standard reference materials USGS-MACS3, HSSr, NanoSr, and NIST SRM 612 across laser diameters ranging from 8 – 40μm. Discussed in section 4.3, laser diameter spot size determines the amount of ablated material transported to each ICP-MS connected in split-stream. This directly impacts the counting statistics involved with increasing accuracy and precision on LA-ICP-MS analyses. Illustrated in section 4.3, variation from the preferred values consistently increased with decreasing laser diameters for both trace element and $^{87}Sr/^{86}Sr$ values, however this effect is exacerbated by lower Sr mass fractions (e.g., NanoSr vs. HSSr) (Tables 5 and 6). Due to the non-linear nature of accuracy and precision with respect to signal intensity/laser diameter (e.g., Figs. 9-11), sudden drastic changes in accuracy and precision vary between reference materials. Monitoring these inflection points, a higher level of precision is consistently achieved at laser spot diameters >15μm for both $^{87}Sr/^{86}Sr$ ratios and trace element measurements for all reference materials (Figs 9-11).

Standard reference materials are used as indicators of what laser diameters will yield the highest quality of data with respect to accuracy and precision when applied to otolith research. For strontium isotope ratios, otoliths with a strontium mass fraction <500 mg/kg will correlate best with analyses done on RM NanoSr, while those >1000 mg/kg are comparable more to RM HSSr. An examination of changes in 2SE (%) across laser diameters for analyses on NanoSr, laser diameters of 25μm and 40μm will yield the most accurate and precise results. Laser diameters below 25μm on otoliths ~500 mg/kg could yield inaccurate data or data with an insufficient level of precision. Data collected on HSSr showed that data collected at laser diameters 12, 15 and 20μm were similar in terms of precision while 25μm laser diameter is of a significantly higher precision than the rest. Since the 8μm laser diameter is of a significantly lower level of precision than other laser diameters tested, laser diameters of 12 – 25 μm on otoliths with strontium mass fractions >1000mg/kg are recommended, with the 25μm laser diameter being preferred regarding accuracy and precision. In terms of acceptable accuracy and precision in trace elements across laser diameters, >60% of all analyses were below 10% variation from the accepted values of NIST SRM 612 and were above the LOD for Sr, Ba, and Zn. The trace element data can be considered accurate and because of the consistently low background and small LOD values, all laser diameters used to measure trace element concentrations can be considered acceptable for otolith research.

In summary the effective and applicable laser diameters used when collecting otolith transect data vary with respect to strontium mass fraction. For mass fractions <500 mg/kg laser diameters of 25 and 40μm are suggested to provide the necessary levels of accuracy and precision while otoliths >1000 mg/kg can utilize a range of laser diameters > 12μm.

5.4. Analysis of Otoliths

During refinement of the methods discussed in this thesis, multiple otoliths with different research questions were analyzed in conjunction with Dr. Heidi Swanson and associated graduate students. Below, I interpret the results of split-stream analysis of two otolith samples from these studies (results presented in section 3.3) and discuss the utility and limitations of the methods applied to different aspects of fish growth and migration. Additional figures can be found in Appendix C and trace element data in Appendix D.

5.4.1. *Diadromous Lake Trout (LAU3-5 40µm)*

Long-lived diadromous fish can undertake complex migratory patterns for ~10–12yrs with growth zones <10µm appearing in otoliths, which require a high spatial resolution to confidently determine the number of Zn oscillations (e.g., years) in the pre-migratory and post-migratory phases of the fish's life. Elucidating migration timing is crucial in the management of fish populations and otoliths from long-lived diadromous fishes can record migrations for >10 years. Timing and patterns in migration can be associated with local environmental change or larger global phenomena, such as climate change (Galappaththi et al., 2019). One otolith of a lake trout (*Salvelinus namaycush*) from Nunavut, Canada was analyzed using a 40µm split-stream setup. As defined in section 3.3, three zones were identified using the Sr concentration transect (Fig. 14b).

The first zone extended from the nucleus of the otolith until ~0.2mm, which is where the first growth ring occurs. The mean $^{87}Sr/^{86}Sr$ isotope ratio of zone 1 is ~0.7240 $\pm$ 0.0067 (2SE) and is indicative of an area of early freshwater growth likely formed during the natal phase (~0.5yr) of the fish's life based on fluctuations in Zn concentrations (seasonal activity influencing metabolic processes due to food availability) and the centricity of the growth ring shown in reflected light images (Campana, 1999) (Fig. 14b). Sr concentrations in this zone increase slightly (50 → 65 mg/kg) while Zn has a single oscillation (~40–85 mg/kg). This period of growth is indicative of a natal phase of a fish's lifetime and is similar to fish spawned in freshwater environments (Section 1; Campbell et al. 2002).

The second zone began at 0.2mm and extended until the end of the second Zn oscillation around 1.6mm (Fig. 14b). The mean $^{87}Sr/^{86}Sr$ isotope ratio of zone 2 was ~0.7204 $\pm$ 0.0015 (2SE) which indicates a change in habitat growth which extends for ~18.5 yrs signaled by the number of oscillations in Zn concentration (Campana, 1999). Concentrations of Sr have very minor fluctuations across this zone (~50–75 mg/kg) while Zn progresses through oscillations (~18.5years) with decreasing maxima (85 → 15 mg/kg) and minima (40 → 10 mg/kg). These minor fluctuations in Sr can indicate minor changes in freshwater habitats but observing the minimal change in $^{87}Sr/^{86}Sr$ signatures between the natal and rearing phases, these regions are likely very close to one another or may vary in the same body of water year-to-year.

The third zone begins after 19 growth rings (e.g., 19 years into the fish's lifetime: >1.6mm). At the beginning of zone 3, the Sr concentrations increased from ~65mg/kg to 300 mg/kg (Fig. 14b). This is indicative of a migration event to oceanic waters confirmed by the strontium isotope signature of ~0.7134 $\pm$ 0.0014 (2SE) in zone 3 which is similar to that of ocean water(0.7092; Kuznetsov et al. 2012; Mokadem et al., 2015) but just outside analytical uncertainty. This is attributed to the averaging effect of the maxima and minima attributed to migrations between freshwater and saltwater. Throughout this zone, oscillations of Sr continue corresponding to that of Zn's oscillations indicating seasonal growth periods and migrations back to freshwater. Zone 3 lasts for eight Zn oscillations correlating to a time of ~8 years (Campana, 1999).

In summary, observing the transect and relevant data we can see that the fish spent approximately a 18.5 years rearing in freshwater. After a period of 19 years, the fish migrated to the ocean for a length of 8 years while periodically migrating between seasons to an area with a higher isotopic ratio.

Split-stream analysis of long-lived freshwater diadromous fish is important for research purposes because the low Sr mass fraction of freshwater fish makes it difficult to retrieve accurate and precise isotopic data at almost all available spot-sizes. With the novel uneven distribution of sample material developed in this thesis, we can utilize smaller laser spot diameters and preserve the otolith for other techniques. This is especially crucial for northern freshwater fish populations which are difficult and expensive to track in the remote areas of northern Canada where indigenous populations depend on these fish (Bennet et al., 2018).

5.4.2. *Diadromous Fish Migration of Arctic Char (40µm & 25µm)*

One otolith of an Arctic char (*Salvelinus alpinus*) from Nunavut was analyzed twice, once with a 25 µm laser diameter (KUG1-1a) and once with a 40 µm laser diameter (KUG1-1b). Three growth zones were identified in the otolith based on a combination of trace element and $^{87}Sr/^{86}Sr$ ratios (section 3.3). Strontium isotope ratios are used to indicate three different areas of habitation during the lifetime of the fish (e.g. Campbell et al., 2002; Fig 15,16).

The first zone extended from the nucleus of the otolith until ~0.2mm, which is where the first growth ring occurs. The mean $^{87}Sr/^{86}Sr$ isotope ratios of zone 1 were ~0.7330 ± 0.0005 (2SE) (40µm) and ~0.743 ± 0.001 (2SE) (25µm) and are indicative of an area of early freshwater growth likely formed during the natal phase (~0.5yr) of the fish's life based on fluctuations in Zn concentrations and the centricity of the growth ring shown in transmitted light images (Fig. 15,16). Sr concentrations in this zone (~400 mg/kg) remain stable for both spot diameters in this zone while Zn has a single oscillation (~60–120 mg/kg) indicating a non-migratory phase across seasons.

The second zone began at 0.2mm and extended until the end of the second Zn oscillation around 0.85mm (Fig. 15b,16b). The mean $^{87}Sr/^{86}Sr$ isotope ratios of zone 1 were ~0.7495 ± 0.0003 (2SE) (40µm) and ~0.7475 ± 0.0007 (2SE) (25µm), which extends for ~1.5yrs signaled by the number of oscillations in Zn concentration (Campana 1999). Concentrations of Sr have very minor fluctuations across this zone (~200–500 mg/kg: Sr) while Zn progresses through 1.5 oscillations (~1.5years) with decreasing maxima (120 → 100 mg/kg) and minima (20 → 15 mg/kg). These minor fluctuations in Sr can indicate changes in freshwater habitats and decreasing Zn concentrations can be attributed to ageing and slower otolith growth (Campbell et al., 2002).

The third zone begins after 2 growth rings (e.g., 2 years into the fish's lifetime). At the beginning of zone 3, the Sr concentrations increased from ~300 mg/kg to 2500 mg/kg (Figs 15b, 16b). This is indicative of a migration event to oceanic waters supported by the strontium isotope signature of ~0.7108 ± 0.0001 (2SE) (25µm) and ~0.7110 ± 0.0001 (2SE) (40µm) in zone 3 resembling that of ocean water (0.7092; Kuznetsov et al., 2012; Mokadem et al., 2015) but just outside analytical uncertainty. Throughout this zone, oscillations of Sr continued corresponding to that of Zn's oscillations, indicating seasonal growth periods and migrations back to freshwater. Zone 3 lasts for 7 Zn oscillations correlating to a time of ~7 years (Campana, 1999).

In summary, observing the transect and relevant data we can see that the fish spent reflects the maternal signal for half a year which before rearing for 1.5years. After a period of 2 years, the fish migrated annually to the ocean for 7 years and returned to an area with a higher isotopic ratio each winter. Such information is important for studies of fish migration because diadromous fish like the one investigated above appear to be dependent upon freshwater ecosystems for the first 2 years of their life. These subtle variations in the timing of the first migration can be a crucial component of evidence required to sustain these populations.

In northern areas where fishing is a dominant career and families are dependent upon these fish, this information is invaluable (Fisheries and Oceans Canada 2012). The combination of both trace element and isotopic data increases the amount of information obtained from each individual otolith, allowing the indication of unsustainable fish populations, and pin-pointing the spawning and rearing areas that are possibly in risk (Pracheil et al., 2014; Carlson et al., 2016).

5.5. Limitations of technique

There are two main factors that dictate the resolution of the isotope and trace element data using split-stream LA-ICP-MS on otolith samples. The first factor is the mass fraction of elements of interest in the otoliths. The second is the spatial resolution of analyses needed on an otolith and, hence, the laser beam diameter. This depends on the research question and the size and spacing of growth zones in otoliths; this varies with the species of fish, the growth environment, and the age of the fish. I explore these limitations using the examples discussed in section 4.3.

LAU3-5 and KUG1-1 are otoliths with a strontium mass fractions of 30-300mg/kg and 250-3000 mg/kg with three distinct zones of strontium concentration and isotopic signatures associated with both. LAU3-5 and KUG1-1b were both analyzed at a laser spot diameter of 40µm but vary in terms of strontium mass fractions, whereas KUG1-1a and KUG1-1b involve analyses on the same otolith at 2 spot sizes (25µm and 40µm).

Although analyzed with the same laser spot size (40µm), otolith sample LAU3-5 (Fig. 14c) has an $^{87}Sr/^{86}Sr$ value that is significantly noisier (i.e., less precise) than that of KUG1-1b (Fig. 16c). This is due to the significantly smaller growth zones and low Sr mass fraction in otolith LAU3-5 compared to KUG1-1a. Comparing LAU3-5 to KUG1-1a, KUG1-1a has significantly more well-defined zones and a more stable signal in both the trace element (Sr) and isotopic ($^{87}Sr/^{86}Sr$) transects (Figs. 14,16). This greatly influences the information that we can infer from isotopic ratios retrieved from the analyses. Important details such as determining natal and rearing $^{87}Sr/^{86}Sr$ signatures depend on high analytical precision which is a function of signal stability and intensity. For otoliths with a high Sr mass fraction in natal and rearing areas, the discrimination between natal and rearing areas is possible due to a higher analytical precision on individual analyses whereas low Sr mass fraction otoliths will not be able to accommodate early growth research. Although an analyst has no control on otoliths with low strontium mass fractions, laser spot diameter can be increased to improve the amount of material processed thus improving the end results. However, with samples such as LAU3-5, increasing laser spot diameter may disguise more information by laterally mixing isotopic (and trace element) signatures by encroaching into neighbouring growth zones. Therefore, there will be a trade-off between laser diameter and the resolution of the Sr isotope ratios.

By comparing two analyses of the same otolith at two laser diameters, we can observe the changes in spatial resolution, precision, and stability directly to one another without considering variations in growth zone width and differences in strontium mass fraction. However, the caveat of this approach is that the two lines are sampling the same growth zones and there is no micro-scale variation from the adjacent positions of the laser line scans; this is considered a necessary but reasonable assumption given the general homogeneity of growth zones in otoliths (Di Franco et al., 2014).

$^{87}Sr/^{86}Sr$ ratios along the KUG1-1a line (25μm laser diameter) do not show a well-defined natal phase with a pronounced lower isotopic ratio whereas this is present in the KUG1-1b scan (40μm laser diameter). Reduced signal intensity would yield a higher and incorrect $^{87}Sr/^{86}Sr$ isotope ratio, resulting in improper characterization of the isotope value of the natal spawning area. The Sr concentration can also be used to distinguish the natal and rearing phases of this otolith (Fig. 15), but on its own provides no estimate of the $^{87}Sr/^{86}Sr$ of the natal environment. This can impact our ability to appropriately characterize the length of transect that needs to be assessed and influence the reduction of that data. Due to the increased spot size, maxima and minima values appear to be stunted compared to a lower spot size. The migratory maxima and minima of KUG1-1a have more square peaks and troughs than KUG1-1b indicating that the period of growth was a significant event but was hidden by a larger spot size due to lateral encroachment of the laser on other growth zones. The reduction of this lateral encroachment is required for a more precise integration of $^{87}Sr/^{86}Sr$ ratios, and by extension a more detailed history of the fish.

In summary, although there are significant benefits to analyzing otolith samples with high strontium mass fractions, and larger laser diameters, the research question dictates the appropriate method. If isotopic signatures of migratory peaks and troughs are the primary focus, then a transect with a smaller laser spot diameter may be necessary to properly resolve those areas and avoid mixing of adjacent domains. This may sacrifice precision on $^{87}Sr/^{86}Sr$ ratios, but otherwise would result in mixed $^{87}Sr/^{86}Sr$ ratios that could be meaningless. If natal sources and rearing phases with large growth zones are the primary focus—and these usually have low mass fractions of Sr—then larger laser diameters can be chosen to characterize those zones and sacrifice spatial resolution for more precise estimates of the $^{87}Sr/^{86}Sr$ value. Therefore, split-stream LA-ICP-MS of otolith samples have the potential to provide new insights into fish growth and migration, but only after the balance between spatial resolution and isotopic precision is addressed for a specific research question.

5.6. Suggested Future Work

Continued long-term analyses of reference materials is recommended to track changes in signal sensitivity and precision to ensure that the technique remains accurate and precise. To ensure that long-term analyses can be constantly updated and assessed, data from split-stream should be uploaded to a University of Waterloo MIG lab database regularly.

Modification of the LASS-ICP-MS to change the distribution of material from 2:1 to 3:1 and even 1:1 (50-50 split) would improve the signal intensity to the MC-ICP-MS which one would anticipate to achieve better accuracy and precision on $^{87}Sr/^{86}Sr$ ratios. These modifications to the split-stream technique should be evaluated long-term using a similar approach to that of this thesis focusing on comparisons with current laboratories (e.g., Hegg et al., 2020). With the high sensitivity of the Agilent 8800, material can still be increased to the NuPlasma II increasing the accuracy and precision of $^{87}Sr/^{86}Sr$ isotope ratios on reference materials and otolith samples. For low concentrations of Sr in particular, the precision of isotope values would benefit from increased sensitivity of the Nu Plasma II. Upgrades are available from the manufacturer that would enable increased sensitivity that may be necessary for reducing spot sizes even further while maintaining usable data. Although originally designed for trace element and Sr isotope ratios on otoliths, the design has applications to various strontium isotope research on other materials. Various applications include U-Pb Geochronology and Hf isotopes on zircons in the field of geochemistry, $^{87}Sr/^{86}Sr$ ratios and trace element concentrations on hydroxyapatite (teeth) for archaeology and calcites for geological applications where precise isotopic data is favourable over precise elemental data.

6. CONCLUSIONS

This thesis presents a new aerosol plumbing design optimized for LASS-ICP-MS analysis of Sr isotopes and trace element concentrations of otoliths. The novel introduction of the ‘loop junction’ used to unevenly distribute the sample material was crucial for determining precise Sr isotope ratios of otoliths. Long-term reproducibility of $^{87}Sr/^{86}Sr$ ratios and trace element concentrations of reference materials demonstrate that this technique is fit for the purpose of most otolith microchemistry studies, although quantifying Sr isotope ratios in small winter growth bands may require single stream analysis. Precision and accuracy improve with increasing laser diameter for isotope and trace element analyses. The application of the LASS-ICP-MS method to two different species of fish demonstrated the expected precision on fish with mass fractions of ~500 mg/kg and >1000 mg/kg. These otolith analyses successfully demonstrated the utility of the LASS-ICP-MS technique for documenting different phases of fish life (i.e., natal, rearing, and migratory) as well as provide linked $^{87}Sr/^{86}Sr$ ratios. Moving forward, optimizing the LASS-ICP-MS technique to resolve Sr isotope variations at laser diameters <20 μm should be a priority that will make this analytical approach useful for a wider variety of fish species.

References

Arai, T., Kotake, A., and Morita, K. 2004. Evidence of downstream migration of Sakhalin taimen, Hucho perryi, as revealed by Sr:Ca ratios of otolith. Ichthyological Research, **51**: 377–380. doi:10.1007/s10228-004-0230-x.

Armbruster, D.A., and Pry, T. 2008. Limit of blank, limit of detection and limit of quantitation. The Clinical biochemist. Reviews, **29**: 49-52. Available from http://www.ncbi.nlm.nih.gov/pubmed/18852857%0Ahttp://www.pubmedcentral.nih.gov/Arcticlerender.fcgi?artid=PMC2556583.

Arslan, Z., and Secor, D.H. 2005. Analysis of trace transition elements and heavy metals in fish otoliths as tracers of habitat use by American eels in the Hudson River estuary. Estuaries, **28**: 382–393. doi:10.1007/BF02693921.

Avigliano, E., Pouilly, M., Bouchez, J., Domanico, A., Sánchez, S., Llamazares, S., Cirsthian, V., Scarabotti, P., Facetti, J.F., Caffetti, J.D., and Volpedo, A. V. 2020. Strontium isotopes ($^{87}Sr/^{86}Sr$) reveal the life history of freshwater migratory fishes in the La Plata Basin. : 1985–2000. doi:10.1002/rra.3727.

Babaluk, J.A., Halden, N.M., Reist, J.D., Kristofferson, A.H., Campbell, J.L., and Teesdale, W.J. 1997. Evidence for non-anadromous behaviour of Arctic charr (*Salvelinus alpinus*) from Lake Hazen, Ellesmere Island, Northwest Territories, Canada, based on scanning proton microprobe analysis of otolith strontium distribution. Arctic, **50**: 224–233. doi:10.14430/arctic1104.

Barnett-Johnson, R., Ramos, F.C., Grimes, C.B., and MacFarlane, R.B. 2005. Validation of Sr isotopes in otoliths by laser ablation multicollector inductively coupled plasma mass spectrometry (LA-MC-ICPMS): Opening avenues in fisheries science applications. Canadian Journal of Fisheries and Aquatic Sciences, **62**: 2425–2430. doi:10.1139/f05-194.

Barnett-Johnson, R., Teel, D.J., and Casillas, E. 2010. Genetic and otolith isotopic markers identify salmon populations in the Columbia River at broad and fine geographic scales. Environmental Biology of Fishes, **89**: 533–546. doi:10.1007/s10641-010-9662-5.

Brennan, S.R., Fernandez, D.P., Zimmerman, C.E., Cerling, T.E., Brown, R.J., and Wooller, M.J. 2015. Strontium isotopes in otoliths of a non-migratory fish (slimy sculpin): Implications for provenance studies. Geochimica et Cosmochimica Acta, **149**: 32–45. Elsevier Ltd. doi:10.1016/j.gca.2014.10.032.

Campana, S.E. 1999. Chemistry and composition of fish otoliths: Pathways, mechanisms and applications. Marine Ecology Progress Series, **188**: 263–297. doi:10.3354/meps188263.

Campana, S.E., Fowler, A.J., and Jones, C.M. 1994. Otolith elemental fingerprinting for stock identification of Atlantic cod (Gadus morhua) using laser ablation ICPMS. Canadian Journal of Fisheries and Aquatic Sciences, **51**: 1942–1950. doi:10.1139/f94-196.

Campana, S.E., Thorrold, S.R., Jones, C.M., Günther, D., Tubrett, M., Longerich, H., Jackson, S., Halden, N.M., Kalish, J.M., Piccoli, P., De Pontual, H., Troadec, H., Panfili, J., Secor, D.H., Severin, K.P., Sie, S.H., Thresher, R., Teesdale, W.J., and Campbell, J.L. 1997. Comparison of accuracy, precision, and sensitivity in elemental assays of fish otoliths using the electron microprobe, proton-induced X-ray emission, and laser ablation inductively coupled plasma mass spectrometry. Canadian Journal of Fisheries and Aquatic Sciences, **54**: 2068–2079.

doi:10.1139/f97-117.

Carlson, R.W. 2013. Thermal Ionization Mass Spectrometry. *In* Treatise on Geochemistry: Second Edition, 2nd edition. Elsevier Ltd. doi:10.1016/B978-0-08-095975-7.01427-3.

Chen, H.L., Shen, K.N., Chang, C.W., Iizuka, Y., and Tzeng, W.N. 2008. Effects of water temperature, salinity and feeding regimes on metamorphosis, growth and otolith Sr:Ca ratios of *Megalops cyprinoides leptocephali*. Aquatic Biology, **3**: 41–50. doi:10.3354/ab00062.

Coote, G.E., and Vickridge, I.C. 1988. Application of a nuclear microprobe to the study of calcified tissues. Nuclear Inst. and Methods in Physics Research, B, **30**: 393–397. doi:10.1016/0168-583X(88)90031-6.

Crook, D.A., Lacksen, K., King, A.J., Buckle, D.J., Tickell, S.J., Woodhead, J.D., Maas, R., Townsend, S.A., and Douglas, M.M. 2017. Temporal and spatial variation in strontium in a tropical river: Implications for otolith chemistry analyses of fish migration. Canadian Journal of Fisheries and Aquatic Sciences, **74**: 533–545. doi:10.1139/cjfas-2016-0153.

Crook, D.A., Wedd, D., and Berra, T.M. 2015. Analysis of otolith $^{87}Sr/^{86}Sr$ to elucidate salinity histories of Nurseryfish Kurtus gulliveri (Perciformes:Kurtidae) in a tropical lowland river in northern Australia. Freshwater Science, **34**: 609–619. doi:10.1086/681022.

D'Avignon, G., and Rose, G.A. 2013. Otolith elemental fingerprints distinguish Atlantic cod spawning areas in Newfoundland and Labrador. Fisheries Research, **147**: 1–9. doi:10.1016/j.fishres.2013.04.006.

DiMaria, R.A., Miller, J.A., and Hurst, T.P. 2010. Temperature and growth effects on otolith elemental chemistry of larval Pacific cod, Gadus macrocephalus. Environmental Biology of Fishes, **89**: 453–462. doi:10.1007/s10641-010-9665-2.

Eggins, S.M., Grün, R., McCulloch, M.T., Pike, A.W.G., Chappell, J., Kinsley, L., Mortimer, G., Shelley, M., Murray-Wallace, C. V., Spötl, C., and Taylor, L. 2005. In situ U-series dating by laser-ablation multi-collector ICPMS: New prospects for Quaternary geochronology. Quaternary Science Reviews, **24**: 2523–2538. doi:10.1016/j.quascirev.2005.07.006.

Elsdon, T.S., and Gillanders, B.M. 2004. Fish otolith chemistry influenced by exposure to multiple environmental variables. Journal of Experimental Marine Biology and Ecology, **313**: 269–284. doi:10.1016/j.jembe.2004.08.010.

Farrell, J., and Campana, S.E. 1996. Regulation of calcium and strontium deposition on the otoliths of juvenile tilapia, Oreochromis niloticus. Comparative Biochemistry and Physiology - A Physiology, **115**: 103–109. doi:10.1016/0300-9629(96)00015-1.

Fey, D.P., and Greszkiewicz, M. 2021. Effects of temperature on somatic growth, otolith growth, and uncoupling in the otolith to fish size relationship of larval northern pike, Esox lucius L. Fisheries Research, **236**: 105843. Elsevier B.V. doi:10.1016/j.fishres.2020.105843.

Fisheries and Oceans Canada. 2012. Aboriginal Fisheries Strategy. *In* Government of Canada. Available from https://www.dfo-mpo.gc.ca/fisheries-peches/aboriginal-autochtones/afs-srapa-eng.html.

Fowler, A.J., Campana, S.E., Thorrold, S.R., and Jones, C.M. 1995. Experimental assessment of the effect of temperature and salinity on elemental composition of otoliths using laser ablation ICPMS. Canadian Journal of Fisheries and Aquatic Sciences, **52**: 1431–1441. doi:10.1139/f95-138.

Friedrich, L.A., and Halden, N.M. 2008. Alkali element uptake in otoliths: A link between the environment and otolith microchemistry. Environmental Science and Technology, **42**: 3514–3518. doi:10.1021/es072093r.

Füger, A., Méheut, M., Mavromatis, V., Leis, A., and Dietzel, M. 2018. Oxygen isotope fractionation during smithsonite formation from aqueous solutions. Chemical Geology, **495**: 76–89. Elsevier. doi:10.1016/j.chemgeo.2018.08.005.

Fukuda, N., Kuroki, M., Shinoda, A., Yamada, Y., Okamura, A., Aoyama, J., and Tsukamoto, K. 2009. Influence of water temperature and feeding regime on otolith growth in Anguilla japonica glass eels and elvers: Does otolith growth cease at low temperatures? Journal of Fish Biology, **74**: 1915–1933. doi:10.1111/j.1095-8649.2009.02287.x.

Galappaththi, EK, Ford, JD and Bennett, EM. 2019. A framework for assessing community adaptation to climate change in a fisheries context. Environmental Science and Policy, **92**. pp. 17-26. ISSN 1462-9011

Gao, Y., and Bean, D. 2008. Stable isotope analyses of otoliths in identification of hatchery origin of Atlantic salmon (*Salmo salar*) in Maine. Environmental Biology of Fishes, **83**: 429–437. doi:10.1007/s10641-008-9365-3.

Gauldie, R.W. 1986. Vaterite otoliths from chinook salmon (*Oncorhynchus tshawytscha*). New Zealand Journal of Marine and Freshwater Research, **20**: 209–217. doi:10.1080/00288330.1986.9516145.

Gauldie, R.W., and Nelson, D.G.A. 1990. Otolith growth in fishes. Comparative Biochemistry and Physiology -- Part A: Physiology, **97**: 119–135. doi:10.1016/0300-9629(90)90159-P.

Hacker, B.R., Kylander-Clark, A.R.C., Holder, R., Andersen, T.B., Peterman, E.M., Walsh, E.O., and Munnikhuis, J.K. 2015. Monazite response to ultrahigh-pressure subduction from U-Pb dating by laser ablation split stream. Chemical Geology, **409**: 28–41. doi:10.1016/j.chemgeo.2015.05.008.

Halden, N.M., Babaluk, J.A., Campbell, J.L., and Teesdale, W.J. 1995a. Scanning proton microprobe analysis of strontium in an arctic charr, *Salvelinus alpinus*, otolith: implications for the interpretation of anadromy. Environmental Biology of Fishes, **43**: 333–339. doi:10.1007/BF00001166.

Halden, N.M., Campbell, J.L., and Teesdale, W.J. 1995b. PIXE analysis in mineralogy and geochemistry. Canadian Mineralogist, **33**: 293–302.

Halden, N.M., Campbell, J.L., and Teesdale, W.J. 1996. Behaviour and Stock Discrimination. **110**: 592–597.

Halden, N.M., and Friedrich, L.A. 2008. Trace-element distributions in fish otoliths: natural markers of life histories, environmental conditions and exposure to tailings effluence. Mineralogical Magazine, **72**: 593–605. doi:10.1180/minmag.2008.072.2.593.

Halden, N.M., Mejia, S.R., Babaluk, J.A., Reist, J.D., Kristofferson, A.H., Campbell, J.L., and Teesdale, W.J. 2000. Oscillatory zinc distribution in Arctic char (*Salvelinus alpinus*) otoliths: The result of biology or environment? Fisheries Research, **46**: 289–298. doi:10.1016/S0165-7836(00)00154-5.

Hanson, C.E., Hyndes, G.A., and Wang, S.F. 2010. Differentiation of benthic marine primary producers using stable isotopes and fatty acids: Implications to food web studies. Aquatic Botany, **93**: 114–122. Elsevier B.V. doi:10.1016/j.aquabot.2010.04.004.

Harris, L.N., Swanson, H.K., Gilbert, M.J.H., Malley, B.K., Fisk, A.T., and Moore, J.S. 2020. Anadromy and marine habitat use of Lake trout (*Salvelinus namaycush*) from the central Canadian Arctic. Journal of Fish Biology, **96**: 1489–1494. doi:10.1111/jfb.14305.

Hegg, J.C., Fisher, C.M., and Vervoort, J. 2020. Simultaneous determination of $^{87}Sr/^{86}Sr$ and trace-element data in otoliths and other sclerochronological hard structures. bioRxiv,. doi:10.1101/2020.04.24.060640.

Helser, T.E., Kastelle, C.R., McKay, J.L., Orland, I.J., Kozdon, R., and Valley, J.W. 2018. Evaluation of micromilling/conventional isotope ratio mass spectrometry and secondary ion mass spectrometry of $\delta^{18}O$ values in fish otoliths for sclerochronology. Rapid Communications in Mass Spectrometry, **32**: 1781–1790. doi:10.1002/rcm.8231.

Horstwood, M.S.A., Evans, J.A., and Montgomery, J. 2008. Determination of Sr isotopes in calcium phosphates using laser ablation inductively coupled plasma mass spectrometry and their application to archaeological tooth enamel. Geochimica et Cosmochimica Acta, **72**: 5659–5674. Elsevier Ltd. doi:10.1016/j.gca.2008.08.016.

Howland, K.L., Babaluk, J.A., Chiperzak, D., Tallman, R.F., and Low, G. 2009. Variability in diadromous behavior of a northern coregonid based on scanning proton microprobe analysis of otolith strontium. Challenges for diadromous fishes in a dynamic global environment. American Fisheries Society, Symposium, **69**: 121–134.

Ibanez-Mejia, M., Pullen, A., Arenstein, J., Gehrels, G.E., Valley, J., Ducea, M.N., Mora, A.R., Pecha, M., and Ruiz, J. 2015. Unraveling crustal growth and reworking processes in complex zircons from orogenic lower-crust: The Proterozoic Putumayo Orogen of Amazonia. Precambrian Research, **267**: 285–310. Elsevier B.V. doi:10.1016/j.precamres.2015.06.014.

Jackson, S.E., and Günther, D. 2003. The nature and sources of laser induced isotopic fractionation in laser ablation-multicollector-inductively coupled plasma-mass spectrometry. Journal of Analytical Atomic Spectrometry, **18**: 205–212. doi:10.1039/b209620j.

Jochum, K.P., Garbe-Schönberg, D., Veter, M., Stoll, B., Weis, U., Weber, M., Lugli, F., Jentzen, A., Schiebel, R., Wassenburg, J.A., Jacob, D.E., and Haug, G.H. 2019. Nano-Powdered Calcium Carbonate Reference Materials: Significant Progress for Microanalysis? Geostandards and Geoanalytical Research, **43**: 595–609. doi:10.1111/ggr.12292.

Jochum, K.P., Weis, U., Stoll, B., Kuzmin, D., Yang, Q., Raczek, I., Jacob, D.E., Stracke, A., Birbaum, K., Frick, D.A., Günther, D., and Enzweiler, J. 2011. Determination of reference values for NIST SRM 610-617 glasses following ISO guidelines. Geostandards and Geoanalytical Research, **35**: 397–429. doi:10.1111/j.1751-908X.2011.00120.x.

Kalish, J.M. 1989. Otolith microchemistry: validation of the effects of physiology, age and environment on otolith composition. Journal of Experimental Marine Biology and Ecology, **132**: 151–178. doi:10.1016/0022-0981(89)90126-3.

Kennedy, B.P., Blum, J.D., Folt, C.L., and Nislow, K.H. 2000. Using natural strontium isotopic signatures as fish markers: Methodology and application. Canadian Journal of Fisheries and Aquatic Sciences, **57**: 2280–2292. doi:10.1139/f00-206.

Kennedy, B.P., and Folt, C.L. 1997. scientific correspondence Natural isotope markers in salmon DNA fingerprints from fingerprints How many replicons make a nodule ? Unique morphology of the human eye. Nature, **387**: 766–767.

Kennedy, B.P., Klaue, A., Blum, J.D., Folt, C.L., and Nislow, K.H. 2002. Reconstructing the lives of fish using Sr isotopes in otoliths. Canadian Journal of Fisheries and Aquatic Sciences, **59**: 925–929. doi:10.1139/f02-070.

Kuhn, B.K., Birbaum, K., Luo, Y., and Günther, D. 2010. Fundamental studies on the ablation behaviour of Pb/U in NIST 610 and zircon 91500 using laser ablation inductively coupled plasma mass spectrometry with respect to geochronology. Journal of Analytical Atomic Spectrometry, **25**: 21–27. doi:10.1039/b917261k.

Kuznetsov, A.B., Semikhatov, M.A., and Gorokhov, I.M. 2012. The Sr isotope composition of the world ocean, marginal and inland seas: Implications for the Sr isotope stratigraphy. Stratigraphy and Geological Correlation, **20**: 501–515. doi:10.1134/S0869593812060044.

Kylander-Clark, A.R.C., Hacker, B.R., and Cottle, J.M. 2013. Laser-ablation split-stream ICP petrochronology. Chemical Geology, **345**: 99–112. Elsevier B.V. doi:10.1016/j.chemgeo.2013.02.019.

Landaeta, M.F., Castillo-Hidalgo, G., and Bustos, C.A. 2018. Effects of salinity gradients on larval growth and otolith asymmetry of austral hake Merluccius australis. Latin American Journal of Aquatic Research, **46**: 212–218. doi:10.3856/vol46-issue1-fulltext-20.

Loewen, T.N., Reist, J.D., Yang, P., Koleszar, A., Babaluk, J.A., Mochnacz, N., and Halden, N.M. 2015. Discrimination of northern form Dolly Varden Char (*Salvelinus malma malma*) stocks of the North Slope, Yukon and Northwest Territories, Canada via otolith trace elements and $^{87}Sr/^{86}Sr$ isotopes. Fisheries Research, **170**: 116–124. doi:10.1016/j.fishres.2015.05.025.

Longerich, H.P. 2008. Laser ablation-inductively coupled plasma-mass spectrometry (LA-ICP-MS); an introduction. *In* Laser Ablation ICP-MS in the Earth Sciences: Current Practices and Outstanding Issues. *Edited by* Robert Raeside. Mineralogical Association of Canada, Vancouver, BC. pp. 1–16.

Longerich, H.P., Jackson, S.E., and Günther, D. 1996. Laser ablation inductively coupled plasma mass spectrometric transient signal data acquisition and analyte concentration calculation. Journal of Analytical Atomic Spectrometry, **11**: 899–904. doi:10.1039/JA9961100899.

Matta, M.E., Orland, I.J., Ushikubo, T., Helser, T.E., Black, B.A., and Valley, J.W. 2013. Otolith oxygen isotopes measured by high-precision secondary ion mass spectrometry reflect life history of a yellowfin sole (*Limanda aspera*). Rapid Communications in Mass Spectrometry, **27**:

691–699. doi:10.1002/rcm.6502.

McFadden, A., Wade, B., Izzo, C., Gillanders, B.M., Lenehan, C.E., and Pring, A. 2016. Quantitative electron microprobe mapping of otoliths suggests elemental incorporation is affected by organic matrices: Implications for the interpretation of otolith chemistry. Marine and Freshwater Research, **67**: 889–898. doi:10.1071/MF15074.

Miller, J.A., and Kent, A.J.R. 2009. The determination of maternal run time in juvenile Chinook salmon (*Oncorhynchus tshawytscha*) based on Sr/Ca and $^{87}Sr/^{86}Sr$ within otolith cores. Fisheries Research, **95**: 373–378. doi:10.1016/j.fishres.2008.09.030.

Mokadem, F., Parkinson, I.J., Hathorne, E.C., Anand, P., Allen, J.T., and Burton, K.W. 2015. High-precision radiogenic strontium isotope measurements of the modern and glacial ocean: Limits on glacial-interglacial variations in continental weathering. Earth and Planetary Science Letters, **415**: 111–120. Elsevier B.V. doi:10.1016/j.epsl.2015.01.036.

Morrison, C.M., Kunegel-Lion, M., Gallagher, C.P., Wastle, R.J., Lea, E. V., Loewen, T.N., Reist, J.D., Howland, K.L., and Tierney, K.B. 2019. Decoupling of otolith and somatic growth during anadromous migration in a northern salmonid. Canadian Journal of Fisheries and Aquatic Sciences, **76**: 1940–1953. doi:10.1139/cjfas-2018-0306.

Outridge, P.M., Chenery, S.R., Babaluk, J.A., and Reist, J.D. 2002. Analysis of geological Sr isotope markers in fish otoliths with subannual resolution using laser ablation-multicollector-ICP-mass spectrometry. Environmental Geology, **42**: 891–899. doi:10.1007/s00254-002-0596-x.

Palace, V.P., Halden, N.M., Yang, P., Evans, R.E., and Sterling, G. 2007. Determining residence patterns of rainbow trout using laser ablation inductively coupled plasma mass spectrometry (LA-ICP-MS) analysis of selenium in otoliths. Environmental Science and Technology, **41**: 3679–3683. doi:10.1021/es0628093.

Panfili, J., Pontual, H., Troadec, H., and Wright, P.J. 2002. Manual of fish sclerochronology. Ifremer-IRD coedition, Brest, France.

Paton, C., Hellstrom, J., Paul, B., Woodhead, J., and Hergt, J. 2011. Iolite: Freeware for the visualisation and processing of mass spectrometric data. Journal of Analytical Atomic Spectrometry, **26**: 2508–2518. doi:10.1039/c1ja10172b.

Pettke, T., Oberli, F., Audétat, A., Guillong, M., Simon, A.C., Hanley, J.J., and Klemm, L.M. 2012. Recent developments in element concentration and isotope ratio analysis of individual fluid inclusions by laser ablation single and multiple collector ICP-MS. Ore Geology Reviews, **44**: 10–38. Elsevier B.V. doi:10.1016/j.oregeorev.2011.11.001.

Prohaska, T., Irrgeher, J., and Zitek, A. 2016. Simultaneous multi-element and isotope ratio imaging of fish otoliths by laser ablation split stream ICP-MS/MC ICP-MS. Journal of Analytical Atomic Spectrometry, **31**: 1612–1621. Royal Society of Chemistry. doi:10.1039/c6ja00087h.

Radtke, R.L., Dempson, J.B., and Ruzicka, J. 1997. Microprobe analyses of anadromous Arctic charr, *Salvelinus alpinus*, otoliths to infer life history migration events. Polar Biology, **19**: 1–8. doi:10.1007/s003000050209.

Secor, D.H., Henderson-Arzapalo, A., and Piccoli, P.M. 1995. Can otolith microchemistry chart patterns of migration and habitat utilization in anadromous fishes? Journal of Experimental Marine Biology and Ecology, **192**: 15–33. doi:10.1016/0022-0981(95)00054-U.

Serre, S.H., Nielsen, K.E., Fink-Jensen, P., Thomsen, T.B., and Hüssy, K. 2018. Analysis of cod otolith microchemistry by continuous line transects using LA-ICP-MS. Geological Survey of Denmark and Greenland Bulletin, **41**: 91–94. doi:10.34194/geusb.v41.4351.

Severin, K.P., Carroll, J.L., and Norcross, B.L. 1995. Electron microprobe analysis of juvenile walleye pollock, Theragra chalcogramma, otoliths from Alaska: a pilot stock separation study. Environmental Biology of Fishes, **43**: 269–283. doi:10.1007/BF00005859.

Shao, Y., Farkaš, J., Holmden, C., Mosley, L., Kell-Duivestein, I., Izzo, C., Reis-Santos, P., Tyler, J., Törber, P., Frýda, J., Taylor, H., Haynes, D., Tibby, J., and Gillanders, B.M. 2018. Calcium and strontium isotope systematics in the lagoon-estuarine environments of South Australia: Implications for water source mixing, carbonate fluxes and fish migration. Geochimica et Cosmochimica Acta, **239**: 90–108. doi:10.1016/j.gca.2018.07.036.

Shelley, J.M.G., Eggins, S.M., and Kinsley, L.P.J. 1998. Deposition and element fractionation processes during atmospheric pressure laser sampling for analysis by ICP-MS. Applied Surface Science, **127**–**129**: 278–286.

SRM NIST 612.; *Glass*; National Institute of Standards and Technology; U.S. Department of Commerce: Gaithersburg, MD (06 April 2012).

SRM NIST 610.; *Glass*; National Institute of Standards and Technology; U.S. Department of Commerce: Gaithersburg, MD (06 April 2012).

SRM NIST 987.; *Glass*; National Institute of Standards and Technology; U.S. Department of Commerce: Gaithersburg, MD (19 June 2007).

Stroud, R.M. 2013. Transmission Electron Microscope-Based Spectroscopy. *In* Treatise on Geochemistry: Second Edition, 2nd edition. Elsevier Ltd. doi:10.1016/B978-0-08-095975-7.01416-9.

Swanson, H.K., Kidd, K.A., Babaluk, J.A., Wastle, R.J., Yang, P.P., Halden, N.M., and Reist, J.D. 2010. Anadromy in Arctic populations of lake trout (Salvelinus namaycush): Otolith microchemistry, stable isotopes, and comparisons with Arctic char (*Salvelinus alpinus*). Canadian Journal of Fisheries and Aquatic Sciences, **67**: 842–853. doi:10.1139/F10-022.

Tabouret, H., Bareille, G., Claverie, F., Pécheyran, C., Prouzet, P., and Donard, O.F.X. 2010. Simultaneous use of strontium:calcium and barium:calcium ratios in otoliths as markers of habitat: Application to the European eel (*Anguilla anguilla*) in the Adour basin, South West France. Marine Environmental Research, **70**: 35–45. Elsevier Ltd. doi:10.1016/j.marenvres.2010.02.006.

Targett, T.E., Thorrold, S.R., Jones, C.M., and Swart, P.K. 1998. Accurate classification of juvenile weakfish Cynoscion regalis to estuarine nursery areas based on chemical signatures in otoliths. Marine Ecology Progress Series, **173**: 253–265. Available from //000077093600020.

Thirlwall, M.F. 1991. Long-term reproducibility of multicollector Sr and Nd isotope ratio analysis. Chemical Geology, **94**: 85–104. doi:10.1016/S0009-2541(10)80021-X.

Thorrold, S.R., and Shuttleworth, S. 2000. In situ analysis of trace elements and isotope ratios in fish otoliths using laser ablation sector field inductively coupled plasma mass spectrometry. Canadian Journal of Fisheries and Aquatic Sciences, **57**: 1232–1242. doi:10.1139/f00-054.

Thomas, O.R.B., and Swearer, S.E. 2019. Otolith Biochemistry—A Review. Reviews in Fisheries Science and Aquaculture, **27**: 458–489. doi:10.1080/23308249.2019.1627285.

Tzadik, O.E., Curtis, J.S., Granneman, J.E., Kurth, B.N., Pusack, T.J., Wallace, A.A., Hollander, D.J., Peebles, E.B., and Stallings, C.D. 2017. Chemical archives in fishes beyond otoliths : A review on the use of other body parts as chronological recorders of microchemical ecological , and life-history changes. Limnology and Oceanography: Methods,: 26. doi:10.1002/lom3.10153.

Viete, D.R., Kylander-Clark, A.R.C., and Hacker, B.R. 2015. Single-shot laser ablation split stream (SS-LASS) petrochronology deciphers multiple, short-duration metamorphic events. Chemical Geology, **415**: 70–86. doi:10.1016/j.chemgeo.2015.09.013.

Vroon, P.Z., Van Der Wagt, B., Koornneef, J.M., and Davies, G.R. 2008. Problems in obtaining precise and accurate Sr isotope analysis from geological materials using laser ablation MC-ICPMS. Analytical and Bioanalytical Chemistry, **390**: 465–476. doi:10.1007/s00216-007-1742-9.

Walther, B.D., and Limburg, K.E. 2012. The use of otolith chemistry to characterize diadromous migrations. : 796–825. doi:10.1111/j.1095-8649.2012.03371.x.

Weber, M., Lugli, F., Hattendorf, B., Scholz, D., Mertz-Kraus, R., Guinoiseau, D., and Jochum, K.P. 2020. NanoSr – A New Carbonate Microanalytical Reference Material for In Situ Strontium Isotope Analysis. Geostandards and Geoanalytical Research, **44**: 69–83. doi:10.1111/ggr.12296.

Weidman, C.R., and Millner, R. 2000. Weidman and Millner 2000. **46**: 1–16. Available from papers2://publication/uuid/333827FA-F117-4520-A8F6-01C084F74EF2.

Wiederhold JG. 2015. Metal stable isotope signatures as tracers in environmental geochemistry. Environ Sci Technol. **5**: 2606-24. doi: 10.1021/es504683e.

Willmes, M., Glessner, J.J.G., Carleton, S.A., Gerrity, P.C., and Hobbs, J.A. 2016. 87Sr/86Sr isotope ratio analysis by laser ablation MC-ICP-MS in scales, spines, and fin rays as a nonlethal alternative to otoliths for reconstructing fish life history. Canadian Journal of Fisheries and Aquatic Sciences, **73**: 1852–1860. doi:10.1139/cjfas-2016-0103.

Woodhead, J., Swearer, S., Hergt, J., and Maas, R. 2005. In situ Sr-isotope analysis of carbonates by LA-MC-ICP-MS: Interference corrections, high spatial resolution and an example from otolith studies. Journal of Analytical Atomic Spectrometry, **20**: 22–27. doi:10.1039/b412730g.

Wright, P.J., Panfili, J., Morales-Nin, B., Geffen, A. 2002. Types of Calcified Structures: Otoliths. *In* Manual of Fish Sclerochronology. Edited by J. Panfili, H. Pontual, H. Troadec. P.J. Wright. Ifremer-IRD coedition. Brest, France. pp. 31-57.

Yoshimura, T., Tamenori, Y., Suzuki, A., Kawahata, H., Iwasaki, N., Hasegawa, H., Nguyen, L.T., Kuroyanagi, A., Yamazaki, T., Kuroda, J., and Ohkouchi, N. 2017. Altervalent substitution of sodium for calcium in biogenic calcite and aragonite. Geochimica et Cosmochimica Acta, **202**:

21–38. Elsevier Ltd. doi:10.1016/j.gca.2016.12.003.

Yuan, H.L., Gao, S., Dai, M.N., Zong, C.L., Günther, D., Fontaine, G.H., Liu, X.M., and Diwu, C.R. 2008. Simultaneous determinations of U-Pb age, Hf isotopes and trace element compositions of zircon by excimer laser-ablation quadrupole and multiple-collector ICP-MS. Chemical Geology, **247**: 100–118. doi:10.1016/j.chemgeo.2007.10.003.

Zimmerman, C.E., Swanson, H.K., Volk, E.C., and Kent, A.J.R. 2013. Species and life history affect the utility of otolith chemical composition for determining natal stream of origin for pacific salmon. Transactions of the American Fisheries Society, **142**: 1370–1380. doi:10.1080/00028487.2013.811102.

Zitek, A., Sturm, M., Waidbacher, H., and Prohaska, T. 2010. Discrimination of wild and hatchery trout by natural chronological patterns of elements and isotopes in otoliths using LA-ICP-MS. Fisheries Management and Ecology, **17**: 435–445. doi:10.1111/j.1365-2400.2010.00742.x.

Appendix A

Strontium Isotope and Trace Element Data on SRMs

LASS-ICP-MS long-term isotope data for the SRM USGS-MACS3

Sample	Date	Laser Diameter (µm)	Split-Stream	Nitrogen Used	$^{87}Sr/^{86}Sr$ Uncorrected Mean	$^{87}Sr/^{86}Sr$ Uncorrected 2SE	$^{87}Sr/^{86}Sr$ Instrumental Corrected Mean	$^{87}Sr/^{86}Sr$ Instrumental Corrected 2SE	$^{87}Sr/^{86}Sr$ Additional Corrected Mean	$^{87}Sr/^{86}Sr$ Additional Corrected 2SE
USGS_MACS3	2020-08-18	25	Yes	No	0.70769	0.000157	0.707649	0.000163	0.707744	0.000163
USGS_MACS3	2020-08-18	25	Yes	No	0.707539	0.000155	0.707492	0.000160	0.707530	0.000160
USGS_MACS3	2020-08-18	25	Yes	No	0.70757	0.000175	0.707551	0.000186	0.707561	0.000186
USGS_MACS3	2020-08-18	25	Yes	No	0.707554	0.000183	0.707548	0.000196	0.707513	0.000196
USGS_MACS3	2020-08-18	25	Yes	No	0.707643	0.000157	0.707605	0.000159	0.707527	0.000159
USGS_MACS3	2020-08-18	25	Yes	No	0.707608	0.000174	0.707574	0.000178	0.707559	0.000178
USGS_MACS3	2020-08-18	25	Yes	No	0.707657	0.000153	0.707665	0.000160	0.707652	0.000160
USGS_MACS3	2020-08-18	25	Yes	No	0.707632	0.000170	0.707600	0.000176	0.707590	0.000176
USGS_MACS3	2020-08-18	25	Yes	No	0.707511	0.000153	0.707480	0.000159	0.707472	0.000159
USGS_MACS3	2020-08-18	25	Yes	No	0.707545	0.000166	0.707510	0.000172	0.707505	0.000171
USGS_MACS3	2020-08-18	20	Yes	No	0.707546	0.000220	0.707514	0.000221	0.707511	0.000221
USGS_MACS3	2020-08-18	20	Yes	No	0.707649	0.000235	0.707666	0.000253	0.707665	0.000253
USGS_MACS3	2020-08-18	20	Yes	No	0.707552	0.000235	0.707496	0.000251	0.707498	0.000251
USGS_MACS3	2020-08-18	20	Yes	No	0.707545	0.000247	0.707522	0.000270	0.707526	0.000270
USGS_MACS3	2020-08-18	20	Yes	No	0.707624	0.000236	0.707573	0.000256	0.707579	0.000256
USGS_MACS3	2020-08-18	15	Yes	No	0.707395	0.000371	0.707313	0.000390	0.707322	0.000390
USGS_MACS3	2020-08-18	15	Yes	No	0.707623	0.000380	0.707576	0.000411	0.707587	0.000411
USGS_MACS3	2020-08-18	15	Yes	No	0.707561	0.000485	0.707496	0.000521	0.707509	0.000521
USGS_MACS3	2020-08-18	15	Yes	No	0.707399	0.000431	0.707401	0.000451	0.707416	0.000451
USGS_MACS3	2020-08-18	15	Yes	No	0.707481	0.000347	0.707380	0.000377	0.707398	0.000377
USGS_MACS3	2020-08-18	12	Yes	No	0.707533	0.000612	0.707316	0.000635	0.707233	0.000635
USGS_MACS3	2020-08-18	12	Yes	No	0.707568	0.000577	0.707532	0.000623	0.707473	0.000623
USGS_MACS3	2020-08-18	12	Yes	No	0.708095	0.000690	0.708016	0.000725	0.707980	0.000725
USGS_MACS3	2020-08-18	12	Yes	No	0.70779	0.000642	0.707619	0.000702	0.707607	0.000702
USGS_MACS3	2020-08-18	12	Yes	No	0.707904	0.000620	0.707849	0.000663	0.707860	0.000663
USGS_MACS3	2020-08-18	8	Yes	No	0.708002	0.001192	0.707747	0.001254	0.707783	0.001254
USGS_MACS3	2020-08-18	8	Yes	No	0.706965	0.001787	0.707082	0.001898	0.707141	0.001898
USGS_MACS3	2020-08-18	8	Yes	No	0.70833	0.001416	0.708044	0.001472	0.708127	0.001472
USGS_MACS3	2020-08-18	8	Yes	No	0.707013	0.001386	0.706768	0.001476	0.706875	0.001476
USGS_MACS3	2020-08-18	8	Yes	No	0.708295	0.001499	0.708435	0.001707	0.708565	0.001707
USGS_MACS3	2020-10-23	25	Yes	Yes	0.707737	0.000119	0.707613	0.000117	0.707686	0.000117
USGS_MACS3	2020-10-23	25	Yes	Yes	0.707677	0.000128	0.707629	0.000131	0.707702	0.000131
USGS_MACS3	2020-10-23	25	Yes	Yes	0.70764	0.000111	0.707600	0.000114	0.707673	0.000114
USGS_MACS3	2020-10-23	25	Yes	Yes	0.707666	0.000111	0.707627	0.000113	0.707701	0.000113
USGS_MACS3	2020-10-23	25	Yes	Yes	0.707661	0.000112	0.707636	0.000113	0.707710	0.000113
USGS_MACS3	2020-10-23	25	Yes	Yes	0.707675	0.000116	0.707640	0.000119	0.707714	0.000120
USGS_MACS3	2020-10-23	25	Yes	Yes	0.707606	0.000118	0.707576	0.000121	0.707651	0.000121
USGS_MACS3	2020-10-23	20	Yes	Yes	0.707717	0.000219	0.707624	0.000233	0.707698	0.000233
USGS_MACS3	2020-10-23	20	Yes	Yes	0.707746	0.000239	0.707663	0.000248	0.707738	0.000248
USGS_MACS3	2020-10-23	20	Yes	Yes	0.707752	0.000223	0.707730	0.000227	0.707805	0.000227
USGS_MACS3	2020-10-23	20	Yes	Yes	0.707679	0.000235	0.707634	0.000241	0.707709	0.000241

Sample	Date	Laser Diameter (µm)	Split-Stream	Nitrogen Used	$^{87}Sr/^{86}Sr$ Uncorrected Mean	$^{87}Sr/^{86}Sr$ Uncorrected 2SE	$^{87}Sr/^{86}Sr$ Instrumental Corrected Mean	$^{87}Sr/^{86}Sr$ Instrumental Corrected 2SE	$^{87}Sr/^{86}Sr$ Additional Corrected Mean	$^{87}Sr/^{86}Sr$ Additional Corrected 2SE
USGS_MACS3	2020-10-23	20	Yes	Yes	0.707618	0.000212	0.707544	0.000213	0.707620	0.000213
USGS_MACS3	2020-10-23	20	Yes	Yes	0.707851	0.000262	0.707800	0.000263	0.707875	0.000263
USGS_MACS3	2020-10-23	20	Yes	Yes	0.707841	0.000239	0.707713	0.000238	0.707788	0.000238
USGS_MACS3	2020-10-23	15	Yes	Yes	0.708074	0.000782	0.708108	0.000801	0.708184	0.000801
USGS_MACS3	2020-10-23	15	Yes	Yes	0.708357	0.000784	0.708180	0.000798	0.708256	0.000798
USGS_MACS3	2020-10-23	15	Yes	Yes	0.708808	0.000612	0.708108	0.000640	0.708184	0.000640
USGS_MACS3	2020-10-23	15	Yes	Yes	0.707764	0.000630	0.707580	0.000654	0.707657	0.000654
USGS_MACS3	2020-10-23	15	Yes	Yes	0.708313	0.000641	0.708332	0.000663	0.708409	0.000663
USGS_MACS3	2020-10-23	15	Yes	Yes	0.708089	0.000842	0.707883	0.000901	0.707960	0.000901
USGS_MACS3	2020-10-23	15	Yes	Yes	0.707391	0.000796	0.707223	0.000864	0.707301	0.000864
USGS_MACS3	2020-10-23	8	Yes	Yes	0.79351	0.090154	0.795302	0.117594	0.795389	0.117607
USGS_MACS3	2020-10-23	12	Yes	Yes	0.706569	0.001942	0.706979	0.002097	0.707057	0.002097
USGS_MACS3	2020-10-23	12	Yes	Yes	0.708055	0.001872	0.707692	0.002036	0.707770	0.002036
USGS_MACS3	2020-10-23	8	Yes	Yes	0.59135	0.137338	0.551842	0.117680	0.551903	0.117693
USGS_MACS3	2020-10-23	12	Yes	Yes	0.708126	0.001633	0.708150	0.001678	0.708229	0.001679
USGS_MACS3	2020-10-23	8	Yes	Yes	0.642208	0.260964	0.661805	0.278178	0.661878	0.278209
USGS_MACS3	2020-10-23	12	Yes	Yes	0.708646	0.001732	0.708819	0.001800	0.708898	0.001800
USGS_MACS3	2020-10-23	8	Yes	Yes	0.781479	0.085860	0.786997	0.087359	0.787085	0.087369
USGS_MACS3	2020-10-23	12	Yes	Yes	0.708764	0.002401	0.709624	0.002510	0.709704	0.002510
USGS_MACS3	2020-10-23	8	Yes	Yes	0.711503	0.147770	0.659016	0.124880	0.659090	0.124894
USGS_MACS3	2020-10-23	12	Yes	Yes	0.710508	0.003208	0.710202	0.003447	0.710282	0.003447
USGS_MACS3	2020-10-23	8	Yes	Yes	0.730882	0.042839	0.698115	0.051517	0.698194	0.051523
USGS_MACS3	2020-10-23	12	Yes	Yes	0.714837	0.003897	0.714556	0.004266	0.714636	0.004266
USGS_MACS3	2020-10-26	25	Yes	Yes	0.707667	0.000115	0.707635	0.000116	0.707621	0.000116
USGS_MACS3	2020-10-26	25	Yes	Yes	0.707661	0.000109	0.707631	0.000111	0.707628	0.000111
USGS_MACS3	2020-10-26	25	Yes	Yes	0.70753	0.000109	0.707500	0.000110	0.707508	0.000110
USGS_MACS3	2020-10-26	25	Yes	Yes	0.707678	0.000120	0.707626	0.000122	0.707645	0.000122
USGS_MACS3	2020-10-26	25	Yes	Yes	0.707706	0.000116	0.707664	0.000118	0.707695	0.000118
USGS_MACS3	2020-10-26	25	Yes	Yes	0.707675	0.000134	0.707602	0.000134	0.707645	0.000134
USGS_MACS3	2020-10-26	25	Yes	Yes	0.707677	0.000126	0.707638	0.000127	0.707692	0.000127
USGS_MACS3	2020-10-26	20	Yes	Yes	0.707698	0.000183	0.707621	0.000185	0.707684	0.000185
USGS_MACS3	2020-10-26	20	Yes	Yes	0.70767	0.000165	0.707603	0.000175	0.707677	0.000175
USGS_MACS3	2020-10-26	20	Yes	Yes	0.707506	0.000149	0.707453	0.000155	0.707538	0.000155
USGS_MACS3	2020-10-26	20	Yes	Yes	0.707584	0.000170	0.707524	0.000171	0.707621	0.000171
USGS_MACS3	2020-10-26	20	Yes	Yes	0.707669	0.000157	0.707637	0.000159	0.707745	0.000159
USGS_MACS3	2020-10-26	20	Yes	Yes	0.707744	0.000216	0.707573	0.000220	0.707693	0.000220
USGS_MACS3	2020-10-26	20	Yes	Yes	0.707609	0.000153	0.707568	0.000161	0.707699	0.000161
USGS_MACS3	2020-10-26	15	Yes	Yes	0.708178	0.000768	0.707895	0.000841	0.708035	0.000842
USGS_MACS3	2020-10-26	15	Yes	Yes	0.708156	0.000765	0.707924	0.000807	0.708075	0.000807
USGS_MACS3	2020-10-26	15	Yes	Yes	0.706836	0.000847	0.706566	0.000849	0.706728	0.000849
USGS_MACS3	2020-10-26	15	Yes	Yes	0.708135	0.000704	0.708033	0.000738	0.708207	0.000738
USGS_MACS3	2020-10-26	15	Yes	Yes	0.70794	0.000655	0.707752	0.000697	0.707938	0.000697
USGS_MACS3	2020-10-26	15	Yes	Yes	0.707409	0.000833	0.707204	0.000871	0.707401	0.000871
USGS_MACS3	2020-10-26	15	Yes	Yes	0.707299	0.000927	0.706979	0.001014	0.707187	0.001015

Sample	Date	Laser Diameter (µm)	Split-Stream	Nitrogen Used	$^{87}Sr/^{86}Sr$ Uncorrected Mean	$^{87}Sr/^{86}Sr$ Uncorrected 2SE	$^{87}Sr/^{86}Sr$ Instrumental Corrected Mean	$^{87}Sr/^{86}Sr$ Instrumental Corrected 2SE	$^{87}Sr/^{86}Sr$ Additional Corrected Mean	$^{87}Sr/^{86}Sr$ Additional Corrected 2SE
USGS_MACS3	2020-10-26	25	Yes	Yes	0.707564	0.000163	0.707500	0.000166	0.707572	0.000166
USGS_MACS3	2020-10-26	25	Yes	Yes	0.707674	0.000172	0.707684	0.000175	0.707753	0.000175
USGS_MACS3	2020-10-26	25	Yes	Yes	0.707689	0.000241	0.707647	0.000256	0.707713	0.000256
USGS_MACS3	2020-10-26	25	Yes	Yes	0.707716	0.000212	0.707737	0.000219	0.707800	0.000219
USGS_MACS3	2020-10-26	25	Yes	Yes	0.707641	0.000161	0.707639	0.000170	0.707698	0.000170
USGS_MACS3	2020-10-26	20	Yes	Yes	0.707601	0.000233	0.707605	0.000238	0.707661	0.000238
USGS_MACS3	2020-10-26	20	Yes	Yes	0.707562	0.000245	0.707577	0.000246	0.707630	0.000246
USGS_MACS3	2020-10-26	20	Yes	Yes	0.707602	0.000302	0.707512	0.000316	0.707562	0.000316
USGS_MACS3	2020-10-26	20	Yes	Yes	0.707574	0.000303	0.707535	0.000329	0.707582	0.000329
USGS_MACS3	2020-10-26	20	Yes	Yes	0.707818	0.000438	0.707830	0.000450	0.707873	0.000451
USGS_MACS3	2020-10-26	15	Yes	Yes	0.707667	0.000633	0.707676	0.000661	0.707717	0.000661
USGS_MACS3	2020-10-26	15	Yes	Yes	0.708002	0.003091	0.707419	0.003327	0.707458	0.003327
USGS_MACS3	2020-10-26	15	Yes	Yes	0.706595	0.003070	0.706501	0.003158	0.706536	0.003158
USGS_MACS3	2020-10-26	15	Yes	Yes	0.707164	0.002810	0.707009	0.003076	0.707041	0.003076
USGS_MACS3	2020-10-26	8	Yes	Yes	0.710507	0.006093	0.710010	0.006348	0.710034	0.006348
USGS_MACS3	2020-10-26	8	Yes	Yes	0.705638	0.006321	0.705957	0.006928	0.705979	0.006928
USGS_MACS3	2020-10-26	8	Yes	Yes	0.707333	0.005057	0.706933	0.005382	0.706949	0.005382
USGS_MACS3	2020-10-26	8	Yes	Yes	0.706598	0.004502	0.706158	0.004702	0.706171	0.004702
USGS_MACS3	2020-10-26	8	Yes	Yes	0.710364	0.006038	0.710888	0.006335	0.710900	0.006336
USGS_MACS3	2020-11-02	25	Yes	Yes	0.707658	0.000106	0.707628	0.000106	0.707556	0.000106
USGS_MACS3	2020-11-02	25	Yes	Yes	0.70765	0.000105	0.707623	0.000106	0.707557	0.000106
USGS_MACS3	2020-11-02	25	Yes	Yes	0.707603	0.000119	0.707580	0.000119	0.707520	0.000119
USGS_MACS3	2020-11-02	25	Yes	Yes	0.707662	0.000113	0.707642	0.000117	0.707587	0.000117
USGS_MACS3	2020-11-02	25	Yes	Yes	0.707601	0.000109	0.707583	0.000113	0.707534	0.000113
USGS_MACS3	2020-11-02	25	Yes	Yes	0.707637	0.000110	0.707616	0.000116	0.707573	0.000116
USGS_MACS3	2020-11-02	25	Yes	Yes	0.707601	0.000122	0.707578	0.000121	0.707542	0.000121
USGS_MACS3	2020-11-02	25	Yes	Yes	0.707669	0.000130	0.707646	0.000132	0.707607	0.000132
USGS_MACS3	2020-11-02	25	Yes	Yes	0.707613	0.000190	0.707579	0.000192	0.707552	0.000192
USGS_MACS3	2020-11-02	25	Yes	Yes	0.707741	0.000191	0.707727	0.000192	0.707714	0.000192
USGS_MACS3	2020-11-02	25	Yes	Yes	0.707705	0.000154	0.707644	0.000156	0.707646	0.000156
USGS_MACS3	2020-11-02	25	Yes	Yes	0.707596	0.000176	0.707564	0.000177	0.707584	0.000177
USGS_MACS3	2020-11-02	25	Yes	Yes	0.70772	0.000153	0.707769	0.000161	0.707809	0.000161
USGS_MACS3	2020-11-02	25	Yes	Yes	0.707727	0.000132	0.707693	0.000132	0.707753	0.000132
USGS_MACS3	2020-11-02	25	Yes	Yes	0.707597	0.000130	0.707577	0.000132	0.707634	0.000132
USGS_MACS3	2020-11-02	25	Yes	Yes	0.707717	0.000127	0.707692	0.000130	0.707735	0.000130
USGS_MACS3	2020-11-02	25	Yes	Yes	0.707679	0.000120	0.707655	0.000120	0.707685	0.000120
USGS_MACS3	2020-11-02	25	Yes	Yes	0.707614	0.000118	0.707583	0.000120	0.707599	0.000120
USGS_MACS3	2020-11-02	25	Yes	Yes	0.707635	0.000114	0.707598	0.000117	0.707600	0.000117
USGS_MACS3	2020-11-02	25	Yes	Yes	0.707584	0.000124	0.707543	0.000127	0.707532	0.000127
USGS_MACS3	2020-11-02	25	Yes	Yes	0.707696	0.000114	0.707660	0.000116	0.707636	0.000116
USGS_MACS3	2020-11-02	25	Yes	Yes	0.707565	0.000116	0.707550	0.000119	0.707501	0.000119
USGS_MACS3	2020-11-02	25	Yes	Yes	0.707656	0.000107	0.707629	0.000111	0.707583	0.000111
USGS_MACS3	2020-11-02	25	Yes	Yes	0.707614	0.000115	0.707621	0.000118	0.707582	0.000118
USGS_MACS3	2020-11-02	25	Yes	Yes	0.707525	0.000111	0.707494	0.000118	0.707467	0.000118

Sample	Date	Laser Diameter (µm)	Split-Stream	Nitrogen Used	$^{87}Sr/^{86}Sr$ Uncorrected Mean	$^{87}Sr/^{86}Sr$ Uncorrected 2SE	$^{87}Sr/^{86}Sr$ Instrumental Corrected Mean	$^{87}Sr/^{86}Sr$ Instrumental Corrected 2SE	$^{87}Sr/^{86}Sr$ Additional Corrected Mean	$^{87}Sr/^{86}Sr$ Additional Corrected 2SE
USGS_MACS3	2020-11-02	25	Yes	Yes	0.707537	0.000105	0.707512	0.000107	0.707503	0.000107
USGS_MACS3	2020-11-02	25	Yes	Yes	0.707594	0.000107	0.707583	0.000114	0.707597	0.000114
USGS_MACS3	2020-11-02	25	Yes	Yes	0.707537	0.000115	0.707510	0.000121	0.707547	0.000121
USGS_MACS3	2020-11-03	15	Yes	Yes	0.707674	0.000100	0.707651	0.000103	0.707718	0.000103
USGS_MACS3	2020-11-03	15	Yes	Yes	0.707633	0.000125	0.707583	0.000129	0.707598	0.000129
USGS_MACS3	2020-11-03	15	Yes	Yes	0.707549	0.000112	0.707524	0.000115	0.707508	0.000115
USGS_MACS3	2020-11-03	15	Yes	Yes	0.70772	0.000106	0.707695	0.000107	0.707687	0.000107
USGS_MACS3	2020-11-03	15	Yes	Yes	0.707522	0.000142	0.707513	0.000142	0.707563	0.000142
USGS_MACS3	2020-11-03	15	Yes	Yes	0.707697	0.000110	0.707699	0.000110	0.707760	0.000110
USGS_MACS3	2020-11-03	15	Yes	Yes	0.707569	0.000106	0.707530	0.000112	0.707556	0.000112
USGS_MACS3	2020-11-03	15	Yes	Yes	0.707536	0.000207	0.707530	0.000214	0.707608	0.000214
USGS_MACS3	2020-11-03	15	Yes	Yes	0.707407	0.000177	0.707420	0.000185	0.707480	0.000185
USGS_MACS3	2020-11-03	15	Yes	Yes	0.707744	0.000192	0.707681	0.000204	0.707723	0.000204
USGS_MACS3	2020-11-03	15	Yes	Yes	0.707632	0.000187	0.707651	0.000193	0.707676	0.000193
USGS_MACS3	2020-11-03	15	Yes	Yes	0.70761	0.000203	0.707579	0.000210	0.707586	0.000210
USGS_MACS3	2020-11-03	15	Yes	Yes	0.707728	0.000205	0.707652	0.000211	0.707641	0.000211
USGS_MACS3	2020-11-03	15	Yes	Yes	0.707547	0.000173	0.707500	0.000177	0.707472	0.000177
USGS_MACS3	2020-11-03	12	Yes	Yes	0.707744	0.000318	0.707777	0.000322	0.708017	0.000322
USGS_MACS3	2020-11-03	12	Yes	Yes	0.707848	0.000377	0.707878	0.000382	0.708048	0.000382
USGS_MACS3	2020-11-03	12	Yes	Yes	0.707604	0.000360	0.707559	0.000364	0.707687	0.000359
USGS_MACS3	2020-11-03	12	Yes	Yes	0.707566	0.000304	0.707666	0.000323	0.707694	0.000323
USGS_MACS3	2020-11-03	12	Yes	Yes	0.707679	0.000282	0.707758	0.000292	0.707715	0.000292
USGS_MACS3	2020-11-03	12	Yes	Yes	0.707482	0.000323	0.707490	0.000327	0.707377	0.000327
USGS_MACS3	2020-11-03	12	Yes	Yes	0.707591	0.000264	0.707590	0.000283	0.707407	0.000282
USGS_MACS3	2020-11-03	8	Yes	Yes	0.707759	0.000634	0.707797	0.000671	0.707602	0.000671
USGS_MACS3	2020-11-03	8	Yes	Yes	0.70762	0.000780	0.707642	0.000845	0.707548	0.000845
USGS_MACS3	2020-11-03	8	Yes	Yes	0.708063	0.000659	0.708064	0.000697	0.708071	0.000697
USGS_MACS3	2020-11-03	8	Yes	Yes	0.70784	0.000628	0.707874	0.000687	0.707983	0.000687
USGS_MACS3	2020-11-03	8	Yes	Yes	0.707716	0.000551	0.707562	0.000596	0.707773	0.000596
USGS_MACS3	2020-11-03	8	Yes	Yes	0.707509	0.000578	0.707413	0.000613	0.707726	0.000613
USGS_MACS3	2020-11-03	8	Yes	Yes	0.707204	0.000604	0.707193	0.000646	0.707608	0.000646
USGS_MACS3	2020-11-23	25	Yes	Yes	0.707616	0.000167	0.707555	0.000168	0.707576	0.000168
USGS_MACS3	2020-11-23	25	Yes	Yes	0.707548	0.000122	0.707499	0.000127	0.707545	0.000127
USGS_MACS3	2020-11-23	25	Yes	Yes	0.707653	0.000122	0.707620	0.000122	0.707735	0.000122
USGS_MACS3	2020-11-23	25	Yes	Yes	0.70761	0.000136	0.707551	0.000142	0.707637	0.000142
USGS_MACS3	2020-11-23	25	Yes	Yes	0.707576	0.000096	0.707562	0.000099	0.707659	0.000099
USGS_MACS3	2020-11-23	25	Yes	Yes	0.707602	0.000100	0.707570	0.000099	0.707637	0.000099
USGS_MACS3	2020-11-23	25	Yes	Yes	0.707601	0.000128	0.707578	0.000130	0.707623	0.000130
USGS_MACS3	2020-11-23	25	Yes	Yes	0.707699	0.000110	0.707668	0.000111	0.707675	0.000111
USGS_MACS3	2020-11-23	25	Yes	Yes	0.707617	0.000104	0.707593	0.000107	0.707590	0.000107
USGS_MACS3	2020-11-23	25	Yes	Yes	0.707592	0.000102	0.707567	0.000103	0.707620	0.000103
USGS_MACS3	2020-11-23	25	Yes	Yes	0.707622	0.000101	0.707602	0.000103	0.707676	0.000103
USGS_MACS3	2020-11-23	25	Yes	Yes	0.707531	0.000089	0.707490	0.000091	0.707552	0.000091
USGS_MACS3	2020-11-23	25	Yes	Yes	0.707537	0.000090	0.707518	0.000090	0.707488	0.000090

Sample	Date	Laser Diameter (µm)	Split-Stream	Nitrogen Used	$^{87}Sr/^{86}Sr$ Uncorrected Mean	$^{87}Sr/^{86}Sr$ Uncorrected 2SE	$^{87}Sr/^{86}Sr$ Instrumental Corrected Mean	$^{87}Sr/^{86}Sr$ Instrumental Corrected 2SE	$^{87}Sr/^{86}Sr$ Additional Corrected Mean	$^{87}Sr/^{86}Sr$ Additional Corrected 2SE
USGS_MACS3	2020-11-23	25	Yes	Yes	0.707534	0.000088	0.707510	0.000089	0.707481	0.000089
USGS_MACS3	2020-11-23	25	Yes	Yes	0.707554	0.000098	0.707514	0.000098	0.707583	0.000098
USGS_MACS3	2020-11-24	25	Yes	Yes	0.70761	0.000090	0.707581	0.000091	0.707661	0.000091
USGS_MACS3	2020-11-24	25	Yes	Yes	0.707575	0.000081	0.707557	0.000082	0.707674	0.000082
USGS_MACS3	2020-11-24	25	Yes	Yes	0.707653	0.000085	0.707653	0.000087	0.707716	0.000087
USGS_MACS3	2020-11-24	25	Yes	Yes	0.707598	0.000083	0.707574	0.000084	0.707484	0.000084
USGS_MACS3	2020-11-24	25	Yes	Yes	0.707579	0.000075	0.707566	0.000078	0.707685	0.000078
USGS_MACS3	2020-11-24	25	Yes	Yes	0.707635	0.000080	0.707609	0.000082	0.707750	0.000082
USGS_MACS3	2020-11-24	25	Yes	Yes	0.707573	0.000055	0.707564	0.000057	0.707535	0.000057
USGS_MACS3	2020-11-24	25	Yes	Yes	0.707598	0.000052	0.707578	0.000055	0.707745	0.000055
USGS_MACS3	2020-11-24	25	Yes	Yes	0.707597	0.000093	0.707566	0.000093	0.707734	0.000094
USGS_MACS3	2020-11-25	25	Yes	Yes	0.707566	0.000099	0.707553	0.000101	0.707594	0.000101
USGS_MACS3	2020-11-25	25	Yes	Yes	0.707554	0.000107	0.707537	0.000108	0.707608	0.000108
USGS_MACS3	2020-11-25	25	Yes	Yes	0.707561	0.000096	0.707528	0.000097	0.707649	0.000097
USGS_MACS3	2020-11-25	25	Yes	Yes	0.707483	0.000117	0.707463	0.000119	0.707551	0.000119
USGS_MACS3	2020-11-25	25	Yes	Yes	0.707557	0.000145	0.707537	0.000145	0.707577	0.000145
USGS_MACS3	2020-11-25	25	Yes	Yes	0.707583	0.000120	0.707570	0.000121	0.707598	0.000121
USGS_MACS3	2020-11-25	25	Yes	Yes	0.707575	0.000121	0.707535	0.000122	0.707619	0.000122
USGS_MACS3	2020-11-25	25	Yes	Yes	0.707572	0.000113	0.707557	0.000113	0.707600	0.000113
USGS_MACS3	2020-11-25	25	Yes	Yes	0.707586	0.000140	0.707575	0.000140	0.707534	0.000140
USGS_MACS3	2020-11-25	10	Yes	Yes	0.708947	0.006216	0.709585	0.006435	0.709705	0.006436
USGS_MACS3	2020-11-25	10	Yes	Yes	0.705814	0.012177	0.706222	0.013256	0.706335	0.013259
USGS_MACS3	2021-01-05	15	Yes	Yes	0.707897	0.001157	0.707459	0.001211	0.707429	0.001211
USGS_MACS3	2021-01-05	15	Yes	Yes	0.707879	0.001632	0.707946	0.001689	0.707917	0.001689
USGS_MACS3	2021-01-05	15	Yes	Yes	0.70754	0.001634	0.707073	0.001732	0.706993	0.001731
USGS_MACS3	2021-01-06	15	Yes	Yes	0.707703	0.000822	0.707555	0.000931	0.707646	0.000932
USGS_MACS3	2021-01-06	15	Yes	Yes	0.707728	0.001091	0.707776	0.001132	0.707866	0.001132
USGS_MACS3	2021-01-06	15	Yes	Yes	0.707551	0.000882	0.707291	0.000983	0.707402	0.000983
USGS_MACS3	2021-01-06	15	Yes	Yes	0.707361	0.000683	0.707744	0.000715	0.707577	0.000715
USGS_MACS3	2021-01-06	15	Yes	Yes	0.707027	0.000719	0.707630	0.000774	0.707432	0.000773
USGS_MACS3	2021-01-06	15	Yes	Yes	0.706971	0.000798	0.707517	0.000826	0.707648	0.000826
USGS_MACS3	2021-01-06	15	Yes	Yes	0.706353	0.000714	0.707638	0.000796	0.707907	0.000797
USGS_MACS3	2021-01-06	15	Yes	Yes	0.701472	0.001542	0.706521	0.001599	0.706522	0.001599
USGS_MACS3	2021-01-06	15	Yes	Yes	0.707591	0.000456	0.707596	0.000503	0.707728	0.000503
USGS_MACS3	2021-01-06	15	Yes	Yes	0.707757	0.001311	0.707685	0.001465	0.707818	0.001466
USGS_MACS3	2021-02-01	15	Yes	Yes	0.70802	0.000860	0.708010	0.000910	0.708060	0.000910
USGS_MACS3	2021-02-01	15	Yes	Yes	0.70735	0.000550	0.707350	0.000600	0.707400	0.000600
USGS_MACS3	2021-02-01	15	Yes	Yes	0.7069	0.002000	0.706800	0.002200	0.706800	0.002200
USGS_MACS3	2021-02-01	15	Yes	Yes	0.70753	0.000480	0.707560	0.000500	0.707580	0.000500
USGS_MACS3	2021-02-01	15	Yes	Yes	0.70739	0.000500	0.707460	0.000560	0.707460	0.000560
USGS_MACS3	2021-02-02	15	Yes	Yes	0.70749	0.000380	0.707510	0.000400	0.707410	0.000400
USGS_MACS3	2021-02-02	15	Yes	Yes	0.70751	0.000360	0.707280	0.000390	0.707170	0.000390
USGS_MACS3	2021-02-02	15	Yes	Yes	0.70754	0.000920	0.707800	0.001100	0.707700	0.001100
USGS_MACS3	2021-02-02	15	Yes	Yes	0.7075	0.001700	0.707900	0.001800	0.707800	0.001800

Sample	Date	Laser Diameter (µm)	Split-Stream	Nitrogen Used	$^{87}Sr/^{86}Sr$ Uncorrected Mean	$^{87}Sr/^{86}Sr$ Uncorrected 2SE	$^{87}Sr/^{86}Sr$ Instrumental Corrected Mean	$^{87}Sr/^{86}Sr$ Instrumental Corrected 2SE	$^{87}Sr/^{86}Sr$ Additional Corrected Mean	$^{87}Sr/^{86}Sr$ Additional Corrected 2SE
USGS_MACS3	2021-02-02	15	Yes	Yes	0.7073	0.001700	0.707200	0.001800	0.707100	0.001800
USGS_MACS3	2021-02-02	15	Yes	Yes	0.70808	0.000810	0.707960	0.000830	0.707830	0.000830
USGS_MACS3	2021-02-02	15	Yes	Yes	0.7077	0.000600	0.707790	0.000640	0.707650	0.000640
USGS_MACS3	2021-03-03	40	Yes	Yes	0.7076	0.000085	0.707582	0.000086	0.707550	0.000086
USGS_MACS3	2021-03-03	40	Yes	Yes	0.70757	0.000117	0.707559	0.000119	0.707528	0.000119
USGS_MACS3	2021-03-03	40	Yes	Yes	0.707577	0.000100	0.707559	0.000101	0.707531	0.000101
USGS_MACS3	2021-03-03	40	Yes	Yes	0.70772	0.000124	0.707679	0.000127	0.707653	0.000127
USGS_MACS3	2021-03-03	40	Yes	Yes	0.707696	0.000143	0.707671	0.000145	0.707647	0.000145
USGS_MACS3	2021-03-03	40	Yes	Yes	0.707667	0.000151	0.707628	0.000151	0.707606	0.000151
USGS_MACS3	2021-03-03	40	Yes	Yes	0.707732	0.000174	0.707684	0.000176	0.707664	0.000176
USGS_MACS3	2021-03-03	40	Yes	Yes	0.707797	0.000163	0.707760	0.000167	0.707741	0.000167
USGS_MACS3	2021-03-03	40	Yes	Yes	0.70767	0.000182	0.707643	0.000183	0.707626	0.000183
USGS_MACS3	2021-03-04	40	Yes	Yes	0.707449	0.000125	0.707409	0.000129	0.707462	0.000129
USGS_MACS3	2021-03-04	40	Yes	Yes	0.707759	0.000164	0.707705	0.000171	0.707759	0.000172
USGS_MACS3	2021-03-04	40	Yes	Yes	0.707652	0.000150	0.707632	0.000154	0.707694	0.000154
USGS_MACS3	2021-03-04	40	Yes	Yes	0.707865	0.000221	0.707817	0.000223	0.707890	0.000223
USGS_MACS3	2021-03-04	40	Yes	Yes	0.707557	0.000133	0.707556	0.000140	0.707633	0.000140
USGS_MACS3	2021-03-04	40	Yes	Yes	0.707776	0.000213	0.707750	0.000219	0.707837	0.000219
USGS_MACS3	2021-03-04	40	Yes	Yes	0.707697	0.000256	0.707712	0.000270	0.707810	0.000270
USGS_MACS3	2021-03-05	40	Yes	Yes	0.708078	0.000122	0.707506	0.000115	0.707746	0.000115
USGS_MACS3	2021-03-05	40	Yes	Yes	0.715776	0.001621	0.707729	0.000210	0.707954	0.000210
USGS_MACS3	2021-03-05	40	Yes	Yes	0.708879	0.000130	0.707667	0.000126	0.707874	0.000126
USGS_MACS3	2021-03-05	40	Yes	Yes	0.707633	0.000083	0.707574	0.000085	0.707775	0.000085
USGS_MACS3	2021-03-05	40	Yes	Yes	0.707555	0.000113	0.707548	0.000115	0.707728	0.000115
USGS_MACS3	2021-03-05	40	Yes	Yes	0.707677	0.000136	0.707650	0.000135	0.707806	0.000135
USGS_MACS3	2021-03-05	40	Yes	Yes	0.707548	0.000140	0.707513	0.000144	0.707663	0.000144
USGS_MACS3	2021-03-05	40	Yes	Yes	0.707674	0.000137	0.707654	0.000138	0.707780	0.000138
USGS_MACS3	2021-03-05	40	Yes	Yes	0.707668	0.000155	0.707585	0.000153	0.707686	0.000153
USGS_MACS3	2021-03-05	40	Yes	Yes	0.707665	0.000153	0.707643	0.000154	0.707734	0.000154
USGS_MACS3	2021-03-05	40	Yes	Yes	0.707643	0.000212	0.707643	0.000216	0.707707	0.000216
USGS_MACS3	2021-03-05	40	Yes	Yes	0.7077	0.000170	0.707687	0.000169	0.707720	0.000169
USGS_MACS3	2021-03-05	40	Yes	Yes	0.707844	0.000276	0.707869	0.000281	0.707893	0.000281
USGS_MACS3	2021-03-05	40	Yes	Yes	0.707823	0.000292	0.707550	0.000300	0.707515	0.000300
USGS_MACS3	2021-05-27	40	Yes	Yes	0.707655	0.000122	0.707588	0.000124	0.707426	0.000124
USGS_MACS3	2021-05-27	40	Yes	Yes	0.707605	0.000125	0.707572	0.000127	0.707569	0.000127
USGS_MACS3	2021-05-27	40	Yes	Yes	0.70749	0.000130	0.707462	0.000129	0.707602	0.000129
USGS_MACS3	2021-05-27	40	Yes	Yes	0.707437	0.000154	0.707420	0.000155	0.707668	0.000155
USGS_MACS3	2021-05-27	40	Yes	Yes	0.707492	0.000205	0.707458	0.000207	0.707798	0.000207
USGS_MACS3	2021-05-27	40	Yes	Yes	0.707458	0.000157	0.707413	0.000157	0.707839	0.000158
USGS_MACS3	2021-05-27	40	Yes	Yes	0.70748	0.000129	0.707443	0.000128	0.707956	0.000128
USGS_MACS3	2021-05-27	40	Yes	Yes	0.707486	0.000142	0.707439	0.000142	0.708037	0.000142
USGS_MACS3	2021-05-27	40	Yes	Yes	0.707585	0.000128	0.707547	0.000128	0.708221	0.000128

LA-ICP-MS (single-stream) long-term isotope data for the SRM USGS-MACS3

Sample	Date	Laser Diameter (µm)	Split-Stream	Nitrogen Used	$^{87}Sr/^{86}Sr$ Uncorrected Mean	$^{87}Sr/^{86}Sr$ Uncorrected 2SE	$^{87}Sr/^{86}Sr$ Instrumental Corrected Mean	$^{87}Sr/^{86}Sr$ Instrumental Corrected 2SE	$^{87}Sr/^{86}Sr$ Additional Corrected Mean	$^{87}Sr/^{86}Sr$ Additional Corrected 2SE
USGS_MACS3	2020-03-04	10	No	No	0.707311	0.000448042	0.707147	0.000477185	0.707267	0.000477265
USGS_MACS3	2020-03-04	10	No	No	0.707382	0.000476454	0.707309	0.000505389	0.707409	0.000505462
USGS_MACS3	2020-03-04	10	No	No	0.70787	0.00045406	0.70767	0.000491126	0.707727	0.000491162
USGS_MACS3	2020-03-04	50	No	No	0.707702	0.000106835	0.707685	0.000110971	0.70764	0.000110965
USGS_MACS3	2020-03-04	50	No	No	0.707732	0.000111544	0.707694	0.000113888	0.707636	0.000113878
USGS_MACS3	2020-03-04	50	No	No	0.707803	0.000106111	0.707783	0.000108948	0.707727	0.000108938
USGS_MACS3	2020-03-04	50	No	No	0.707686	0.0000582	0.70766	0.0000585	0.707553	0.0000585
USGS_MACS3	2020-03-04	50	No	No	0.707682	0.0000635	0.707665	0.0000642	0.707553	0.0000642
USGS_MACS3	2020-03-04	50	No	No	0.707704	0.0000664	0.70768	0.0000673	0.707554	0.0000672
USGS_MACS3	2020-07-29	25	No	No	0.707633	0.000052	0.707605	0.000054311	0.707616	0.0000543
USGS_MACS3	2020-07-29	25	No	No	0.707637	0.0000572	0.707622	0.0000585	0.707623	0.0000585
USGS_MACS3	2020-07-29	25	No	No	0.707628	0.0000532	0.707605	0.0000547	0.707583	0.0000547
USGS_MACS3	2020-07-29	25	No	No	0.707596	0.0000557	0.70755	0.000057002	0.707519	0.000056998
USGS_MACS3	2020-07-29	25	No	No	0.707605	0.0000509	0.707549	0.0000523	0.707622	0.0000523
USGS_MACS3	2020-07-29	25	No	No	0.707588	0.0000469	0.707563	0.0000483	0.707631	0.00004833
USGS_MACS3	2020-07-29	25	No	No	0.70757	0.0000466	0.70755	0.000048648	0.707613	0.0000487
USGS_MACS3	2020-07-29	25	No	No	0.707609	0.0000464	0.707575	0.0000478	0.707634	0.0000479
USGS_MACS3	2020-07-30	25	No	No	0.707585	0.000059	0.707566	0.0000616	0.707631	0.0000616
USGS_MACS3	2020-07-30	25	No	No	0.707593	0.0000585	0.707558	0.000061	0.707565	0.000061
USGS_MACS3	2020-07-30	25	No	No	0.707623	0.000057909	0.707591	0.0000606	0.707571	0.0000606
USGS_MACS3	2020-07-30	25	No	No	0.707592	0.0000559	0.707568	0.0000586	0.70756	0.0000586
USGS_MACS3	2020-07-31	25	No	No	0.707631	0.000063436	0.70759	0.0000654	0.707652	0.0000655
USGS_MACS3	2020-07-31	25	No	No	0.707643	0.0000621	0.707599	0.0000644	0.707646	0.0000644
USGS_MACS3	2020-07-31	25	No	No	0.707588	0.0000644	0.707547	0.0000667	0.707582	0.0000667
USGS_MACS3	2020-07-31	25	No	No	0.707609	0.0000561	0.707573	0.0000586	0.707644	0.000058633
USGS_MACS3	2020-07-31	25	No	No	0.707615	0.00006	0.707564	0.0000624	0.707636	0.0000624
USGS_MACS3	2020-07-31	25	No	No	0.707585	0.0000577	0.707552	0.0000598	0.707575	0.0000598
USGS_MACS3	2020-07-31	25	No	No	0.707558	0.0000604	0.707511	0.0000617	0.707517	0.0000617
USGS_MACS3	2020-07-31	25	No	No	0.707645	0.0000587	0.707602	0.0000615	0.707591	0.0000615
USGS_MACS3	2020-10-19	25	No	No	0.707833	0.00137814	0.707162	0.00150791	0.707794	0.00150925
USGS_MACS3	2020-10-19	25	No	No	0.708254	0.00169776	0.708287	0.00177354	0.708871	0.00177499
USGS_MACS3	2020-10-19	25	No	No	0.708219	0.00148426	0.708249	0.00152826	0.708784	0.00152941
USGS_MACS3	2020-10-19	25	No	No	0.707139	0.00148253	0.706873	0.00162154	0.707359	0.00162267
USGS_MACS3	2020-10-19	25	No	No	0.706392	0.00167334	0.706189	0.00174171	0.706625	0.00174279
USGS_MACS3	2020-10-19	25	No	No	0.70667	0.00180404	0.706842	0.00191553	0.707231	0.00191658
USGS_MACS3	2020-10-19	25	No	No	0.707397	0.00186693	0.707664	0.00203606	0.70803	0.00203712
USGS_MACS3	2020-10-19	25	No	No	0.70863	0.00178224	0.708977	0.0018642	0.709295	0.00186504
USGS_MACS3	2020-10-19	25	No	No	0.708049	0.00201307	0.707851	0.00210741	0.70812	0.00210821
USGS_MACS3	2020-10-19	25	No	No	0.706494	0.00199954	0.706777	0.00219294	0.706997	0.00219363
USGS_MACS3	2020-10-19	25	No	No	0.707894	0.000278423	0.707779	0.000285618	0.707729	0.000285588
USGS_MACS3	2020-10-19	25	No	No	0.707927	0.000282739	0.707864	0.000289053	0.707835	0.000289039

Sample	Date	Laser Diameter (µm)	Split-Stream	Nitrogen Used	$^{87}Sr/^{86}Sr$ Uncorrected Mean	$^{87}Sr/^{86}Sr$ Uncorrected 2SE	$^{87}Sr/^{86}Sr$ Instrumental Corrected Mean	$^{87}Sr/^{86}Sr$ Instrumental Corrected 2SE	$^{87}Sr/^{86}Sr$ Additional Corrected Mean	$^{87}Sr/^{86}Sr$ Additional Corrected 2SE
USGS_MACS3	2020-10-19	25	No	No	0.707819	0.000252523	0.707751	0.000271459	0.707743	0.000271457
USGS_MACS3	2020-10-19	25	No	No	0.707802	0.000270599	0.7077	0.000295747	0.707713	0.00029574
USGS_MACS3	2020-10-19	25	No	No	0.707681	0.000337387	0.707629	0.000353105	0.70766	0.000353133
USGS_MACS3	2020-10-19	25	No	No	0.707861	0.000297662	0.707739	0.000326444	0.707782	0.000326466
USGS_MACS3	2020-10-19	25	No	No	0.707791	0.000329928	0.707717	0.00035344	0.707764	0.000353463
USGS_MACS3	2020-10-19	25	No	No	0.707965	0.000290788	0.707884	0.000311091	0.707933	0.000311113
USGS_MACS3	2020-10-19	25	No	No	0.707615	0.000284746	0.70754	0.000295297	0.707583	0.000295318
USGS_MACS3	2020-10-19	25	No	No	0.707721	0.000367031	0.707677	0.000358896	0.707708	0.000358914
USGS_MACS3	2020-10-19	25	No	No	0.707833	0.000645532	0.707511	0.000669098	0.707671	0.000669248
USGS_MACS3	2020-10-19	25	No	No	0.708222	0.000590871	0.707984	0.000621368	0.708163	0.000621526
USGS_MACS3	2020-10-19	25	No	No	0.70766	0.000695724	0.707687	0.000725158	0.707884	0.000725367
USGS_MACS3	2020-10-19	25	No	No	0.707894	0.000697599	0.707684	0.000747442	0.7079	0.000747664
USGS_MACS3	2020-10-19	25	No	No	0.707588	0.000693311	0.707443	0.000737838	0.707677	0.00073808
USGS_MACS3	2020-10-19	25	No	No	0.708049	0.000663538	0.707887	0.000699346	0.70814	0.0006996
USGS_MACS3	2020-10-19	25	No	No	0.707957	0.000694307	0.708006	0.000727802	0.708269	0.000728073
USGS_MACS3	2020-10-19	25	No	No	0.707775	0.000626041	0.707495	0.000653805	0.707776	0.000654063
USGS_MACS3	2020-10-19	25	No	No	0.707889	0.000723394	0.707672	0.00074961	0.707972	0.000749928
USGS_MACS3	2020-10-19	25	No	No	0.707356	0.000661894	0.707179	0.000719965	0.707497	0.000720284
USGS_MACS3	2020-10-19	25	No	No	0.708013	0.000990169	0.708013	0.00107243	0.708474	0.00107312
USGS_MACS3	2020-10-19	25	No	No	0.708087	0.00102066	0.708128	0.00109578	0.70854	0.00109643
USGS_MACS3	2020-10-19	25	No	No	0.707774	0.000881513	0.707541	0.00093459	0.707905	0.000935073
USGS_MACS3	2020-10-19	25	No	No	0.707916	0.000983081	0.7079	0.0010388	0.708216	0.00103929
USGS_MACS3	2020-10-19	25	No	No	0.708146	0.000927135	0.707925	0.000997453	0.708192	0.00099784
USGS_MACS3	2020-10-19	25	No	No	0.708031	0.00105506	0.707834	0.00112645	0.708054	0.00112682
USGS_MACS3	2020-10-19	25	No	No	0.707894	0.0013253	0.708338	0.00142039	0.708536	0.00142078
USGS_MACS3	2020-10-19	25	No	No	0.708399	0.00103004	0.708065	0.00110435	0.708214	0.0011046
USGS_MACS3	2020-10-19	25	No	No	0.707912	0.00115537	0.707664	0.00132506	0.707765	0.00132525
USGS_MACS3	2020-10-19	25	No	No	0.707994	0.00109443	0.70791	0.00113733	0.707962	0.00113742
USGS_MACS3	2020-10-23	25	No	Yes	0.707655	0.0000812	0.70761	0.0000826	0.707582	0.0000826
USGS_MACS3	2020-10-23	25	No	Yes	0.707695	0.0000824	0.707658	0.0000831	0.707635	0.0000831
USGS_MACS3	2020-10-23	25	No	Yes	0.70769	0.000101086	0.70764	0.000101984	0.707624	0.000101979
USGS_MACS3	2020-10-23	25	No	Yes	0.707638	0.0000899	0.707606	0.0000904	0.707595	0.0000904
USGS_MACS3	2020-10-23	25	No	Yes	0.707695	0.000084941	0.707661	0.0000854	0.707657	0.0000854
USGS_MACS3	2020-10-23	25	No	Yes	0.707618	0.000087	0.707579	0.000087847	0.707582	0.0000878
USGS_MACS3	2020-10-23	25	No	Yes	0.707656	0.0000767	0.707626	0.0000781	0.707632	0.0000781
USGS_MACS3	2020-10-23	25	No	Yes	0.707696	0.0000899	0.707653	0.0000907	0.707667	0.0000907
USGS_MACS3	2020-10-23	25	No	Yes	0.707607	0.0000831	0.707569	0.0000835	0.707592	0.0000835
USGS_MACS3	2020-10-23	25	No	Yes	0.707611	0.0000834	0.70757	0.000084	0.707602	0.000084
USGS_MACS3	2020-10-23	25	No	Yes	0.707652	0.000146303	0.707636	0.000146507	0.707613	0.000146503
USGS_MACS3	2020-10-23	25	No	Yes	0.708012	0.000149186	0.707578	0.000140502	0.707556	0.000140498
USGS_MACS3	2020-10-23	25	No	Yes	0.707656	0.000115767	0.707628	0.000116758	0.707608	0.000116756
USGS_MACS3	2020-10-23	25	No	Yes	0.707634	0.000107494	0.707609	0.000110304	0.707592	0.000110302
USGS_MACS3	2020-10-23	25	No	Yes	0.707631	0.000088	0.707601	0.0000897	0.707585	0.0000897
USGS_MACS3	2020-10-23	25	No	Yes	0.707628	0.000146339	0.707607	0.000147753	0.707593	0.00014775

Sample	Date	Laser Diameter (µm)	Split-Stream	Nitrogen Used	$^{87}Sr/^{86}Sr$ Uncorrected Mean	$^{87}Sr/^{86}Sr$ Uncorrected 2SE	$^{87}Sr/^{86}Sr$ Instrumental Corrected Mean	$^{87}Sr/^{86}Sr$ Instrumental Corrected 2SE	$^{87}Sr/^{86}Sr$ Additional Corrected Mean	$^{87}Sr/^{86}Sr$ Additional Corrected 2SE
USGS_MACS3	2020-10-23	25	No	Yes	0.707992	0.000140	0.707705	0.000136	0.707693	0.000136
USGS_MACS3	2020-10-23	25	No	Yes	0.707672	0.000110	0.707647	0.000112	0.707636	0.000112
USGS_MACS3	2020-10-23	25	No	Yes	0.707635	0.000103	0.707604	0.000106	0.707595	0.000106
USGS_MACS3	2020-10-23	25	No	Yes	0.707636	0.000125	0.707602	0.000128	0.707595	0.000128
USGS_MACS3	2020-10-23	25	No	Yes	0.707618	0.000095	0.707572	0.000101	0.707560	0.000101
USGS_MACS3	2020-10-23	25	No	Yes	0.707624	0.000098	0.707588	0.000100	0.707581	0.000100
USGS_MACS3	2020-10-23	25	No	Yes	0.707585	0.000104	0.707549	0.000104	0.707547	0.000104
USGS_MACS3	2020-10-23	25	No	Yes	0.707540	0.000091	0.707501	0.000093	0.707505	0.000093
USGS_MACS3	2020-10-23	25	No	Yes	0.707700	0.000113	0.707640	0.000113	0.707649	0.000113
USGS_MACS3	2020-10-23	25	No	Yes	0.707636	0.000095	0.707600	0.000096	0.707614	0.000096
USGS_MACS3	2020-10-23	25	No	Yes	0.707673	0.000114	0.707642	0.000116	0.707659	0.000116
USGS_MACS3	2020-10-23	25	No	Yes	0.707621	0.000109	0.707613	0.000110	0.707635	0.000110
USGS_MACS3	2020-10-23	25	No	Yes	0.707558	0.000103	0.707534	0.000104	0.707561	0.000104
USGS_MACS3	2020-10-23	25	No	Yes	0.707630	0.000103	0.707597	0.000104	0.707630	0.000104
USGS_MACS3	2020-10-23	25	No	Yes	0.707651	0.000144	0.707610	0.000143	0.707603	0.000143
USGS_MACS3	2020-10-23	25	No	Yes	0.707579	0.000135	0.707538	0.000136	0.707517	0.000136
USGS_MACS3	2020-10-23	25	No	Yes	0.707562	0.000133	0.707533	0.000134	0.707498	0.000134
USGS_MACS3	2020-10-23	25	No	Yes	0.707612	0.000142	0.707585	0.000143	0.707537	0.000143
USGS_MACS3	2020-10-23	25	No	Yes	0.707683	0.000142	0.707679	0.000145	0.707624	0.000145
USGS_MACS3	2020-10-23	25	No	Yes	0.707653	0.000148	0.707633	0.000150	0.707581	0.000150
USGS_MACS3	2020-10-23	25	No	Yes	0.707588	0.000155	0.707556	0.000156	0.707518	0.000156
USGS_MACS3	2020-10-23	20	No	Yes	0.707866	0.000189	0.707604	0.000192	0.707585	0.000192
USGS_MACS3	2020-10-23	20	No	Yes	0.707673	0.000185	0.707586	0.000190	0.707584	0.000190
USGS_MACS3	2020-10-23	20	No	Yes	0.707734	0.000163	0.707674	0.000170	0.707685	0.000170
USGS_MACS3	2020-10-23	20	No	Yes	0.707579	0.000166	0.707560	0.000164	0.707581	0.000164
USGS_MACS3	2020-10-23	20	No	Yes	0.707517	0.000183	0.707483	0.000186	0.707510	0.000186
USGS_MACS3	2020-10-23	20	No	Yes	0.707654	0.000184	0.707610	0.000191	0.707635	0.000191
USGS_MACS3	2020-10-23	20	No	Yes	0.707696	0.000182	0.707668	0.000189	0.707684	0.000189
USGS_MACS3	2020-10-23	15	No	Yes	0.708061	0.000802	0.707977	0.000841	0.707980	0.000841
USGS_MACS3	2020-10-23	15	No	Yes	0.707583	0.000586	0.707338	0.000609	0.707327	0.000609
USGS_MACS3	2020-10-23	15	No	Yes	0.707812	0.000498	0.707828	0.000508	0.707802	0.000508
USGS_MACS3	2020-10-23	15	No	Yes	0.707505	0.000628	0.707535	0.000651	0.707495	0.000651
USGS_MACS3	2020-10-23	15	No	Yes	0.707691	0.000638	0.707497	0.000671	0.707445	0.000671
USGS_MACS3	2020-10-23	15	No	Yes	0.707399	0.000817	0.707308	0.000881	0.707248	0.000881
USGS_MACS3	2020-10-23	15	No	Yes	0.708203	0.000660	0.708154	0.000689	0.708094	0.000689
USGS_MACS3	2020-10-23	8	No	Yes	0.703615	0.031762	0.702104	0.035296	0.702055	0.035293
USGS_MACS3	2020-10-23	12	No	Yes	0.708011	0.001841	0.708222	0.001947	0.708179	0.001947
USGS_MACS3	2020-10-23	8	No	Yes	0.719214	0.021563	0.710840	0.025323	0.710818	0.025323
USGS_MACS3	2020-10-23	12	No	Yes	0.708141	0.001664	0.707936	0.001845	0.707920	0.001845
USGS_MACS3	2020-10-23	8	No	Yes	0.718422	0.043345	0.706291	0.045027	0.706295	0.045027
USGS_MACS3	2020-10-23	12	No	Yes	0.708729	0.002062	0.709482	0.002159	0.709492	0.002159
USGS_MACS3	2020-10-23	8	No	Yes	0.721771	0.041394	0.704328	0.044121	0.704349	0.044123
USGS_MACS3	2020-10-23	12	No	Yes	0.709344	0.002413	0.709809	0.002591	0.709831	0.002591
USGS_MACS3	2020-10-23	8	No	Yes	0.730424	0.025306	0.744942	0.026611	0.744963	0.026612

Sample	Date	Laser Diameter (µm)	Split-Stream	Nitrogen Used	$^{87}Sr/^{86}Sr$ Uncorrected Mean	$^{87}Sr/^{86}Sr$ Uncorrected 2SE	$^{87}Sr/^{86}Sr$ Instrumental Corrected Mean	$^{87}Sr/^{86}Sr$ Instrumental Corrected 2SE	$^{87}Sr/^{86}Sr$ Additional Corrected Mean	$^{87}Sr/^{86}Sr$ Additional Corrected 2SE
USGS_MACS3	2020-10-23	12	No	Yes	0.708370	0.001795	0.708799	0.001902	0.708815	0.001902
USGS_MACS3	2020-10-23	8	No	Yes	0.673942	0.078602	0.667626	0.077471	0.667629	0.077471
USGS_MACS3	2020-10-23	12	No	Yes	0.708116	0.002111	0.708088	0.002253	0.708086	0.002253
USGS_MACS3	2020-10-23	8	No	Yes	0.697573	0.031032	0.687625	0.032133	0.687606	0.032133
USGS_MACS3	2020-10-23	12	No	Yes	0.709427	0.002832	0.709877	0.002938	0.709851	0.002937

LASS-ICP-MS long-term isotope data for the in-house gastropod shell HSSr

Sample	Date	Laser Diameter (µm)	Split-Stream	Nitrogen Used	$^{87}Sr/^{86}Sr$ Uncorrected Mean	$^{87}Sr/^{86}Sr$ Uncorrected 2SE	$^{87}Sr/^{86}Sr$ Instrumental Corrected Mean	$^{87}Sr/^{86}Sr$ Instrumental Corrected 2SE	$^{87}Sr/^{86}Sr$ Additional Corrected Mean	$^{87}Sr/^{86}Sr$ Additional Corrected 2SE
HSSr	2020-08-18	8	Yes	No	0.708913	0.002088	0.708740	0.002215	0.708757	0.002215
HSSr	2020-08-18	8	Yes	No	0.709772	0.001938	0.709356	0.002095	0.709396	0.002095
HSSr	2020-08-18	8	Yes	No	0.708985	0.001558	0.709057	0.001613	0.709121	0.001613
HSSr	2020-08-18	8	Yes	No	0.709017	0.001571	0.709196	0.001679	0.709284	0.001679
HSSr	2020-08-18	8	Yes	No	0.709239	0.001483	0.709448	0.001636	0.709560	0.001636
HSSr	2020-08-18	12	Yes	No	0.709736	0.000783	0.709516	0.000850	0.709414	0.000850
HSSr	2020-08-18	12	Yes	No	0.709313	0.000870	0.709185	0.000918	0.709106	0.000918
HSSr	2020-08-18	12	Yes	No	0.709363	0.000784	0.709257	0.000843	0.709202	0.000843
HSSr	2020-08-18	12	Yes	No	0.709368	0.000815	0.708955	0.000887	0.708924	0.000887
HSSr	2020-08-18	12	Yes	No	0.709195	0.000924	0.709088	0.001040	0.709081	0.001040
HSSr	2020-08-18	15	Yes	No	0.709471	0.000543	0.709435	0.000581	0.709441	0.000581
HSSr	2020-08-18	15	Yes	No	0.709207	0.000618	0.708976	0.000656	0.708986	0.000656
HSSr	2020-08-18	15	Yes	No	0.709181	0.000552	0.709117	0.000567	0.709128	0.000567
HSSr	2020-08-18	15	Yes	No	0.708741	0.000507	0.708759	0.000554	0.708773	0.000554
HSSr	2020-08-18	15	Yes	No	0.709450	0.000516	0.709200	0.000561	0.709216	0.000561
HSSr	2020-08-18	20	Yes	No	0.709375	0.000399	0.709257	0.000410	0.709253	0.000410
HSSr	2020-08-18	20	Yes	No	0.709558	0.000368	0.709495	0.000399	0.709492	0.000399
HSSr	2020-08-18	20	Yes	No	0.709280	0.000337	0.709202	0.000358	0.709202	0.000358
HSSr	2020-08-18	20	Yes	No	0.709187	0.000343	0.709168	0.000360	0.709170	0.000360
HSSr	2020-08-18	20	Yes	No	0.709329	0.000331	0.709252	0.000354	0.709256	0.000354
HSSr	2020-08-18	25	Yes	No	0.709166	0.000217	0.709074	0.000225	0.709157	0.000225
HSSr	2020-08-18	25	Yes	No	0.709286	0.000218	0.709207	0.000234	0.709237	0.000234
HSSr	2020-08-18	25	Yes	No	0.709222	0.000291	0.709041	0.000317	0.709045	0.000317
HSSr	2020-08-18	25	Yes	No	0.709470	0.000299	0.709294	0.000314	0.709249	0.000314
HSSr	2020-08-18	25	Yes	No	0.709327	0.000208	0.709253	0.000221	0.709167	0.000221
HSSr	2020-08-18	25	Yes	No	0.709485	0.000279	0.709371	0.000288	0.709355	0.000288
HSSr	2020-08-18	25	Yes	No	0.709170	0.000237	0.709070	0.000256	0.709055	0.000256
HSSr	2020-08-18	25	Yes	No	0.709141	0.000236	0.709036	0.000248	0.709024	0.000248
HSSr	2020-08-18	25	Yes	No	0.709277	0.000211	0.709176	0.000219	0.709166	0.000219
HSSr	2020-08-18	25	Yes	No	0.709283	0.000199	0.709188	0.000201	0.709180	0.000201
HSSr	2020-10-23	8	Yes	Yes	0.709431	0.001560	0.709161	0.001620	0.709239	0.001620
HSSr	2020-10-23	8	Yes	Yes	0.708416	0.001431	0.708535	0.001529	0.708613	0.001529
HSSr	2020-10-23	8	Yes	Yes	0.709158	0.001318	0.708869	0.001426	0.708948	0.001427
HSSr	2020-10-23	8	Yes	Yes	0.709436	0.001712	0.709602	0.001815	0.709680	0.001815
HSSr	2020-10-23	8	Yes	Yes	0.709804	0.001779	0.709521	0.001955	0.709601	0.001955
HSSr	2020-10-23	8	Yes	Yes	0.709604	0.001479	0.709251	0.001514	0.709330	0.001514
HSSr	2020-10-23	8	Yes	Yes	0.709401	0.001468	0.708981	0.001481	0.709061	0.001481
HSSr	2020-10-23	12	Yes	Yes	0.709235	0.001120	0.709226	0.001176	0.709304	0.001176
HSSr	2020-10-23	12	Yes	Yes	0.709220	0.000884	0.709186	0.000932	0.709264	0.000933
HSSr	2020-10-23	12	Yes	Yes	0.709266	0.000843	0.709296	0.000921	0.709374	0.000921
HSSr	2020-10-23	12	Yes	Yes	0.709348	0.000986	0.709292	0.001058	0.709371	0.001058
HSSr	2020-10-23	12	Yes	Yes	0.709191	0.000880	0.708711	0.000955	0.708791	0.000955

Sample	Date	Laser Diameter (µm)	Split-Stream	Nitrogen Used	$^{87}Sr/^{86}Sr$ Uncorrected Mean	$^{87}Sr/^{86}Sr$ Uncorrected 2SE	$^{87}Sr/^{86}Sr$ Instrumental Corrected Mean	$^{87}Sr/^{86}Sr$ Instrumental Corrected 2SE	$^{87}Sr/^{86}Sr$ Additional Corrected Mean	$^{87}Sr/^{86}Sr$ Additional Corrected 2SE
HSSr	2020-10-23	12	Yes	Yes	0.709417	0.000973	0.709234	0.000992	0.709313	0.000992
HSSr	2020-10-23	12	Yes	Yes	0.709575	0.000716	0.709340	0.000774	0.709420	0.000774
HSSr	2020-10-23	15	Yes	Yes	0.709679	0.000508	0.709584	0.000550	0.709660	0.000550
HSSr	2020-10-23	15	Yes	Yes	0.708903	0.000472	0.708997	0.000506	0.709073	0.000506
HSSr	2020-10-23	15	Yes	Yes	0.709445	0.000454	0.709420	0.000486	0.709497	0.000486
HSSr	2020-10-23	15	Yes	Yes	0.708890	0.000504	0.708775	0.000509	0.708852	0.000509
HSSr	2020-10-23	15	Yes	Yes	0.709055	0.000520	0.709084	0.000547	0.709161	0.000547
HSSr	2020-10-23	15	Yes	Yes	0.708691	0.000521	0.708698	0.000548	0.708775	0.000548
HSSr	2020-10-23	15	Yes	Yes	0.709287	0.000498	0.709056	0.000520	0.709134	0.000520
HSSr	2020-10-23	20	Yes	Yes	0.709144	0.000253	0.708978	0.000265	0.709052	0.000265
HSSr	2020-10-23	20	Yes	Yes	0.709275	0.000297	0.709207	0.000327	0.709282	0.000327
HSSr	2020-10-23	20	Yes	Yes	0.709279	0.000286	0.709310	0.000303	0.709385	0.000303
HSSr	2020-10-23	20	Yes	Yes	0.709090	0.000306	0.708959	0.000316	0.709034	0.000316
HSSr	2020-10-23	20	Yes	Yes	0.709070	0.000312	0.708888	0.000333	0.708963	0.000333
HSSr	2020-10-23	20	Yes	Yes	0.709294	0.000298	0.709182	0.000318	0.709258	0.000318
HSSr	2020-10-23	20	Yes	Yes	0.709065	0.000317	0.709040	0.000316	0.709115	0.000316
HSSr	2020-10-23	25	Yes	Yes	0.709282	0.000160	0.709196	0.000167	0.709270	0.000167
HSSr	2020-10-23	25	Yes	Yes	0.709254	0.000202	0.709196	0.000210	0.709270	0.000210
HSSr	2020-10-26	8	Yes	Yes	0.706880	0.004491	0.705912	0.004670	0.705938	0.004670
HSSr	2020-10-26	8	Yes	Yes	0.711277	0.003894	0.710142	0.004326	0.710165	0.004326
HSSr	2020-10-26	8	Yes	Yes	0.709496	0.003223	0.709598	0.003498	0.709617	0.003498
HSSr	2020-10-26	8	Yes	Yes	0.710528	0.003653	0.709588	0.003895	0.709604	0.003895
HSSr	2020-10-26	8	Yes	Yes	0.708058	0.006443	0.709209	0.007185	0.709221	0.007185
HSSr	2020-10-26	12	Yes	Yes	0.709373	0.001159	0.709002	0.001227	0.709216	0.001228
HSSr	2020-10-26	15	Yes	Yes	0.709126	0.000507	0.708892	0.000551	0.709029	0.000551
HSSr	2020-10-26	15	Yes	Yes	0.709146	0.000361	0.708986	0.000384	0.709134	0.000385
HSSr	2020-10-26	15	Yes	Yes	0.709129	0.000314	0.708937	0.000330	0.709097	0.000330
HSSr	2020-10-26	15	Yes	Yes	0.709254	0.000396	0.709194	0.000420	0.709365	0.000420
HSSr	2020-10-26	15	Yes	Yes	0.709140	0.000424	0.709021	0.000443	0.709204	0.000443
HSSr	2020-10-26	15	Yes	Yes	0.709057	0.000547	0.708856	0.000567	0.709051	0.000567
HSSr	2020-10-26	15	Yes	Yes	0.708970	0.000358	0.708749	0.000379	0.708955	0.000379
HSSr	2020-10-26	15	Yes	Yes	0.709165	0.001060	0.709025	0.001137	0.709067	0.001137
HSSr	2020-10-26	15	Yes	Yes	0.709200	0.001237	0.708994	0.001371	0.709034	0.001371
HSSr	2020-10-26	15	Yes	Yes	0.709395	0.001453	0.709134	0.001622	0.709171	0.001622
HSSr	2020-10-26	15	Yes	Yes	0.709581	0.001592	0.709625	0.001635	0.709658	0.001635
HSSr	2020-10-26	15	Yes	Yes	0.709777	0.001323	0.709839	0.001432	0.709869	0.001432
HSSr	2020-10-26	20	Yes	Yes	0.709433	0.000285	0.709250	0.000306	0.709310	0.000306
HSSr	2020-10-26	20	Yes	Yes	0.709192	0.000225	0.709059	0.000237	0.709130	0.000237
HSSr	2020-10-26	20	Yes	Yes	0.709125	0.000205	0.709040	0.000220	0.709123	0.000220
HSSr	2020-10-26	20	Yes	Yes	0.709239	0.000235	0.709144	0.000240	0.709238	0.000240
HSSr	2020-10-26	20	Yes	Yes	0.709193	0.000251	0.709098	0.000270	0.709204	0.000270
HSSr	2020-10-26	20	Yes	Yes	0.709533	0.000325	0.709448	0.000326	0.709565	0.000326
HSSr	2020-10-26	20	Yes	Yes	0.709108	0.000227	0.708992	0.000241	0.709120	0.000241
HSSr	2020-10-26	20	Yes	Yes	0.709034	0.000678	0.708900	0.000722	0.708958	0.000722
HSSr	2020-10-26	20	Yes	Yes	0.708691	0.000574	0.708522	0.000617	0.708577	0.000617

Sample	Date	Laser Diameter (µm)	Split-Stream	Nitrogen Used	$^{87}Sr/^{86}Sr$ Uncorrected Mean	$^{87}Sr/^{86}Sr$ Uncorrected 2SE	$^{87}Sr/^{86}Sr$ Instrumental Corrected Mean	$^{87}Sr/^{86}Sr$ Instrumental Corrected 2SE	$^{87}Sr/^{86}Sr$ Additional Corrected Mean	$^{87}Sr/^{86}Sr$ Additional Corrected 2SE
HSSr	2020-10-26	20	Yes	Yes	0.709224	0.000578	0.709233	0.000613	0.709284	0.000613
HSSr	2020-10-26	20	Yes	Yes	0.709222	0.000631	0.709227	0.000662	0.709275	0.000662
HSSr	2020-10-26	20	Yes	Yes	0.709763	0.000974	0.709467	0.001012	0.709512	0.001012
HSSr	2020-10-26	25	Yes	Yes	0.709260	0.000175	0.709117	0.000182	0.709099	0.000182
HSSr	2020-10-26	25	Yes	Yes	0.709268	0.000152	0.709167	0.000162	0.709161	0.000162
HSSr	2020-10-26	25	Yes	Yes	0.709275	0.000136	0.709194	0.000143	0.709199	0.000143
HSSr	2020-10-26	25	Yes	Yes	0.709328	0.000165	0.709214	0.000176	0.709231	0.000176
HSSr	2020-10-26	25	Yes	Yes	0.709300	0.000177	0.709189	0.000183	0.709217	0.000183
HSSr	2020-10-26	25	Yes	Yes	0.709109	0.000214	0.708935	0.000228	0.708975	0.000228
HSSr	2020-10-26	25	Yes	Yes	0.709268	0.000159	0.709155	0.000166	0.709206	0.000166
HSSr	2020-10-26	25	Yes	Yes	0.709148	0.000399	0.708996	0.000417	0.709069	0.000417
HSSr	2020-10-26	25	Yes	Yes	0.709337	0.000351	0.709286	0.000373	0.709356	0.000373
HSSr	2020-10-26	25	Yes	Yes	0.709557	0.000387	0.709379	0.000413	0.709446	0.000413
HSSr	2020-10-26	25	Yes	Yes	0.709050	0.000426	0.708888	0.000448	0.708952	0.000448
HSSr	2020-10-26	25	Yes	Yes	0.709108	0.000565	0.709000	0.000598	0.709060	0.000598
HSSr	2020-11-02	8	Yes	Yes	0.709101	0.000790	0.709011	0.000826	0.709147	0.000826
HSSr	2020-11-02	8	Yes	Yes	0.709269	0.000702	0.709103	0.000739	0.709241	0.000739
HSSr	2020-11-02	8	Yes	Yes	0.709178	0.000799	0.709263	0.000848	0.709402	0.000848
HSSr	2020-11-02	8	Yes	Yes	0.708658	0.000796	0.708497	0.000849	0.708637	0.000849
HSSr	2020-11-02	8	Yes	Yes	0.709462	0.000765	0.709325	0.000816	0.709468	0.000816
HSSr	2020-11-02	8	Yes	Yes	0.709089	0.000776	0.708868	0.000840	0.709012	0.000840
HSSr	2020-11-02	8	Yes	Yes	0.709265	0.000841	0.709156	0.000909	0.709301	0.000910
HSSr	2020-11-02	25	Yes	Yes	0.709306	0.000137	0.709175	0.000144	0.709101	0.000144
HSSr	2020-11-02	25	Yes	Yes	0.709326	0.000144	0.709236	0.000144	0.709168	0.000144
HSSr	2020-11-02	25	Yes	Yes	0.709272	0.000150	0.709122	0.000152	0.709060	0.000152
HSSr	2020-11-02	25	Yes	Yes	0.709223	0.000151	0.709041	0.000160	0.708985	0.000160
HSSr	2020-11-02	25	Yes	Yes	0.709229	0.000164	0.709079	0.000173	0.709029	0.000173
HSSr	2020-11-02	25	Yes	Yes	0.709255	0.000145	0.709155	0.000150	0.709111	0.000150
HSSr	2020-11-02	25	Yes	Yes	0.709308	0.000163	0.709219	0.000166	0.709181	0.000166
HSSr	2020-11-02	25	Yes	Yes	0.709315	0.000093	0.709204	0.000095	0.709162	0.000095
HSSr	2020-11-02	25	Yes	Yes	0.709301	0.000087	0.709192	0.000090	0.709163	0.000090
HSSr	2020-11-02	25	Yes	Yes	0.709294	0.000078	0.709193	0.000082	0.709177	0.000082
HSSr	2020-11-02	25	Yes	Yes	0.709296	0.000079	0.709193	0.000085	0.709191	0.000085
HSSr	2020-11-02	25	Yes	Yes	0.709308	0.000080	0.709217	0.000081	0.709232	0.000081
HSSr	2020-11-02	25	Yes	Yes	0.709227	0.000087	0.709089	0.000092	0.709124	0.000092
HSSr	2020-11-02	25	Yes	Yes	0.709233	0.000078	0.709113	0.000081	0.709167	0.000081
HSSr	2020-11-02	25	Yes	Yes	0.709207	0.000097	0.709119	0.000100	0.709179	0.000100
HSSr	2020-11-02	25	Yes	Yes	0.709249	0.000103	0.709140	0.000106	0.709187	0.000106
HSSr	2020-11-02	25	Yes	Yes	0.709199	0.000102	0.709127	0.000107	0.709160	0.000107
HSSr	2020-11-02	25	Yes	Yes	0.709277	0.000107	0.709182	0.000109	0.709201	0.000109
HSSr	2020-11-02	25	Yes	Yes	0.709233	0.000104	0.709133	0.000107	0.709139	0.000107
HSSr	2020-11-02	25	Yes	Yes	0.709276	0.000109	0.709170	0.000108	0.709163	0.000108
HSSr	2020-11-02	25	Yes	Yes	0.709312	0.000098	0.709220	0.000100	0.709199	0.000100
HSSr	2020-11-02	25	Yes	Yes	0.709268	0.000109	0.709183	0.000115	0.709133	0.000115
HSSr	2020-11-02	25	Yes	Yes	0.709317	0.000101	0.709244	0.000107	0.709197	0.000107

Sample	Date	Laser Diameter (μm)	Split-Stream	Nitrogen Used	$^{87}Sr/^{86}Sr$ Uncorrected Mean	$^{87}Sr/^{86}Sr$ Uncorrected 2SE	$^{87}Sr/^{86}Sr$ Instrumental Corrected Mean	$^{87}Sr/^{86}Sr$ Instrumental Corrected 2SE	$^{87}Sr/^{86}Sr$ Additional Corrected Mean	$^{87}Sr/^{86}Sr$ Additional Corrected 2SE
HSSr	2020-11-02	25	Yes	Yes	0.709318	0.000113	0.709239	0.000113	0.709197	0.000113
HSSr	2020-11-02	25	Yes	Yes	0.709253	0.000112	0.709183	0.000118	0.709152	0.000118
HSSr	2020-11-02	25	Yes	Yes	0.709330	0.000105	0.709266	0.000110	0.709251	0.000110
HSSr	2020-11-02	25	Yes	Yes	0.709202	0.000118	0.709111	0.000121	0.709119	0.000121
HSSr	2020-11-02	25	Yes	Yes	0.709193	0.000117	0.709131	0.000121	0.709162	0.000121
HSSr	2020-11-03	8	Yes	Yes	0.709768	0.000836	0.709612	0.000924	0.709390	0.000924
HSSr	2020-11-03	8	Yes	Yes	0.709030	0.000795	0.709139	0.000826	0.709018	0.000826
HSSr	2020-11-03	8	Yes	Yes	0.709338	0.000783	0.709333	0.000840	0.709315	0.000840
HSSr	2020-11-03	8	Yes	Yes	0.708836	0.000792	0.708869	0.000876	0.708952	0.000876
HSSr	2020-11-03	8	Yes	Yes	0.709274	0.000717	0.709028	0.000769	0.709214	0.000770
HSSr	2020-11-03	8	Yes	Yes	0.709190	0.000758	0.708626	0.000829	0.708913	0.000829
HSSr	2020-11-03	8	Yes	Yes	0.709336	0.000775	0.709074	0.000853	0.709464	0.000853
HSSr	2020-11-03	12	Yes	Yes	0.709122	0.000334	0.709043	0.000357	0.709302	0.000357
HSSr	2020-11-03	12	Yes	Yes	0.709112	0.000356	0.708866	0.000378	0.709054	0.000379
HSSr	2020-11-03	12	Yes	Yes	0.709300	0.000361	0.709148	0.000382	0.709265	0.000382
HSSr	2020-11-03	12	Yes	Yes	0.709063	0.000338	0.709030	0.000364	0.709077	0.000364
HSSr	2020-11-03	12	Yes	Yes	0.709101	0.000353	0.708962	0.000374	0.708938	0.000374
HSSr	2020-11-03	12	Yes	Yes	0.709709	0.000350	0.709496	0.000385	0.709401	0.000385
HSSr	2020-11-03	12	Yes	Yes	0.709411	0.000343	0.709368	0.000376	0.709202	0.000376
HSSr	2020-11-03	15	Yes	Yes	0.709211	0.000095	0.709086	0.000094	0.709169	0.000094
HSSr	2020-11-03	15	Yes	Yes	0.709302	0.000100	0.709168	0.000109	0.709194	0.000109
HSSr	2020-11-03	15	Yes	Yes	0.709287	0.000094	0.709158	0.000095	0.709149	0.000095
HSSr	2020-11-03	15	Yes	Yes	0.709367	0.000099	0.709248	0.000100	0.709230	0.000100
HSSr	2020-11-03	15	Yes	Yes	0.709212	0.000102	0.709091	0.000105	0.709126	0.000105
HSSr	2020-11-03	15	Yes	Yes	0.709205	0.000071	0.709090	0.000075	0.709140	0.000075
HSSr	2020-11-03	15	Yes	Yes	0.709198	0.000099	0.709089	0.000106	0.709154	0.000106
HSSr	2020-11-03	15	Yes	Yes	0.709270	0.000104	0.709158	0.000111	0.709195	0.000111
HSSr	2020-11-03	15	Yes	Yes	0.709280	0.000232	0.709199	0.000240	0.709281	0.000240
HSSr	2020-11-03	15	Yes	Yes	0.709139	0.000243	0.709006	0.000246	0.709071	0.000246
HSSr	2020-11-03	15	Yes	Yes	0.709220	0.000237	0.709137	0.000243	0.709184	0.000243
HSSr	2020-11-03	15	Yes	Yes	0.709188	0.000244	0.709082	0.000250	0.709111	0.000250
HSSr	2020-11-03	15	Yes	Yes	0.709167	0.000247	0.709094	0.000259	0.709106	0.000259
HSSr	2020-11-03	15	Yes	Yes	0.709431	0.000247	0.709343	0.000259	0.709338	0.000259
HSSr	2020-11-03	15	Yes	Yes	0.709289	0.000260	0.709157	0.000279	0.709133	0.000279
HSSr	2020-11-23	25	Yes	Yes	0.709212	0.000183	0.709145	0.000193	0.709169	0.000193
HSSr	2020-11-23	25	Yes	Yes	0.709429	0.000335	0.709184	0.000366	0.709212	0.000366
HSSr	2020-11-23	25	Yes	Yes	0.709154	0.000195	0.709075	0.000205	0.709126	0.000205
HSSr	2020-11-23	25	Yes	Yes	0.709280	0.000197	0.709178	0.000214	0.709226	0.000214
HSSr	2020-11-23	25	Yes	Yes	0.709131	0.000117	0.709061	0.000122	0.708994	0.000122
HSSr	2020-11-23	25	Yes	Yes	0.709168	0.000114	0.709114	0.000119	0.709047	0.000119
HSSr	2020-11-23	25	Yes	Yes	0.709133	0.000109	0.709090	0.000115	0.709023	0.000115
HSSr	2020-11-23	25	Yes	Yes	0.709235	0.000093	0.709190	0.000098	0.709192	0.000098
HSSr	2020-11-23	25	Yes	Yes	0.709149	0.000099	0.709079	0.000102	0.709081	0.000102
HSSr	2020-11-23	25	Yes	Yes	0.709181	0.000105	0.709109	0.000111	0.709101	0.000111
HSSr	2020-11-23	25	Yes	Yes	0.709207	0.000111	0.709131	0.000113	0.709114	0.000113

Sample	Date	Laser Diameter (µm)	Split-Stream	Nitrogen Used	$^{87}Sr/^{86}Sr$ Uncorrected Mean	$^{87}Sr/^{86}Sr$ Uncorrected 2SE	$^{87}Sr/^{86}Sr$ Instrumental Corrected Mean	$^{87}Sr/^{86}Sr$ Instrumental Corrected 2SE	$^{87}Sr/^{86}Sr$ Additional Corrected Mean	$^{87}Sr/^{86}Sr$ Additional Corrected 2SE
HSSr	2020-11-23	25	Yes	Yes	0.709248	0.000102	0.709170	0.000108	0.709144	0.000108
HSSr	2020-11-23	25	Yes	Yes	0.709251	0.000096	0.709180	0.000098	0.709065	0.000098
HSSr	2020-11-23	25	Yes	Yes	0.709201	0.000090	0.709123	0.000095	0.709083	0.000095
HSSr	2020-11-23	25	Yes	Yes	0.709171	0.000089	0.709102	0.000090	0.709087	0.000090
HSSr	2020-11-23	25	Yes	Yes	0.709166	0.000091	0.709114	0.000094	0.709064	0.000094
HSSr	2020-11-23	25	Yes	Yes	0.709275	0.000095	0.709206	0.000096	0.709269	0.000096
HSSr	2020-11-23	25	Yes	Yes	0.709268	0.000086	0.709190	0.000086	0.709233	0.000086
HSSr	2020-11-23	25	Yes	Yes	0.709192	0.000083	0.709107	0.000084	0.709150	0.000084
HSSr	2020-11-24	25	Yes	Yes	0.709160	0.000095	0.709096	0.000098	0.709068	0.000098
HSSr	2020-11-24	25	Yes	Yes	0.709130	0.000105	0.709059	0.000111	0.709031	0.000111
HSSr	2020-11-24	25	Yes	Yes	0.709175	0.000093	0.709113	0.000097	0.709109	0.000097
HSSr	2020-11-24	25	Yes	Yes	0.709327	0.000090	0.709267	0.000093	0.709167	0.000093
HSSr	2020-11-24	25	Yes	Yes	0.709124	0.000089	0.709057	0.000093	0.709036	0.000093
HSSr	2020-11-24	25	Yes	Yes	0.709101	0.000083	0.709034	0.000088	0.709021	0.000088
HSSr	2020-11-24	25	Yes	Yes	0.709274	0.000089	0.709205	0.000096	0.709150	0.000096
HSSr	2020-11-24	25	Yes	Yes	0.709079	0.000093	0.709008	0.000096	0.708998	0.000096
HSSr	2020-11-24	25	Yes	Yes	0.709258	0.000085	0.709192	0.000089	0.709178	0.000089
HSSr	2020-11-25	10	Yes	Yes	0.709183	0.001012	0.709057	0.001082	0.707210	0.001080
HSSr	2020-11-25	10	Yes	Yes	0.709287	0.001053	0.709063	0.001158	0.710213	0.001160
HSSr	2020-11-25	25	Yes	Yes	0.709197	0.000083	0.709122	0.000082	0.709123	0.000082
HSSr	2020-11-25	25	Yes	Yes	0.709272	0.000091	0.709167	0.000093	0.709167	0.000093
HSSr	2020-11-25	25	Yes	Yes	0.709242	0.000083	0.709135	0.000083	0.709135	0.000083
HSSr	2020-11-25	25	Yes	Yes	0.709175	0.000072	0.709104	0.000074	0.709105	0.000074
HSSr	2020-11-25	25	Yes	Yes	0.709155	0.000083	0.709055	0.000084	0.709071	0.000084
HSSr	2020-11-25	25	Yes	Yes	0.709178	0.000087	0.709088	0.000088	0.709113	0.000088
HSSr	2020-11-25	25	Yes	Yes	0.709195	0.000080	0.709136	0.000080	0.709226	0.000080
HSSr	2020-11-25	25	Yes	Yes	0.709234	0.000077	0.709148	0.000081	0.709164	0.000081
HSSr	2020-11-25	25	Yes	Yes	0.709175	0.000076	0.709092	0.000078	0.709075	0.000078
HSSr	2020-11-25	25	Yes	Yes	0.709184	0.000084	0.709133	0.000088	0.709151	0.000088
HSSr	2020-11-25	25	Yes	Yes	0.709283	0.000084	0.709217	0.000087	0.709213	0.000087
HSSr	2020-11-25	25	Yes	Yes	0.709236	0.000084	0.709152	0.000086	0.709130	0.000086
HSSr	2021-01-05	15	Yes	Yes	0.709288	0.000258	0.709206	0.000273	0.709300	0.000273
HSSr	2021-01-05	15	Yes	Yes	0.709191	0.000274	0.709257	0.000298	0.708863	0.000298
HSSr	2021-01-05	15	Yes	Yes	0.709224	0.000297	0.709149	0.000323	0.709631	0.000323
HSSr	2021-01-05	15	Yes	Yes	0.709011	0.000368	0.708958	0.000385	0.709440	0.000385
HSSr	2021-01-05	15	Yes	Yes	0.709443	0.000349	0.709314	0.000381	0.709796	0.000381
HSSr	2021-01-06	15	Yes	Yes	0.709151	0.000307	0.709085	0.000312	0.709176	0.000312
HSSr	2021-01-06	15	Yes	Yes	0.709021	0.000477	0.708954	0.000502	0.709175	0.000502
HSSr	2021-01-06	15	Yes	Yes	0.709128	0.000459	0.708981	0.000475	0.709082	0.000475
HSSr	2021-01-06	15	Yes	Yes	0.709665	0.000403	0.709402	0.000407	0.709228	0.000407
HSSr	2021-01-06	15	Yes	Yes	0.709482	0.000397	0.709521	0.000423	0.709328	0.000423
HSSr	2021-01-06	15	Yes	Yes	0.709024	0.000392	0.708928	0.000389	0.709067	0.000389
HSSr	2021-01-06	15	Yes	Yes	0.709181	0.000374	0.708854	0.000419	0.709122	0.000420
HSSr	2021-01-06	15	Yes	Yes	0.709650	0.000417	0.709237	0.000445	0.709231	0.000445
HSSr	2021-01-06	15	Yes	Yes	0.709085	0.000352	0.709043	0.000369	0.709176	0.000369

Sample	Date	Laser Diameter (µm)	Split-Stream	Nitrogen Used	$^{87}Sr/^{86}Sr$ Uncorrected Mean	$^{87}Sr/^{86}Sr$ Uncorrected 2SE	$^{87}Sr/^{86}Sr$ Instrumental Corrected Mean	$^{87}Sr/^{86}Sr$ Instrumental Corrected 2SE	$^{87}Sr/^{86}Sr$ Additional Corrected Mean	$^{87}Sr/^{86}Sr$ Additional Corrected 2SE
HSSr	2021-01-06	15	Yes	Yes	0.709123	0.000372	0.708931	0.000407	0.709176	0.000407
HSSr	2021-02-01	15	Yes	Yes	0.709300	0.000500	0.709330	0.000510	0.709390	0.000510
HSSr	2021-02-01	15	Yes	Yes	0.709280	0.000500	0.709090	0.000530	0.709150	0.000530
HSSr	2021-02-01	15	Yes	Yes	0.709050	0.000710	0.709170	0.000750	0.709220	0.000750
HSSr	2021-02-01	15	Yes	Yes	0.709100	0.000740	0.709010	0.000770	0.709070	0.000770
HSSr	2021-02-01	15	Yes	Yes	0.709100	0.000770	0.709270	0.000800	0.709330	0.000800
HSSr	2021-02-01	15	Yes	Yes	0.708800	0.000740	0.708740	0.000760	0.708800	0.000760
HSSr	2021-02-01	15	Yes	Yes	0.709030	0.000920	0.709010	0.000970	0.709070	0.000970
HSSr	2021-02-01	15	Yes	Yes	0.709320	0.000740	0.709170	0.000780	0.709220	0.000780
HSSr	2021-02-02	15	Yes	Yes	0.708970	0.000410	0.708980	0.000420	0.709010	0.000420
HSSr	2021-02-02	15	Yes	Yes	0.709360	0.000440	0.709310	0.000470	0.709350	0.000470
HSSr	2021-02-02	15	Yes	Yes	0.709310	0.000650	0.709200	0.000710	0.709230	0.000710
HSSr	2021-02-02	15	Yes	Yes	0.709370	0.000630	0.709480	0.000680	0.709510	0.000680
HSSr	2021-02-02	15	Yes	Yes	0.709370	0.000740	0.709330	0.000760	0.709360	0.000760
HSSr	2021-02-02	15	Yes	Yes	0.709170	0.000830	0.709230	0.000910	0.709260	0.000910
HSSr	2021-02-02	15	Yes	Yes	0.709460	0.000750	0.709130	0.000760	0.709150	0.000760
HSSr	2021-02-02	15	Yes	Yes	0.709350	0.000540	0.709400	0.000590	0.709430	0.000590
HSSr	2021-02-02	15	Yes	Yes	0.709420	0.000890	0.709280	0.000940	0.709310	0.000940
HSSr	2021-02-02	15	Yes	Yes	0.709920	0.000700	0.709840	0.000740	0.709870	0.000740

LA-ICP-MS (single-stream) long-term isotope data for the in-house gastropod shell HSSr

Sample	Date	Laser Diameter (µm)	Split-Stream	Nitrogen Used	$^{87}Sr/^{86}Sr$ Uncorrected Mean	$^{87}Sr/^{86}Sr$ Uncorrected 2SE	$^{87}Sr/^{86}Sr$ Instrumental Corrected Mean	$^{87}Sr/^{86}Sr$ Instrumental Corrected 2SE	$^{87}Sr/^{86}Sr$ Additional Corrected Mean	$^{87}Sr/^{86}Sr$ Additional Corrected 2SE
HSSr	2020-03-03	25	No	No	0.709171	0.000162	0.708981	0.000164	0.709120	0.000164
HSSr	2020-03-03	25	No	No	0.709162	0.000141	0.709052	0.000153	0.709175	0.000154
HSSr	2020-03-03	25	No	No	0.709182	0.000161	0.709000	0.000175	0.709096	0.000175
HSSr	2020-03-03	25	No	No	0.709318	0.000141	0.709179	0.000148	0.709259	0.000148
HSSr	2020-03-03	25	No	No	0.709319	0.000153	0.709195	0.000165	0.709248	0.000165
HSSr	2020-03-03	25	No	No	0.709323	0.000145	0.709201	0.000157	0.709237	0.000157
HSSr	2020-03-03	25	No	No	0.709235	0.000159	0.709107	0.000168	0.709118	0.000168
HSSr	2020-03-03	25	No	No	0.709331	0.000363	0.709132	0.000393	0.709126	0.000393
HSSr	2020-03-03	25	No	No	0.709171	0.000332	0.709114	0.000348	0.709100	0.000348
HSSr	2020-03-03	25	No	No	0.709211	0.000368	0.709129	0.000384	0.709108	0.000384
HSSr	2020-03-03	25	No	No	0.709336	0.000160	0.709185	0.000173	0.709156	0.000173
HSSr	2020-03-04	25	No	No	0.709144	0.000110	0.709012	0.000114	0.709151	0.000114
HSSr	2020-03-04	25	No	No	0.709236	0.000102	0.709071	0.000109	0.709205	0.000109
HSSr	2020-03-04	25	No	No	0.709194	0.000104	0.709063	0.000109	0.709178	0.000109
HSSr	2020-03-04	25	No	No	0.709222	0.000114	0.709065	0.000121	0.709156	0.000121
HSSr	2020-03-04	25	No	No	0.709284	0.000107	0.709144	0.000112	0.709185	0.000112
HSSr	2020-03-04	50	No	No	0.709371	0.000084	0.709275	0.000090	0.709222	0.000090
HSSr	2020-03-04	50	No	No	0.709254	0.000081	0.709175	0.000087	0.709126	0.000087
HSSr	2020-03-04	50	No	No	0.709306	0.000092	0.709216	0.000096	0.709169	0.000096
HSSr	2020-03-04	50	No	No	0.709354	0.000089	0.709259	0.000095	0.709199	0.000095
HSSr	2020-03-04	50	No	No	0.709307	0.000090	0.709220	0.000094	0.709167	0.000094
HSSr	2020-03-04	50	No	No	0.709354	0.000041	0.709235	0.000042	0.709129	0.000042
HSSr	2020-03-04	50	No	No	0.709360	0.000038	0.709254	0.000040	0.709148	0.000040
HSSr	2020-03-04	50	No	No	0.709355	0.000042	0.709249	0.000043	0.709142	0.000043
HSSr	2020-03-04	50	No	No	0.709349	0.000040	0.709249	0.000041	0.709133	0.000041
HSSr	2020-03-04	50	No	No	0.709317	0.000042	0.709228	0.000043	0.709100	0.000043
HSSr	2020-07-29	25	No	No	0.709132	0.000072	0.709086	0.000077	0.709148	0.000077
HSSr	2020-07-29	25	No	No	0.709238	0.000071	0.709173	0.000076	0.709206	0.000076
HSSr	2020-07-29	25	No	No	0.709169	0.000085	0.709185	0.000089	0.709185	0.000089
HSSr	2020-07-29	25	No	No	0.709255	0.000071	0.709187	0.000076	0.709184	0.000076
HSSr	2020-07-29	25	No	No	0.709218	0.000072	0.709162	0.000077	0.709160	0.000077
HSSr	2020-07-29	25	No	No	0.709222	0.000084	0.709204	0.000088	0.709208	0.000088
HSSr	2020-07-29	25	No	No	0.709218	0.000073	0.709145	0.000078	0.709148	0.000078
HSSr	2020-07-29	25	No	No	0.709238	0.000073	0.709158	0.000077	0.709152	0.000077
HSSr	2020-07-29	25	No	No	0.709301	0.000135	0.709212	0.000146	0.709179	0.000145
HSSr	2020-07-29	25	No	No	0.709342	0.000074	0.709268	0.000078	0.709225	0.000078
HSSr	2020-07-29	25	No	No	0.709242	0.000139	0.709117	0.000149	0.709117	0.000149
HSSr	2020-07-29	25	No	No	0.709259	0.000074	0.709154	0.000079	0.709180	0.000079
HSSr	2020-07-29	25	No	No	0.709215	0.000072	0.709110	0.000078	0.709168	0.000078
HSSr	2020-07-29	25	No	No	0.709165	0.000050	0.709091	0.000053	0.709167	0.000053
HSSr	2020-07-29	25	No	No	0.709191	0.000052	0.709099	0.000055	0.709174	0.000055
HSSr	2020-07-29	25	No	No	0.709123	0.000077	0.709061	0.000083	0.709133	0.000083

Sample	Date	Laser Diameter (μm)	Split-Stream	Nitrogen Used	$^{87}Sr/^{86}Sr$ Uncorrected Mean	$^{87}Sr/^{86}Sr$ Uncorrected 2SE	$^{87}Sr/^{86}Sr$ Instrumental Corrected Mean	$^{87}Sr/^{86}Sr$ Instrumental Corrected 2SE	$^{87}Sr/^{86}Sr$ Additional Corrected Mean	$^{87}Sr/^{86}Sr$ Additional Corrected 2SE
HSSr	2020-07-29	25	No	No	0.709193	0.000054	0.709103	0.000057	0.709173	0.000057
HSSr	2020-07-29	25	No	No	0.709198	0.000055	0.709108	0.000058	0.709178	0.000058
HSSr	2020-07-29	25	No	No	0.709226	0.000079	0.709220	0.000084	0.709287	0.000084
HSSr	2020-07-29	25	No	No	0.709208	0.000055	0.709138	0.000058	0.709203	0.000058
HSSr	2020-07-29	25	No	No	0.709166	0.000055	0.709091	0.000059	0.709155	0.000059
HSSr	2020-07-29	25	No	No	0.709252	0.000132	0.709162	0.000142	0.709224	0.000142
HSSr	2020-07-29	25	No	No	0.709174	0.000056	0.709098	0.000061	0.709159	0.000061
HSSr	2020-07-29	25	No	No	0.709280	0.000124	0.709139	0.000133	0.709197	0.000133
HSSr	2020-07-29	25	No	No	0.709157	0.000057	0.709069	0.000060	0.709126	0.000060
HSSr	2020-07-29	25	No	No	0.709218	0.000057	0.709148	0.000061	0.709203	0.000061
HSSr	2020-07-30	25	No	No	0.709180	0.000069	0.709093	0.000074	0.709200	0.000074
HSSr	2020-07-30	25	No	No	0.709132	0.000072	0.709041	0.000078	0.709136	0.000078
HSSr	2020-07-30	25	No	No	0.709213	0.000097	0.709155	0.000103	0.709212	0.000103
HSSr	2020-07-30	25	No	No	0.709179	0.000074	0.709104	0.000078	0.709147	0.000078
HSSr	2020-07-30	25	No	No	0.709240	0.000076	0.709167	0.000080	0.709194	0.000080
HSSr	2020-07-30	25	No	No	0.709259	0.000095	0.709206	0.000100	0.709208	0.000100
HSSr	2020-07-30	25	No	No	0.709213	0.000078	0.709117	0.000083	0.709110	0.000083
HSSr	2020-07-30	25	No	No	0.709308	0.000078	0.709232	0.000084	0.709216	0.000084
HSSr	2020-07-30	25	No	No	0.709428	0.000190	0.709333	0.000202	0.709314	0.000202
HSSr	2020-07-30	25	No	No	0.709245	0.000088	0.709176	0.000093	0.709160	0.000093
HSSr	2020-07-30	25	No	No	0.709375	0.000183	0.709269	0.000197	0.709268	0.000197
HSSr	2020-07-30	25	No	No	0.709282	0.000086	0.709199	0.000092	0.709224	0.000092
HSSr	2020-07-30	25	No	No	0.709170	0.000084	0.709063	0.000090	0.709111	0.000090
HSSr	2020-07-31	25	No	No	0.709301	0.000102	0.709137	0.000107	0.709192	0.000107
HSSr	2020-07-31	25	No	No	0.709239	0.000103	0.709083	0.000111	0.709152	0.000111
HSSr	2020-07-31	25	No	No	0.709293	0.000106	0.709151	0.000113	0.709179	0.000113
HSSr	2020-07-31	25	No	No	0.709300	0.000101	0.709157	0.000108	0.709187	0.000109
HSSr	2020-07-31	25	No	No	0.709271	0.000100	0.709105	0.000104	0.709194	0.000105
HSSr	2020-07-31	25	No	No	0.709204	0.000093	0.709046	0.000100	0.709145	0.000100
HSSr	2020-07-31	25	No	No	0.709330	0.000104	0.709172	0.000109	0.709181	0.000109
HSSr	2020-07-31	25	No	No	0.709268	0.000097	0.709129	0.000104	0.709226	0.000104
HSSr	2020-07-31	25	No	No	0.709001	0.000095	0.708929	0.000103	0.709134	0.000103
HSSr	2020-10-19	25	No	No	0.708309	0.001675	0.708383	0.001861	0.709040	0.001863
HSSr	2020-10-19	25	No	No	0.708803	0.001546	0.708152	0.001674	0.708760	0.001676
HSSr	2020-10-19	25	No	No	0.708881	0.001355	0.709021	0.001570	0.709581	0.001571
HSSr	2020-10-19	25	No	No	0.708474	0.001370	0.708471	0.001526	0.708982	0.001527
HSSr	2020-10-19	25	No	No	0.709063	0.001373	0.708932	0.001480	0.709395	0.001481
HSSr	2020-10-19	25	No	No	0.708888	0.001454	0.708851	0.001569	0.709266	0.001570
HSSr	2020-10-19	25	No	No	0.709079	0.001263	0.709029	0.001405	0.709371	0.001405
HSSr	2020-10-19	25	No	No	0.708428	0.001243	0.708848	0.001308	0.709142	0.001309
HSSr	2020-10-19	25	No	No	0.708489	0.001222	0.708880	0.001321	0.709126	0.001322
HSSr	2020-10-19	25	No	No	0.708945	0.001392	0.708822	0.001395	0.709019	0.001396
HSSr	2020-10-19	25	No	No	0.709353	0.000204	0.709267	0.000209	0.709205	0.000209
HSSr	2020-10-19	25	No	No	0.709243	0.000198	0.709157	0.000204	0.709117	0.000204
HSSr	2020-10-19	25	No	No	0.709293	0.000195	0.709245	0.000204	0.709227	0.000204

Sample	Date	Laser Diameter (μm)	Split-Stream	Nitrogen Used	$^{87}Sr/^{86}Sr$ Uncorrected Mean	$^{87}Sr/^{86}Sr$ Uncorrected 2SE	$^{87}Sr/^{86}Sr$ Instrumental Corrected Mean	$^{87}Sr/^{86}Sr$ Instrumental Corrected 2SE	$^{87}Sr/^{86}Sr$ Additional Corrected Mean	$^{87}Sr/^{86}Sr$ Additional Corrected 2SE
HSSr	2020-10-19	25	No	No	0.709286	0.000188	0.709251	0.000195	0.709253	0.000195
HSSr	2020-10-19	25	No	No	0.709163	0.000201	0.709093	0.000218	0.709115	0.000218
HSSr	2020-10-19	25	No	No	0.709242	0.000205	0.709115	0.000214	0.709153	0.000214
HSSr	2020-10-19	25	No	No	0.709130	0.000213	0.709009	0.000229	0.709058	0.000229
HSSr	2020-10-19	25	No	No	0.709333	0.000209	0.709189	0.000229	0.709235	0.000229
HSSr	2020-10-19	25	No	No	0.709125	0.000208	0.708996	0.000219	0.709034	0.000219
HSSr	2020-10-19	25	No	No	0.709417	0.000209	0.709320	0.000224	0.709344	0.000224
HSSr	2020-10-19	25	No	No	0.708893	0.000579	0.708849	0.000601	0.708999	0.000601
HSSr	2020-10-19	25	No	No	0.709165	0.000502	0.708890	0.000526	0.709059	0.000526
HSSr	2020-10-19	25	No	No	0.709192	0.000490	0.709178	0.000530	0.709367	0.000530
HSSr	2020-10-19	25	No	No	0.709090	0.000454	0.708949	0.000482	0.709155	0.000482
HSSr	2020-10-19	25	No	No	0.709328	0.000525	0.709306	0.000547	0.709532	0.000547
HSSr	2020-10-19	25	No	No	0.709060	0.000512	0.708896	0.000546	0.709141	0.000547
HSSr	2020-10-19	25	No	No	0.708712	0.000522	0.708757	0.000541	0.709029	0.000541
HSSr	2020-10-19	25	No	No	0.708928	0.000496	0.708773	0.000517	0.709064	0.000517
HSSr	2020-10-19	25	No	No	0.709141	0.000467	0.708886	0.000511	0.709195	0.000512
HSSr	2020-10-19	25	No	No	0.709052	0.000456	0.708870	0.000489	0.709199	0.000490
HSSr	2020-10-19	25	No	No	0.708358	0.000631	0.708431	0.000674	0.708917	0.000674
HSSr	2020-10-19	25	No	No	0.709192	0.000678	0.709044	0.000738	0.709481	0.000738
HSSr	2020-10-19	25	No	No	0.708684	0.000652	0.708613	0.000685	0.709001	0.000685
HSSr	2020-10-19	25	No	No	0.708846	0.000610	0.708787	0.000661	0.709128	0.000661
HSSr	2020-10-19	25	No	No	0.709168	0.000617	0.709142	0.000640	0.709434	0.000640
HSSr	2020-10-19	25	No	No	0.709108	0.000687	0.708803	0.000751	0.709047	0.000751
HSSr	2020-10-19	25	No	No	0.709380	0.000703	0.709352	0.000768	0.709526	0.000768
HSSr	2020-10-19	25	No	No	0.709147	0.000704	0.709265	0.000745	0.709390	0.000745
HSSr	2020-10-19	25	No	No	0.708970	0.000642	0.708712	0.000688	0.708789	0.000688
HSSr	2020-10-19	25	No	No	0.709335	0.000687	0.709113	0.000719	0.709141	0.000720
HSSr	2020-10-23	8	No	Yes	0.709303	0.000716	0.709207	0.000724	0.709153	0.000724
HSSr	2020-10-23	8	No	Yes	0.708756	0.001165	0.708816	0.001207	0.708786	0.001207
HSSr	2020-10-23	8	No	Yes	0.709061	0.001287	0.708791	0.001388	0.708789	0.001388
HSSr	2020-10-23	8	No	Yes	0.708573	0.001197	0.708489	0.001251	0.708507	0.001251
HSSr	2020-10-23	8	No	Yes	0.709437	0.001066	0.709255	0.001090	0.709277	0.001090
HSSr	2020-10-23	8	No	Yes	0.709556	0.000765	0.709549	0.000810	0.709557	0.000810
HSSr	2020-10-23	8	No	Yes	0.710266	0.001241	0.710027	0.001332	0.710013	0.001332
HSSr	2020-10-23	12	No	Yes	0.709570	0.000363	0.709463	0.000384	0.709405	0.000384
HSSr	2020-10-23	12	No	Yes	0.709094	0.000448	0.708970	0.000470	0.708934	0.000470
HSSr	2020-10-23	12	No	Yes	0.709695	0.000571	0.709525	0.000571	0.709517	0.000571
HSSr	2020-10-23	12	No	Yes	0.708983	0.000472	0.708911	0.000513	0.708926	0.000513
HSSr	2020-10-23	12	No	Yes	0.709024	0.000402	0.709034	0.000416	0.709057	0.000416
HSSr	2020-10-23	12	No	Yes	0.709083	0.000369	0.709038	0.000392	0.709051	0.000392
HSSr	2020-10-23	12	No	Yes	0.709376	0.000523	0.709310	0.000582	0.709302	0.000582
HSSr	2020-10-23	15	No	Yes	0.709274	0.000285	0.709175	0.000299	0.709185	0.000299
HSSr	2020-10-23	15	No	Yes	0.709364	0.000288	0.709300	0.000312	0.709296	0.000312
HSSr	2020-10-23	15	No	Yes	0.709220	0.000353	0.709118	0.000387	0.709099	0.000387
HSSr	2020-10-23	15	No	Yes	0.709231	0.000305	0.709121	0.000336	0.709087	0.000336

Sample	Date	Laser Diameter (µm)	Split-Stream	Nitrogen Used	$^{87}Sr/^{86}Sr$ Uncorrected Mean	$^{87}Sr/^{86}Sr$ Uncorrected 2SE	$^{87}Sr/^{86}Sr$ Instrumental Corrected Mean	$^{87}Sr/^{86}Sr$ Instrumental Corrected 2SE	$^{87}Sr/^{86}Sr$ Additional Corrected Mean	$^{87}Sr/^{86}Sr$ Additional Corrected 2SE
HSSr	2020-10-23	15	No	Yes	0.709149	0.000279	0.709126	0.000304	0.709079	0.000304
HSSr	2020-10-23	15	No	Yes	0.709462	0.000274	0.709433	0.000297	0.709376	0.000297
HSSr	2020-10-23	15	No	Yes	0.709301	0.000316	0.709303	0.000326	0.709242	0.000326
HSSr	2020-10-23	20	No	Yes	0.709152	0.000157	0.709073	0.000162	0.709044	0.000162
HSSr	2020-10-23	20	No	Yes	0.709165	0.000159	0.709070	0.000170	0.709060	0.000170
HSSr	2020-10-23	20	No	Yes	0.709401	0.000187	0.709282	0.000199	0.709287	0.000199
HSSr	2020-10-23	20	No	Yes	0.709255	0.000183	0.709183	0.000189	0.709199	0.000189
HSSr	2020-10-23	20	No	Yes	0.709243	0.000150	0.709150	0.000156	0.709175	0.000156
HSSr	2020-10-23	20	No	Yes	0.709065	0.000148	0.709038	0.000154	0.709065	0.000154
HSSr	2020-10-23	20	No	Yes	0.709280	0.000145	0.709189	0.000157	0.709210	0.000157
HSSr	2020-10-23	25	No	Yes	0.709282	0.000111	0.709202	0.000115	0.709171	0.000115
HSSr	2020-10-23	25	No	Yes	0.709253	0.000109	0.709176	0.000112	0.709151	0.000112
HSSr	2020-10-23	25	No	Yes	0.709306	0.000108	0.709225	0.000113	0.709205	0.000113
HSSr	2020-10-23	25	No	Yes	0.709221	0.000107	0.709152	0.000106	0.709138	0.000106
HSSr	2020-10-23	25	No	Yes	0.709228	0.000111	0.709137	0.000112	0.709129	0.000112
HSSr	2020-10-23	25	No	Yes	0.709366	0.000118	0.709297	0.000124	0.709296	0.000124
HSSr	2020-10-23	25	No	Yes	0.709297	0.000106	0.709228	0.000108	0.709238	0.000108
HSSr	2020-10-23	25	No	Yes	0.709215	0.000097	0.709151	0.000103	0.709170	0.000103
HSSr	2020-10-23	25	No	Yes	0.709164	0.000113	0.709087	0.000114	0.709115	0.000114
HSSr	2020-10-23	25	No	Yes	0.709236	0.000102	0.709131	0.000104	0.709167	0.000104
HSSr	2020-10-23	25	No	Yes	0.709281	0.000131	0.709217	0.000136	0.709193	0.000136
HSSr	2020-10-23	25	No	Yes	0.709257	0.000113	0.709191	0.000116	0.709168	0.000116
HSSr	2020-10-23	25	No	Yes	0.709230	0.000117	0.709166	0.000120	0.709145	0.000120
HSSr	2020-10-23	25	No	Yes	0.709313	0.000118	0.709253	0.000122	0.709235	0.000122
HSSr	2020-10-23	25	No	Yes	0.709309	0.000126	0.709250	0.000130	0.709234	0.000130
HSSr	2020-10-23	25	No	Yes	0.709172	0.000122	0.709102	0.000122	0.709087	0.000122
HSSr	2020-10-23	25	No	Yes	0.709259	0.000110	0.709182	0.000115	0.709170	0.000115
HSSr	2020-10-23	25	No	Yes	0.709229	0.000119	0.709141	0.000125	0.709131	0.000125
HSSr	2020-10-23	25	No	Yes	0.709289	0.000119	0.709216	0.000122	0.709208	0.000122
HSSr	2020-10-23	25	No	Yes	0.709278	0.000114	0.709204	0.000114	0.709198	0.000114
HSSr	2020-10-23	25	No	Yes	0.709247	0.000154	0.709205	0.000161	0.709190	0.000161
HSSr	2020-10-23	25	No	Yes	0.709182	0.000141	0.709117	0.000146	0.709107	0.000146
HSSr	2020-10-23	25	No	Yes	0.709246	0.000148	0.709193	0.000152	0.709188	0.000152
HSSr	2020-10-23	25	No	Yes	0.709303	0.000136	0.709206	0.000142	0.709207	0.000142
HSSr	2020-10-23	25	No	Yes	0.709272	0.000156	0.709174	0.000161	0.709181	0.000161
HSSr	2020-10-23	25	No	Yes	0.709280	0.000153	0.709221	0.000159	0.709233	0.000159
HSSr	2020-10-23	25	No	Yes	0.709174	0.000144	0.709080	0.000148	0.709100	0.000148
HSSr	2020-10-23	25	No	Yes	0.709289	0.000149	0.709237	0.000155	0.709262	0.000155
HSSr	2020-10-23	25	No	Yes	0.709200	0.000132	0.709152	0.000138	0.709181	0.000138
HSSr	2020-10-23	25	No	Yes	0.709151	0.000155	0.709086	0.000157	0.709121	0.000157
HSSr	2020-10-23	25	No	Yes	0.709214	0.000108	0.709153	0.000112	0.709155	0.000112
HSSr	2020-10-23	25	No	Yes	0.709322	0.000115	0.709232	0.000120	0.709218	0.000120
HSSr	2020-10-23	25	No	Yes	0.709240	0.000138	0.709155	0.000140	0.709126	0.000140
HSSr	2020-10-23	25	No	Yes	0.709287	0.000118	0.709186	0.000123	0.709144	0.000123
HSSr	2020-10-23	25	No	Yes	0.709308	0.000107	0.709231	0.000111	0.709178	0.000111

Sample	Date	Laser Diameter (µm)	Split-Stream	Nitrogen Used	$^{87}Sr/^{86}Sr$ Uncorrected Mean	$^{87}Sr/^{86}Sr$ Uncorrected 2SE	$^{87}Sr/^{86}Sr$ Instrumental Corrected Mean	$^{87}Sr/^{86}Sr$ Instrumental Corrected 2SE	$^{87}Sr/^{86}Sr$ Additional Corrected Mean	$^{87}Sr/^{86}Sr$ Additional Corrected 2SE
HSSr	2020-10-23	25	No	Yes	0.709318	0.000112	0.709301	0.000119	0.709246	0.000119
HSSr	2020-10-23	25	No	Yes	0.709396	0.000119	0.709307	0.000122	0.709261	0.000122
HSSr	2020-10-23	25	No	Yes	0.709205	0.000154	0.709116	0.000160	0.709189	0.000160
HSSr	2020-10-23	25	No	Yes	0.709306	0.000195	0.709190	0.000201	0.709264	0.000201
HSSr	2020-10-23	25	No	Yes	0.709164	0.000199	0.708996	0.000204	0.709070	0.000204
HSSr	2020-10-23	25	No	Yes	0.709197	0.000197	0.709057	0.000211	0.709131	0.000211
HSSr	2020-10-23	25	No	Yes	0.709088	0.000198	0.708949	0.000212	0.709023	0.000212
HSSr	2020-03-03	25	No	No	0.709171	0.000162	0.708981	0.000164	0.709120	0.000164
HSSr	2020-03-03	25	No	No	0.709162	0.000141	0.709052	0.000153	0.709175	0.000154
HSSr	2020-03-03	25	No	No	0.709182	0.000161	0.709000	0.000175	0.709096	0.000175
HSSr	2020-03-03	25	No	No	0.709318	0.000141	0.709179	0.000148	0.709259	0.000148
HSSr	2020-03-03	25	No	No	0.709319	0.000153	0.709195	0.000165	0.709248	0.000165
HSSr	2020-03-03	25	No	No	0.709323	0.000145	0.709201	0.000157	0.709237	0.000157
HSSr	2020-03-03	25	No	No	0.709235	0.000159	0.709107	0.000168	0.709118	0.000168
HSSr	2020-03-03	25	No	No	0.709331	0.000363	0.709132	0.000393	0.709126	0.000393
HSSr	2020-03-03	25	No	No	0.709171	0.000332	0.709114	0.000348	0.709100	0.000348
HSSr	2020-03-03	25	No	No	0.709211	0.000368	0.709129	0.000384	0.709108	0.000384
HSSr	2020-03-03	25	No	No	0.709336	0.000160	0.709185	0.000173	0.709156	0.000173
HSSr	2020-03-04	25	No	No	0.709144	0.000110	0.709012	0.000114	0.709151	0.000114
HSSr	2020-03-04	25	No	No	0.709236	0.000102	0.709071	0.000109	0.709205	0.000109
HSSr	2020-03-04	25	No	No	0.709194	0.000104	0.709063	0.000109	0.709178	0.000109
HSSr	2020-03-04	25	No	No	0.709222	0.000114	0.709065	0.000121	0.709156	0.000121
HSSr	2020-03-04	25	No	No	0.709284	0.000107	0.709144	0.000112	0.709185	0.000112
HSSr	2020-03-04	50	No	No	0.709371	0.000084	0.709275	0.000090	0.709222	0.000090
HSSr	2020-03-04	50	No	No	0.709254	0.000081	0.709175	0.000087	0.709126	0.000087
HSSr	2020-03-04	50	No	No	0.709306	0.000092	0.709216	0.000096	0.709169	0.000096
HSSr	2020-03-04	50	No	No	0.709354	0.000089	0.709259	0.000095	0.709199	0.000095
HSSr	2020-03-04	50	No	No	0.709307	0.000090	0.709220	0.000094	0.709167	0.000094
HSSr	2020-03-04	50	No	No	0.709354	0.000041	0.709235	0.000042	0.709129	0.000042
HSSr	2020-03-04	50	No	No	0.709360	0.000038	0.709254	0.000040	0.709148	0.000040
HSSr	2020-03-04	50	No	No	0.709355	0.000042	0.709249	0.000043	0.709142	0.000043
HSSr	2020-03-04	50	No	No	0.709349	0.000040	0.709249	0.000041	0.709133	0.000041
HSSr	2020-03-04	50	No	No	0.709317	0.000042	0.709228	0.000043	0.709100	0.000043
HSSr	2020-07-29	25	No	No	0.709132	0.000072	0.709086	0.000077	0.709148	0.000077
HSSr	2020-07-29	25	No	No	0.709238	0.000071	0.709173	0.000076	0.709206	0.000076
HSSr	2020-07-29	25	No	No	0.709169	0.000085	0.709185	0.000089	0.709185	0.000089
HSSr	2020-07-29	25	No	No	0.709255	0.000071	0.709187	0.000076	0.709184	0.000076
HSSr	2020-07-29	25	No	No	0.709218	0.000072	0.709162	0.000077	0.709160	0.000077
HSSr	2020-07-29	25	No	No	0.709222	0.000084	0.709204	0.000088	0.709208	0.000088
HSSr	2020-07-29	25	No	No	0.709218	0.000073	0.709145	0.000078	0.709148	0.000078
HSSr	2020-07-29	25	No	No	0.709238	0.000073	0.709158	0.000077	0.709152	0.000077
HSSr	2020-07-29	25	No	No	0.709301	0.000135	0.709212	0.000146	0.709179	0.000145
HSSr	2020-07-29	25	No	No	0.709342	0.000074	0.709268	0.000078	0.709225	0.000078
HSSr	2020-07-29	25	No	No	0.709242	0.000139	0.709117	0.000149	0.709117	0.000149
HSSr	2020-07-29	25	No	No	0.709259	0.000074	0.709154	0.000079	0.709180	0.000079

Sample	Date	Laser Diameter (µm)	Split-Stream	Nitrogen Used	$^{87}Sr/^{86}Sr$ Uncorrected Mean	$^{87}Sr/^{86}Sr$ Uncorrected 2SE	$^{87}Sr/^{86}Sr$ Instrumental Corrected Mean	$^{87}Sr/^{86}Sr$ Instrumental Corrected 2SE	$^{87}Sr/^{86}Sr$ Additional Corrected Mean	$^{87}Sr/^{86}Sr$ Additional Corrected 2SE
HSSr	2020-07-29	25	No	No	0.709215	0.000072	0.709110	0.000078	0.709168	0.000078
HSSr	2020-07-29	25	No	No	0.709165	0.000050	0.709091	0.000053	0.709167	0.000053
HSSr	2020-07-29	25	No	No	0.709191	0.000052	0.709099	0.000055	0.709174	0.000055
HSSr	2020-07-29	25	No	No	0.709123	0.000077	0.709061	0.000083	0.709133	0.000083
HSSr	2020-07-29	25	No	No	0.709193	0.000054	0.709103	0.000057	0.709173	0.000057
HSSr	2020-07-29	25	No	No	0.709198	0.000055	0.709108	0.000058	0.709178	0.000058
HSSr	2020-07-29	25	No	No	0.709226	0.000079	0.709220	0.000084	0.709287	0.000084
HSSr	2020-07-29	25	No	No	0.709208	0.000055	0.709138	0.000058	0.709203	0.000058
HSSr	2020-07-29	25	No	No	0.709166	0.000055	0.709091	0.000059	0.709155	0.000059
HSSr	2020-07-29	25	No	No	0.709252	0.000132	0.709162	0.000142	0.709224	0.000142
HSSr	2020-07-29	25	No	No	0.709174	0.000056	0.709098	0.000061	0.709159	0.000061
HSSr	2020-07-29	25	No	No	0.709280	0.000124	0.709139	0.000133	0.709197	0.000133
HSSr	2020-07-29	25	No	No	0.709157	0.000057	0.709069	0.000060	0.709126	0.000060
HSSr	2020-07-29	25	No	No	0.709218	0.000057	0.709148	0.000061	0.709203	0.000061
HSSr	2020-07-30	25	No	No	0.709180	0.000069	0.709093	0.000074	0.709200	0.000074
HSSr	2020-07-30	25	No	No	0.709132	0.000072	0.709041	0.000078	0.709136	0.000078
HSSr	2020-07-30	25	No	No	0.709213	0.000097	0.709155	0.000103	0.709212	0.000103
HSSr	2020-07-30	25	No	No	0.709179	0.000074	0.709104	0.000078	0.709147	0.000078
HSSr	2020-07-30	25	No	No	0.709240	0.000076	0.709167	0.000080	0.709194	0.000080

LASS-ICP-MS long-term isotope data for the SRM NanoSr

Sample	Date	Laser Diameter (μm)	Split-Stream	Nitrogen Used	$^{87}Sr/^{86}Sr$ Uncorrected Mean	$^{87}Sr/^{86}Sr$ Uncorrected 2SE	$^{87}Sr/^{86}Sr$ Instrumental Corrected Mean	$^{87}Sr/^{86}Sr$ Instrumental Corrected 2SE	$^{87}Sr/^{86}Sr$ Additional Corrected Mean	$^{87}Sr/^{86}Sr$ Additional Corrected 2SE
NanoSr	2021-02-02	40	Yes	Yes	0.708640	0.001762	0.705907	0.001857	0.705899	0.001857
NanoSr	2021-02-02	40	Yes	Yes	0.707424	0.001096	0.707610	0.001161	0.707600	0.001161
NanoSr	2021-02-02	40	Yes	Yes	0.718624	0.001421	0.707543	0.001524	0.707531	0.001524
NanoSr	2021-02-03	25	Yes	Yes	0.712433	0.001447	0.709096	0.001440	0.709086	0.001440
NanoSr	2021-02-03	25	Yes	Yes	0.710529	0.001133	0.707744	0.001262	0.707726	0.001262
NanoSr	2021-02-03	25	Yes	Yes	0.710315	0.002026	0.707611	0.002302	0.707554	0.002302
NanoSr	2021-02-03	25	Yes	Yes	0.709994	0.001399	0.707879	0.001519	0.707798	0.001519
NanoSr	2021-02-03	25	Yes	Yes	0.709336	0.001352	0.707660	0.001414	0.707576	0.001414
NanoSr	2021-02-03	25	Yes	Yes	0.709409	0.000867	0.707605	0.000923	0.707590	0.000923
NanoSr	2021-02-03	25	Yes	Yes	0.710017	0.001112	0.707470	0.001214	0.707471	0.001214
NanoSr	2021-02-03	25	Yes	Yes	0.709779	0.000978	0.707010	0.001052	0.707024	0.001052
NanoSr	2021-02-03	25	Yes	Yes	0.707690	0.001335	0.706903	0.001385	0.706932	0.001385
NanoSr	2021-02-03	25	Yes	Yes	0.710051	0.000935	0.708529	0.000940	0.708497	0.000940
NanoSr	2021-02-03	25	Yes	Yes	0.710691	0.003483	0.706507	0.003462	0.706409	0.003461
NanoSr	2021-02-04	25	Yes	Yes	0.709324	0.000960	0.706238	0.001009	0.706260	0.001009
NanoSr	2021-02-04	25	Yes	Yes	0.711009	0.001045	0.708039	0.001124	0.707960	0.001124
NanoSr	2021-02-04	25	Yes	Yes	0.709898	0.001055	0.706994	0.001030	0.707012	0.001030
NanoSr	2021-02-04	25	Yes	Yes	0.710826	0.000702	0.707529	0.000749	0.707519	0.000749
NanoSr	2021-02-04	25	Yes	Yes	0.710201	0.000686	0.707045	0.000749	0.707128	0.000750
NanoSr	2021-02-04	25	Yes	Yes	0.711359	0.001008	0.708145	0.001020	0.708138	0.001020
NanoSr	2021-02-04	25	Yes	Yes	0.712125	0.000676	0.707725	0.000727	0.707710	0.000727
NanoSr	2021-02-04	25	Yes	Yes	0.712146	0.000820	0.707892	0.000860	0.707923	0.000860
NanoSr	2021-02-04	25	Yes	Yes	0.711170	0.000744	0.707500	0.000814	0.707516	0.000814
NanoSr	2021-02-02	25	Yes	Yes	0.707129	0.004483	0.706642	0.004623	0.706620	0.004623
NanoSr	2021-02-02	25	Yes	Yes	0.708206	0.003362	0.708231	0.003659	0.708207	0.003659
NanoSr	2021-02-02	25	Yes	Yes	0.716506	0.004175	0.705976	0.004571	0.705951	0.004571
NanoSr	2021-02-02	20	Yes	Yes	0.706949	0.009908	0.704442	0.010286	0.704406	0.010286
NanoSr	2021-02-02	20	Yes	Yes	0.708980	0.005359	0.708168	0.005895	0.708130	0.005894
NanoSr	2021-02-02	20	Yes	Yes	0.721006	0.008067	0.707999	0.008325	0.707959	0.008325
NanoSr	2021-02-02	15	Yes	Yes	0.721457	0.016520	0.715626	0.016482	0.715576	0.016480
NanoSr	2021-02-02	15	Yes	Yes	0.705381	0.011682	0.705143	0.013276	0.705092	0.013275
NanoSr	2021-02-02	15	Yes	Yes	0.712492	0.019922	0.691614	0.020604	0.691562	0.020603
NanoSr	2021-02-02	12	Yes	Yes	0.684750	0.068982	0.693466	0.070002	0.693403	0.069995
NanoSr	2021-02-02	12	Yes	Yes	0.696383	0.026608	0.694087	0.028002	0.694023	0.028000
NanoSr	2021-02-02	12	Yes	Yes	0.734040	0.042528	0.709884	0.044855	0.709817	0.044851
NanoSr	2021-02-02	10	Yes	Yes	0.716467	0.026366	0.704835	0.027462	0.704758	0.027459
NanoSr	2021-02-02	10	Yes	Yes	0.706715	0.019799	0.704018	0.020998	0.703939	0.020995
NanoSr	2021-02-02	10	Yes	Yes	0.731569	0.030410	0.733770	0.034658	0.733687	0.034654
NanoSr	2021-03-03	40	Yes	Yes	0.707876	0.000338	0.707474	0.000370	0.707454	0.000370
NanoSr	2021-03-03	40	Yes	Yes	0.708187	0.000340	0.707694	0.000367	0.707655	0.000367
NanoSr	2021-03-03	40	Yes	Yes	0.708302	0.000324	0.707797	0.000348	0.707741	0.000348
NanoSr	2021-03-03	40	Yes	Yes	0.707913	0.000379	0.707406	0.000412	0.707338	0.000412

NanoSr	2021-03-03	40	Yes	Yes	0.708052	0.000374	0.707624	0.000407	0.707538	0.000407
NanoSr	2021-03-03	40	Yes	Yes	0.707798	0.000359	0.707276	0.000384	0.707175	0.000384
NanoSr	2021-03-03	40	Yes	Yes	0.708154	0.000357	0.707805	0.000388	0.707697	0.000388
NanoSr	2021-03-03	40	Yes	Yes	0.708027	0.000379	0.707463	0.000405	0.707345	0.000405
NanoSr	2021-03-03	40	Yes	Yes	0.708056	0.000370	0.707618	0.000399	0.707494	0.000399
NanoSr	2021-03-04	40	Yes	Yes	0.708191	0.000352	0.707735	0.000388	0.707707	0.000388
NanoSr	2021-03-04	40	Yes	Yes	0.707633	0.000440	0.707194	0.000467	0.707152	0.000467
NanoSr	2021-03-04	40	Yes	Yes	0.707839	0.000429	0.707469	0.000463	0.707411	0.000463
NanoSr	2021-03-04	40	Yes	Yes	0.708056	0.000542	0.707598	0.000574	0.707531	0.000574
NanoSr	2021-03-04	40	Yes	Yes	0.707754	0.000522	0.707168	0.000572	0.707088	0.000572
NanoSr	2021-03-04	40	Yes	Yes	0.708269	0.000497	0.707844	0.000534	0.707753	0.000534
NanoSr	2021-03-05	40	Yes	Yes	0.707696	0.000402	0.707089	0.000433	0.707073	0.000433
NanoSr	2021-03-05	40	Yes	Yes	0.707881	0.000389	0.707490	0.000422	0.707468	0.000422
NanoSr	2021-03-05	40	Yes	Yes	0.707654	0.000422	0.707168	0.000478	0.707139	0.000478
NanoSr	2021-03-05	40	Yes	Yes	0.707422	0.000417	0.706838	0.000441	0.706806	0.000441
NanoSr	2021-03-05	40	Yes	Yes	0.708158	0.000443	0.707684	0.000481	0.707645	0.000481
NanoSr	2021-03-05	40	Yes	Yes	0.707684	0.000462	0.707208	0.000479	0.707159	0.000479
NanoSr	2021-03-05	40	Yes	Yes	0.708168	0.000445	0.707710	0.000467	0.707657	0.000467
NanoSr	2021-03-05	40	Yes	Yes	0.708259	0.000416	0.707830	0.000437	0.707767	0.000437
NanoSr	2021-03-05	40	Yes	Yes	0.707721	0.000421	0.707207	0.000445	0.707132	0.000445
NanoSr	2021-03-05	40	Yes	Yes	0.708159	0.000439	0.707514	0.000468	0.707433	0.000468
NanoSr	2021-03-05	40	Yes	Yes	0.707835	0.000431	0.707149	0.000464	0.707055	0.000464
NanoSr	2021-03-05	40	Yes	Yes	0.707985	0.000472	0.707656	0.000503	0.707547	0.000502
NanoSr	2021-03-05	40	Yes	Yes	0.708097	0.000409	0.707648	0.000425	0.707534	0.000425
NanoSr	2021-03-05	40	Yes	Yes	0.708010	0.000423	0.707718	0.000450	0.707592	0.000450
NanoSr	2021-03-05	40	Yes	Yes	0.708033	0.000420	0.707620	0.000445	0.707485	0.000445
NanoSr	2021-05-27	40	Yes	Yes	0.708292	0.000263	0.707747	0.000276	0.707706	0.000276
NanoSr	2021-05-27	40	Yes	Yes	0.708181	0.000287	0.707708	0.000299	0.707724	0.000299
NanoSr	2021-05-27	40	Yes	Yes	0.707531	0.000304	0.707043	0.000356	0.707119	0.000356
NanoSr	2021-05-27	40	Yes	Yes	0.707926	0.000326	0.707401	0.000350	0.707512	0.000350
NanoSr	2021-05-27	40	Yes	Yes	0.707744	0.000343	0.707328	0.000363	0.707456	0.000363
NanoSr	2021-05-27	40	Yes	Yes	0.706672	0.000357	0.706857	0.000363	0.706988	0.000363
NanoSr	2021-05-27	40	Yes	Yes	0.707691	0.000348	0.707100	0.000382	0.707217	0.000382
NanoSr	2021-05-27	40	Yes	Yes	0.707323	0.000372	0.707010	0.000389	0.707089	0.000389
NanoSr	2021-05-27	40	Yes	Yes	0.707493	0.000349	0.706964	0.000374	0.706990	0.000374

LASS-ICP-MS and LA-ICP-MS (single-stream) long-term trace element data for NIST SRM 612

Date	Laser Diameter	Split	Nitrogen	^{66}Zn Mean	^{66}Zn 2SE	^{66}Zn LOD Pettke	^{88}Sr Mean	^{88}Sr 2SE	^{88}Sr LOD Pettke	^{137}Ba Mean	^{137}Ba 2SE	^{137}Ba LOD Pettke
2020-10-26	25	Yes	No	41.51	1.27	0.33	79.22	1.24	0.06	39.41	1.18	0.01
2020-10-26	25	Yes	No	41.40	1.13	0.33	79.52	1.12	0.10	38.98	1.06	0.09
2020-10-26	25	Yes	No	40.26	1.15	0.34	79.97	1.17	0.08	39.67	1.14	0.05
2020-10-26	25	Yes	No	41.02	1.28	0.39	79.61	1.11	0.09	39.64	1.10	0.08
2020-10-26	25	Yes	No	39.97	1.14	0.38	79.91	1.18	0.09	40.45	1.16	0.05
2020-10-26	25	Yes	Yes	40.11	1.11	0.36	78.93	1.14	0.06	40.77	1.20	0.01
2020-10-26	25	Yes	Yes	41.20	0.90	0.35	79.24	0.85	0.02	40.60	0.89	0.01
2020-10-26	25	Yes	Yes	41.48	1.02	0.33	80.53	0.81	0.02	41.83	0.93	0.06
2020-10-26	25	Yes	Yes	41.58	1.03	0.35	79.42	0.86	0.03	39.83	0.91	0.04
2020-10-26	25	Yes	Yes	42.34	1.06	0.34	80.34	0.83	0.03	41.00	0.98	0.06
2020-10-26	25	Yes	Yes	42.89	0.99	0.35	80.69	0.96	0.02	41.16	0.87	0.05
2020-10-26	20	Yes	Yes	40.31	1.38	0.48	79.08	1.41	0.15	38.59	1.36	0.10
2020-10-26	20	Yes	Yes	41.08	1.40	0.52	79.72	1.42	0.24	39.64	1.30	0.12
2020-10-26	20	Yes	Yes	40.45	1.45	0.52	79.67	1.40	0.24	39.83	1.46	0.08
2020-10-26	20	Yes	Yes	41.42	1.34	0.48	80.80	1.46	0.29	40.77	1.42	0.14
2020-10-26	20	Yes	Yes	39.81	1.51	0.52	79.13	1.37	0.31	39.20	1.31	0.14
2020-10-26	20	Yes	Yes	40.24	1.51	0.54	79.29	1.27	0.16	40.81	1.46	0.17
2020-10-26	20	Yes	Yes	44.75	1.26	0.57	86.16	1.27	0.04	44.02	1.24	0.09
2020-10-26	20	Yes	Yes	33.23	1.01	0.44	63.52	0.81	0.04	31.89	0.93	0.06
2020-10-26	20	Yes	Yes	32.47	0.92	0.47	62.99	0.84	0.03	31.26	0.90	0.04
2020-10-26	20	Yes	Yes	47.05	1.31	0.55	86.33	1.06	0.05	44.16	1.28	0.10
2020-10-26	15	Yes	Yes	41.45	2.07	1.08	78.63	1.52	0.10	37.77	1.64	0.26
2020-10-26	15	Yes	Yes	42.21	2.16	1.05	78.83	1.66	0.15	38.65	2.04	0.15
2020-10-26	15	Yes	Yes	40.52	1.95	0.98	79.66	1.68	0.09	39.24	1.75	0.04
2020-10-26	15	Yes	Yes	43.24	2.04	0.96	78.67	1.64	0.10	41.62	1.88	0.19
2020-10-26	15	Yes	Yes	40.86	2.10	0.98	78.52	1.62	0.09	39.16	1.81	0.16
2020-10-26	15	Yes	Yes	40.98	2.17	1.02	79.63	1.58	0.10	38.02	1.72	0.04
2020-10-26	15	Yes	Yes	43.12	1.67	1.10	78.21	1.61	0.07	40.44	1.64	0.03
2020-10-26	15	Yes	Yes	42.22	1.56	1.00	80.38	1.83	0.06	42.23	1.83	0.11
2020-10-26	15	Yes	Yes	40.19	1.75	1.14	77.62	1.44	0.05	39.39	1.70	0.03
2020-10-26	15	Yes	Yes	40.24	1.72	1.17	79.42	1.63	0.08	40.08	1.64	0.03
2020-10-26	8	Yes	Yes	39.07	2.90	2.30	79.07	2.73	0.49	41.65	2.88	1.33
2020-10-26	8	Yes	Yes	38.78	3.08	3.57	80.36	2.67	0.20	39.13	2.87	0.65
2020-10-26	8	Yes	Yes	42.98	3.12	3.48	81.01	2.24	0.31	39.64	2.71	0.65
2020-10-26	8	Yes	Yes	40.97	3.10	3.42	77.35	2.38	0.22	37.87	2.97	0.84
2020-11-02	25	Yes	Yes	38.39	1.10	0.35	78.03	0.87	0.06	39.18	0.97	0.05
2020-11-02	25	Yes	Yes	38.44	1.01	0.36	79.33	0.90	0.09	38.91	0.91	0.01

Date	Laser Diameter	Split	Nitrogen	^{66}Zn Mean	^{66}Zn 2SE	^{66}Zn LOD Pettke	^{88}Sr Mean	^{88}Sr 2SE	^{88}Sr LOD Pettke	^{137}Ba Mean	^{137}Ba 2SE	^{137}Ba LOD Pettke
2020-11-02	25	Yes	Yes	39.09	1.09	0.38	78.66	0.89	0.08	39.17	0.93	0.04
2020-11-02	25	Yes	Yes	38.10	1.01	0.41	77.88	0.89	0.08	39.82	0.98	0.04
2020-11-02	25	Yes	Yes	40.20	1.21	0.40	79.79	0.93	0.08	40.37	1.00	0.01
2020-11-02	25	Yes	Yes	40.68	1.05	0.37	79.10	0.90	0.09	39.55	0.96	0.04
2020-11-02	25	Yes	Yes	40.14	1.15	0.39	78.96	0.94	0.09	39.52	0.95	0.06
2020-11-02	25	Yes	Yes	39.17	0.99	nan	79.55	0.96	nan	39.44	0.90	nan
2020-11-02	25	Yes	Yes	39.89	1.08	nan	79.49	0.90	nan	40.11	0.93	nan
2020-11-02	25	Yes	Yes	39.29	1.03	nan	79.35	1.00	nan	39.96	1.01	nan
2020-11-02	25	Yes	Yes	39.78	0.96	nan	78.91	0.89	nan	38.70	0.99	nan
2020-11-02	25	Yes	Yes	38.83	0.92	nan	78.98	0.99	nan	40.01	0.92	nan
2020-11-02	25	Yes	Yes	38.86	4.92	nan	78.29	4.71	nan	40.80	2.07	nan
2020-11-02	25	Yes	Yes	42.82	4.42	nan	82.07	4.32	nan	38.77	1.26	nan
2020-11-02	25	Yes	Yes	41.70	1.19	0.30	80.50	0.91	0.04	41.43	0.95	0.06
2020-11-02	25	Yes	Yes	41.40	1.03	0.35	78.83	0.94	0.05	39.73	0.92	0.04
2020-11-02	25	Yes	Yes	41.51	1.01	0.33	78.63	0.91	0.06	39.09	0.93	0.05
2020-11-02	25	Yes	Yes	41.82	1.14	0.33	78.76	0.90	0.07	39.67	0.97	0.03
2020-11-02	25	Yes	Yes	42.55	1.05	0.34	78.99	0.85	0.05	39.70	0.97	0.03
2020-11-02	25	Yes	Yes	42.12	1.16	0.32	78.64	0.83	0.04	40.26	0.95	0.07
2020-11-02	25	Yes	Yes	41.28	1.19	0.36	79.25	0.89	0.04	39.84	1.09	0.08
2020-11-02	25	Yes	Yes	40.28	1.04	0.33	80.75	1.04	0.05	40.20	0.88	0.04
2020-11-02	25	Yes	Yes	41.24	1.02	0.29	79.09	0.89	0.03	39.15	0.90	0.05
2020-11-02	25	Yes	Yes	41.79	1.03	0.35	79.04	0.88	0.04	40.11	0.78	0.05
2020-11-02	25	Yes	Yes	41.30	1.12	0.33	78.43	0.87	0.05	39.66	0.88	0.05
2020-11-02	25	Yes	Yes	41.14	1.01	0.34	78.74	0.84	0.03	40.16	0.95	0.05
2020-11-02	25	Yes	Yes	40.62	1.05	0.32	79.45	0.93	0.04	38.93	0.82	0.05
2020-11-02	25	Yes	Yes	41.61	0.97	0.33	78.98	0.89	0.03	39.04	0.94	0.04
2020-11-02	25	Yes	Yes	41.04	0.85	0.30	78.43	0.88	0.16	40.20	0.78	0.06
2020-11-02	25	Yes	Yes	41.63	0.82	0.30	79.58	0.86	0.14	40.43	0.79	0.04
2020-11-02	25	Yes	Yes	42.18	0.90	0.32	78.96	0.88	0.13	40.99	0.79	0.05
2020-11-02	25	Yes	Yes	41.65	0.86	0.31	80.17	0.70	0.11	40.41	0.75	0.05
2020-11-02	25	Yes	Yes	42.17	0.94	0.29	78.39	0.83	0.16	40.91	0.86	0.06
2020-11-02	25	Yes	Yes	42.25	0.92	0.28	71.13	0.78	0.35	40.68	0.82	0.09
2020-11-02	25	Yes	Yes	42.01	0.86	0.28	74.45	0.77	0.24	40.28	0.81	0.10
2020-11-02	15	Yes	Yes	39.15	1.06	0.28	79.07	1.05	0.12	39.38	0.96	0.07
2020-11-02	15	Yes	Yes	40.41	1.33	0.34	79.82	1.06	0.10	39.86	1.13	0.08
2020-11-02	15	Yes	Yes	41.25	1.15	0.27	73.70	1.06	0.09	41.54	1.07	0.05
2020-11-02	15	Yes	Yes	39.35	1.10	0.34	80.49	1.04	0.14	37.75	1.05	0.19
2020-11-02	8	Yes	Yes	41.05	3.49	3.43	83.24	2.42	0.27	42.54	3.63	0.72
2020-11-02	8	Yes	Yes	40.55	3.33	3.08	82.33	2.72	0.27	41.18	3.43	0.45

Date	Laser Diameter	Split	Nitrogen	^{66}Zn Mean	^{66}Zn 2SE	^{66}Zn LOD Pettke	^{88}Sr Mean	^{88}Sr 2SE	^{88}Sr LOD Pettke	^{137}Ba Mean	^{137}Ba 2SE	^{137}Ba LOD Pettke
2020-11-02	8	Yes	Yes	44.13	3.75	3.02	81.14	2.42	0.31	41.17	3.25	0.72
2020-11-02	8	Yes	Yes	41.26	3.75	3.06	82.17	2.86	0.32	39.30	3.05	0.11
2020-11-02	8	Yes	Yes	40.79	3.74	3.08	81.07	2.72	0.38	38.81	3.13	0.11
2020-11-02	8	Yes	Yes	39.82	3.32	2.70	79.86	2.63	0.25	39.45	3.07	0.11
2020-11-02	8	Yes	Yes	40.60	3.62	3.05	81.91	2.43	0.50	44.24	3.54	0.58
2020-11-03	15	Yes	Yes	41.14	1.76	0.81	79.27	1.52	0.14	38.93	1.71	0.15
2020-11-03	15	Yes	Yes	42.61	4.13	0.82	78.22	3.68	0.13	41.08	3.94	0.22
2020-11-03	15	Yes	Yes	41.12	1.65	0.88	79.44	1.68	0.10	40.14	1.84	0.12
2020-11-03	15	Yes	Yes	43.49	2.96	0.67	76.77	2.43	0.16	41.28	1.74	0.15
2020-11-03	15	Yes	Yes	44.16	2.04	0.83	79.87	2.00	0.14	40.49	2.69	0.15
2020-11-03	15	Yes	Yes	41.99	2.26	0.82	80.14	1.78	0.17	38.38	1.67	0.20
2020-11-03	15	Yes	Yes	42.98	2.93	0.86	80.53	3.13	0.16	39.28	1.73	0.20
2020-11-03	8	Yes	Yes	41.05	3.35	2.88	76.49	2.72	0.29	37.67	3.27	0.42
2020-11-03	8	Yes	Yes	40.79	2.95	2.40	78.17	3.26	0.41	38.32	3.31	0.58
2020-11-03	8	Yes	Yes	44.61	7.77	2.72	80.27	2.66	0.55	40.03	3.27	0.79
2020-11-03	8	Yes	Yes	42.19	4.06	2.64	77.33	2.84	0.60	37.27	3.25	0.11
2020-11-03	8	Yes	Yes	44.94	3.61	2.88	75.54	2.25	0.56	37.15	2.67	0.95
2020-11-03	8	Yes	Yes	43.13	4.13	3.07	82.62	4.01	0.63	45.06	4.63	0.12
2020-11-03	8	Yes	Yes	45.02	4.99	2.62	81.14	3.16	0.52	36.42	3.09	0.91
2020-11-03	12	Yes	Yes	40.53	2.44	1.36	77.88	1.83	0.21	37.14	2.31	0.26
2020-11-03	12	Yes	Yes	44.46	8.73	1.34	78.89	3.10	0.29	37.92	2.41	0.42
2020-11-03	12	Yes	Yes	42.86	3.24	1.46	80.09	2.08	0.23	41.09	2.29	0.27
2020-11-03	12	Yes	Yes	43.16	2.26	1.32	77.53	3.48	0.26	37.73	2.17	0.20
2020-11-03	12	Yes	Yes	43.89	2.36	1.28	78.57	2.68	0.18	38.32	2.43	0.26
2020-11-03	12	Yes	Yes	41.39	2.64	1.26	79.09	1.89	0.24	39.34	2.24	0.27
2020-11-03	12	Yes	Yes	41.37	2.08	1.42	79.49	2.51	0.26	40.88	2.52	0.27
2020-11-23	25	Yes	Yes	41.25	0.85	0.38	79.55	0.75	0.12	39.99	0.82	0.03
2020-11-23	25	Yes	Yes	41.48	0.90	0.44	80.13	0.78	0.10	39.96	0.77	0.07
2020-11-23	25	Yes	Yes	39.17	0.99	0.29	79.55	0.96	0.13	39.44	0.90	0.17
2020-11-23	25	Yes	Yes	39.89	1.08	0.31	79.49	0.90	0.08	40.11	0.93	0.07
2020-11-23	25	Yes	Yes	39.29	1.03	0.26	79.35	1.00	0.09	39.96	1.01	0.05
2020-11-23	25	Yes	Yes	39.78	0.96	0.30	78.91	0.89	0.11	38.70	0.99	0.07
2020-11-23	25	Yes	Yes	38.83	0.92	0.25	78.98	0.99	0.08	40.01	0.92	0.07
2020-11-23	25	Yes	Yes	38.86	4.92	0.27	78.29	4.71	0.09	40.80	2.07	0.07
2020-11-23	25	Yes	Yes	42.82	4.42	0.29	82.07	4.32	0.12	38.77	1.26	0.05
2020-11-25	25	Yes	Yes	41.36	0.89	0.35	78.51	0.72	0.05	39.86	0.67	0.12
2020-11-25	25	Yes	Yes	43.09	0.96	0.33	79.05	0.68	0.07	40.75	0.74	0.10
2020-11-25	25	Yes	Yes	42.45	1.14	0.42	77.37	0.86	0.08	41.00	0.81	0.30
2020-11-25	25	Yes	Yes	42.57	0.96	0.44	79.54	0.77	0.09	40.52	0.85	0.23

Date	**Laser Diameter**	**Split**	**Nitrogen**	**^{66}Zn Mean**	**^{66}Zn 2SE**	**^{66}Zn LOD Pettke**	**^{88}Sr Mean**	**^{88}Sr 2SE**	**^{88}Sr LOD Pettke**	**^{137}Ba Mean**	**^{137}Ba 2SE**	**^{137}Ba LOD Pettke**
2020-11-25	25	Yes	Yes	42.44	1.05	0.61	80.97	2.63	0.10	40.65	0.82	0.22
2020-11-25	25	Yes	Yes	42.02	1.06	0.42	79.29	0.83	0.08	39.88	0.82	0.18
2020-11-25	25	Yes	Yes	43.16	1.08	0.45	79.15	0.90	0.10	39.56	0.80	0.28
2020-11-25	25	Yes	Yes	43.54	1.03	0.52	79.01	0.88	0.09	40.36	0.92	0.21
2020-11-25	25	Yes	Yes	42.53	1.03	0.43	79.93	0.85	0.11	39.99	0.91	0.23
2020-11-25	25	Yes	Yes	41.43	0.99	0.45	78.94	0.80	0.19	41.03	0.89	0.28
2020-11-25	10	Yes	Yes	37.70	2.46	2.15	81.97	1.99	0.31	38.45	2.17	0.32
2020-11-25	10	Yes	Yes	38.50	2.42	2.49	79.06	1.85	0.33	40.14	2.37	0.33
2021-01-05	15	Yes	Yes	43.79	2.28	1.73	82.23	2.47	0.51	39.43	1.98	0.30
2021-01-05	15	Yes	Yes	43.58	2.87	1.96	79.72	2.14	0.13	41.88	2.65	0.19
2021-01-05	15	Yes	Yes	42.78	2.82	2.01	80.06	2.26	0.18	40.40	2.77	0.43
2021-01-05	15	Yes	Yes	40.86	2.36	1.93	79.04	2.79	0.29	40.38	2.73	0.32
2021-01-05	15	Yes	Yes	42.44	3.42	2.06	80.64	2.33	0.18	41.13	2.50	0.42
2021-01-06	15	Yes	Yes	43.90	2.75	1.48	81.08	2.65	0.21	39.89	2.11	0.06
2021-01-06	15	Yes	Yes	41.22	2.06	1.41	79.78	2.28	0.08	39.01	2.31	0.20
2021-01-06	15	Yes	Yes	43.79	2.15	0.98	78.90	2.04	0.41	39.81	2.16	0.21
2021-01-06	15	Yes	Yes	45.30	2.29	1.04	78.42	2.34	0.44	40.93	2.05	0.30
2021-01-06	15	Yes	Yes	44.27	2.48	1.12	78.48	2.36	0.51	41.57	2.45	0.28
2021-01-06	15	Yes	Yes	42.99	2.51	1.03	74.93	2.36	0.62	38.13	2.17	0.37
2021-01-06	15	Yes	Yes	44.92	2.11	0.99	76.23	2.25	0.47	40.05	2.17	0.49
2021-01-06	15	Yes	Yes	43.73	2.41	1.08	71.72	1.97	0.52	36.64	1.88	0.32
2021-01-06	15	Yes	Yes	44.59	2.29	1.12	78.08	1.89	0.35	37.96	2.02	0.26
2021-01-06	15	Yes	Yes	45.70	2.30	1.14	80.24	1.93	0.30	41.40	1.95	0.20
2021-02-04	25	Yes	Yes	37.18	1.39	0.39	80.68	1.07	0.03	40.14	1.14	0.05
2021-02-04	25	Yes	Yes	37.13	1.52	0.42	79.04	1.09	0.03	41.07	1.19	0.08
2021-02-04	25	Yes	Yes	38.09	1.39	0.43	79.65	1.14	0.04	39.32	1.28	0.08
2021-02-04	25	Yes	Yes	38.88	1.41	0.47	78.76	1.25	0.06	39.25	1.41	0.08
2021-02-04	25	Yes	Yes	35.90	1.19	0.32	79.61	1.24	0.04	39.04	1.14	0.09
2021-02-04	25	Yes	Yes	38.42	1.60	0.32	78.32	1.22	0.04	40.35	1.25	0.07
2021-02-04	25	Yes	Yes	37.34	1.46	0.62	78.28	1.10	0.04	39.83	1.38	0.09
2021-02-04	25	Yes	Yes	39.19	1.68	0.62	78.99	1.16	0.05	40.57	1.25	0.09
2021-02-04	25	Yes	Yes	39.90	1.59	0.55	77.73	1.20	0.05	38.99	1.35	0.09
2021-02-04	25	Yes	Yes	39.32	1.58	0.58	79.50	1.31	0.04	38.62	1.49	0.08
2021-02-04	25	Yes	Yes	41.24	1.83	0.63	79.00	1.15	0.05	39.97	1.44	0.10
2021-02-04	25	Yes	Yes	38.96	1.49	0.51	80.17	1.31	0.05	41.34	1.59	0.13
2021-02-04	25	Yes	Yes	37.37	1.47	0.47	79.20	1.42	0.04	40.73	1.45	0.09
2021-03-03	40	Yes	Yes	41.01	0.68	0.36	78.09	0.58	0.03	38.68	0.60	0.03
2021-03-03	40	Yes	Yes	38.53	0.73	0.34	79.14	0.70	0.02	39.85	0.64	0.03
2021-03-03	40	Yes	Yes	39.33	0.66	0.30	78.77	0.56	0.01	39.41	0.63	0.04

Date	Laser Diameter	Split	Nitrogen	^{66}Zn Mean	^{66}Zn 2SE	^{66}Zn LOD Pettke	^{88}Sr Mean	^{88}Sr 2SE	^{88}Sr LOD Pettke	^{137}Ba Mean	^{137}Ba 2SE	^{137}Ba LOD Pettke
2021-03-03	40	Yes	Yes	38.87	0.75	0.30	78.46	0.63	0.02	41.06	1.28	0.05
2021-03-03	40	Yes	Yes	39.72	0.71	0.27	78.98	0.69	0.02	39.98	0.64	0.05
2021-03-04	40	Yes	Yes	38.66	0.74	0.27	78.98	0.63	0.02	39.13	0.65	0.04
2021-03-04	40	Yes	Yes	39.81	0.65	0.23	80.34	0.56	0.01	40.32	0.60	0.03
2021-03-04	40	Yes	Yes	37.54	0.68	0.22	80.93	0.56	0.02	41.37	0.64	0.04
2021-03-04	40	Yes	Yes	38.68	0.71	0.23	82.37	0.61	0.02	42.23	0.64	0.02
2021-03-04	40	Yes	Yes	37.58	0.63	0.22	81.99	0.59	0.03	41.66	0.70	0.03
2021-03-05	40	Yes	Yes	39.06	0.69	0.22	78.09	0.51	0.02	38.79	0.58	0.05
2021-03-05	40	Yes	Yes	38.97	0.63	0.19	77.96	0.46	0.02	38.77	0.55	0.04
2021-03-05	40	Yes	Yes	39.76	0.68	0.19	79.10	0.52	0.02	40.43	0.60	0.03
2021-03-05	40	Yes	Yes	39.84	0.70	0.20	78.86	0.54	0.02	39.61	0.64	0.04
2021-03-05	40	Yes	Yes	40.07	0.69	0.21	79.54	0.52	0.03	40.09	0.68	0.04
2021-03-05	40	Yes	Yes	38.57	0.70	0.19	78.46	0.52	0.02	39.66	0.60	0.03
2021-03-05	40	Yes	Yes	39.00	0.68	0.18	79.72	0.55	0.03	40.03	0.57	0.03
2021-03-05	40	Yes	Yes	38.90	0.68	0.18	78.76	0.56	0.03	38.86	0.61	0.02
2021-05-27	40	Yes	Yes	37.77	0.66	0.20	83.52	0.64	0.01	40.42	0.61	0.02
2021-05-27	40	Yes	Yes	38.39	0.65	0.20	80.25	0.68	0.05	40.42	0.62	0.02
2021-05-27	40	Yes	Yes	38.44	0.69	0.19	80.12	0.63	0.02	40.64	0.57	0.08
2021-05-27	40	Yes	Yes	37.98	0.79	0.20	80.37	0.68	0.02	39.70	0.69	0.06
2021-05-27	40	Yes	Yes	38.17	0.64	0.21	80.77	0.68	0.02	40.16	0.60	0.02
2021-04-26	65	No	No	39.07	0.74	0.04	78.39	0.49	0.00	39.12	0.45	0.00
2021-04-26	65	No	No	39.20	0.81	0.04	78.28	0.52	0.01	39.52	0.54	0.01
2021-04-26	65	No	No	39.06	0.69	0.07	78.54	0.54	0.01	39.34	0.54	0.01
2021-04-26	65	No	No	39.10	0.45	0.03	78.46	0.56	0.00	39.34	0.46	0.01
2021-04-26	65	No	No	39.10	0.33	0.03	78.46	0.55	0.00	39.20	0.40	0.01
2021-04-26	65	No	No	39.27	0.37	0.03	77.84	0.58	0.00	39.27	0.48	0.01
2021-04-27	65	No	No	39.12	0.35	0.02	78.81	0.59	0.01	39.52	0.46	0.02
2021-04-27	65	No	No	39.10	0.33	0.03	78.41	0.68	0.01	39.26	0.49	0.02
2021-04-27	65	No	No	39.06	0.36	0.02	78.76	0.83	0.00	39.20	0.43	0.01
2021-04-27	65	No	No	38.95	0.61	0.03	78.61	1.13	0.01	39.23	0.69	0.01
2021-04-27	65	No	No	39.07	0.31	0.02	77.93	0.63	0.00	39.25	0.43	0.01
2021-04-27	65	No	No	39.10	0.32	nan	78.52	0.79	nan	39.28	0.47	nan

Appendix B

NISTSRM 610 and 612 GeoREM preferred values

GeoREM preferred values for NIST SRM 610 and NIST SRM 612

	NIST612 Preferred Value (ppm)	NIST612 2SE (ppm)	NIST610 Preferred Value (ppm)	NIST610 2SE (ppm)
Ag	22	0.3	251	9
Al	10743	-	10319	-
As	35.7	5.5	325	18
Au	4.77	0.31	23.6	1.7
B	34.3	1.7	350	56
Ba	39.3	0.9	452	9
Be	37.5	1.5	476	31
Bi	30.2	2.3	384	26
Ca	85049	-	81476	-
Cd	28.1	1.1	270	16
Ce	38.4	0.7	453	8
Cl	142	58	274	67
Co	35.5	1	410	10
Cr	36.4	1.5	408	10
Cs	42.7	1.8	366	9
Cu	37.8	1.5	441	15
Dy	35.5	0.7	437	11
Er	38	0.9	455	14
Eu	35.6	0.8	447	12
F	80	89	304	-
Fe	51	2	458	9
Ga	36.9	1.5	433	13
Gd	37.3	0.9	449	12
Ge	36.1	3.8	447	78
Hf	36.7	1.2	435	12
Ho	38.3	0.8	449	12
In	38.9	2.1	434	19
K	62.3	2.4	464	21
La	36	0.7	440	10
Li	40.2	1.3	468	24
Lu	37	0.9	439	8
Mg	68	5.1	432	29
Mn	38.7	0.9	444	13
Mo	37.4	1.5	417	21
Na	101640	-	99415	-
Nb	38.9	2.1	465	34
Nd	35.5	0.7	430	8
Ni	38.8	0.2	458.7	4
P	46.6	6.9	413	46
Pb	38.57	0.2	426	1
Pd	1.05	0.1	1.21	0.44

Pr	37.9	1	448	7
Pt	2.51	0.1	3.12	0.08
Rb	31.4	0.4	425.7	1
Re	6.63	0.61	49.9	3.7
Rh	0.91	0.02	1.29	0.07
S	377	70	575	32
Sb	34.7	1.8	396	19
Sc	39.9	2.5	455	10
Se	-	-	138	42
Si	337068	-	325848	-
Sm	37.7	0.8	453	11
Sn	38.6	1.3	430	29
Sr	78.4	0.2	515.5	1
Ta	37.6	1.9	446	33
Tb	37.6	1.1	437	9
Th	37.79	0.08	457.2	1
Ti	44	2.3	452	10
Tl	14.9	0.5	59.6	2.8
Tm	36.8	0.6	435	10
U	37.38	0.08	461.5	1
V	38.8	1.2	450	9
W	38	1.1	444	29
Y	38.3	1.4	462	11
Yb	39.2	0.9	450	9
Zn	39.1	1.7	460	18
Zr	37.9	1.2	448	9

Appendix C

Supplementary Figures

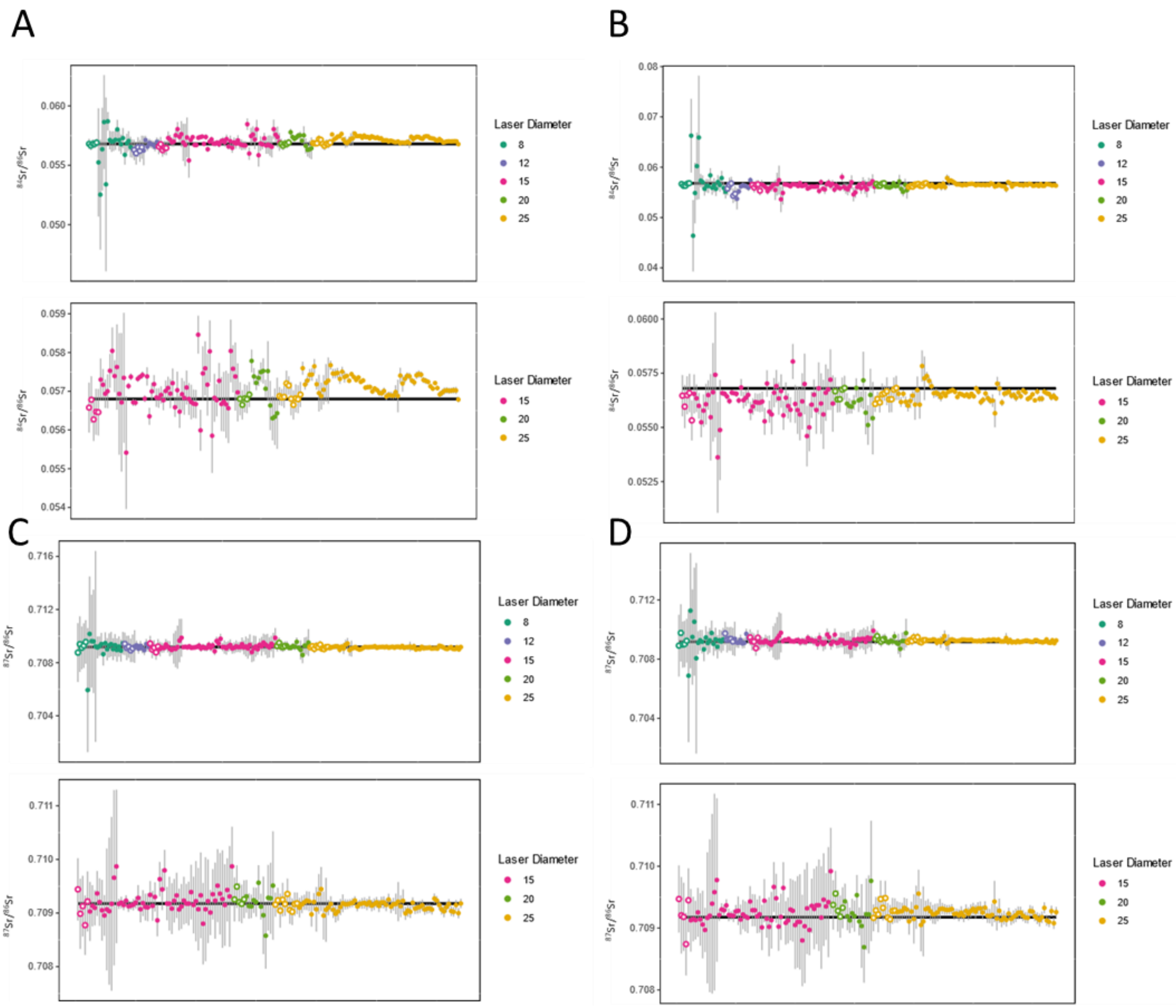

LASS-ICP-MS long-term isotopic data plots for a. $^{84}Sr/^{86}Sr$ uncorrected values b. $^{84}Sr/^{86}Sr$ instrumental corrected values c. $^{87}Sr/^{86}Sr$ uncorrected values d. $^{87}Sr/^{86}Sr$ instrumental corrected values. Closed circle data points indicate the use of nitrogen while open circles indicate no use of nitrogen.

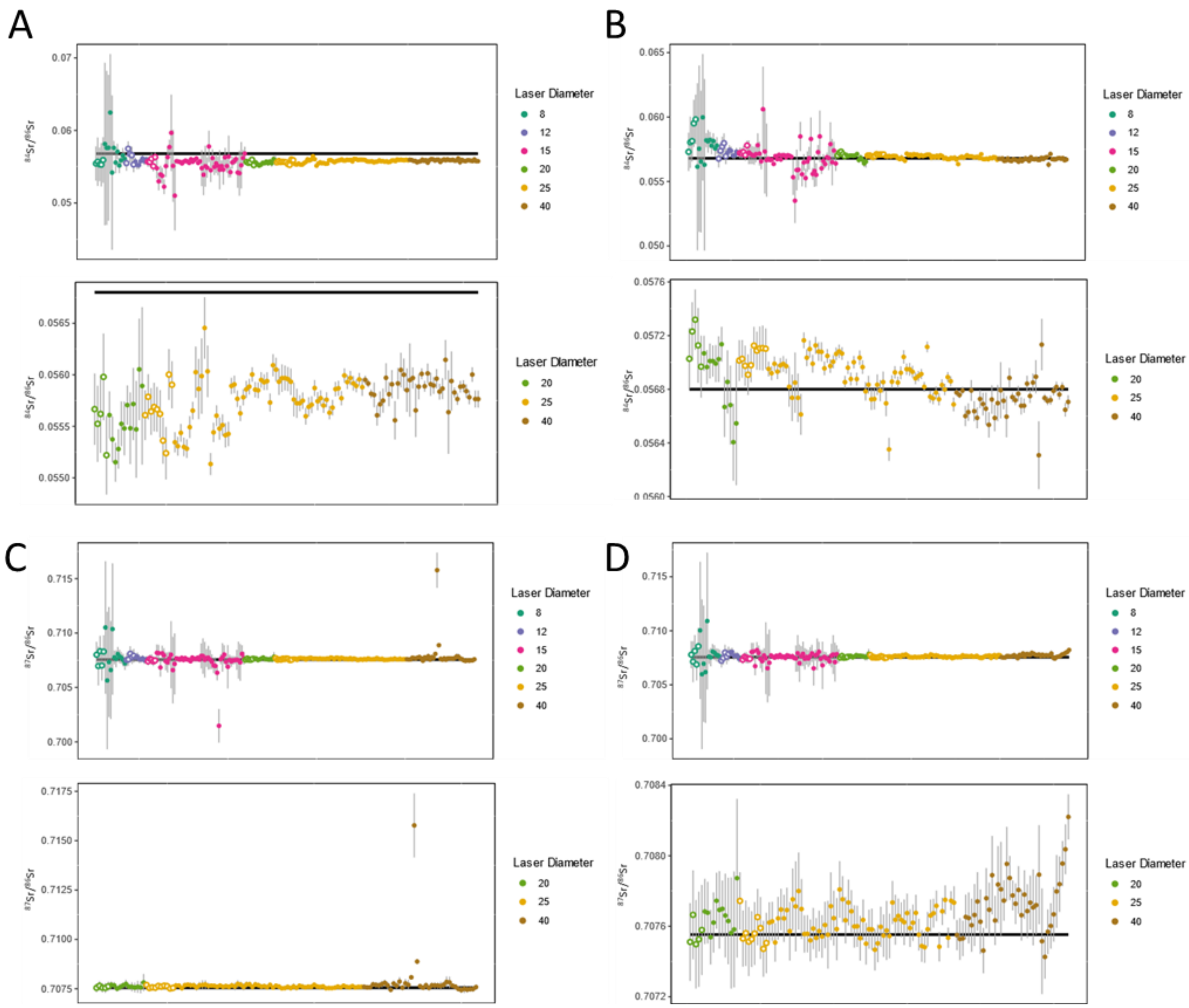

LASS-ICP-MS long-term isotopic data plots for a. $^{84}Sr/^{86}Sr$ uncorrected values b. $^{84}Sr/^{86}Sr$ instrumental corrected values c. $^{87}Sr/^{86}Sr$ uncorrected values d. $^{87}Sr/^{86}Sr$ instrumental corrected values. Closed circle data points indicate the use of nitrogen while open circles indicate no use of nitrogen.

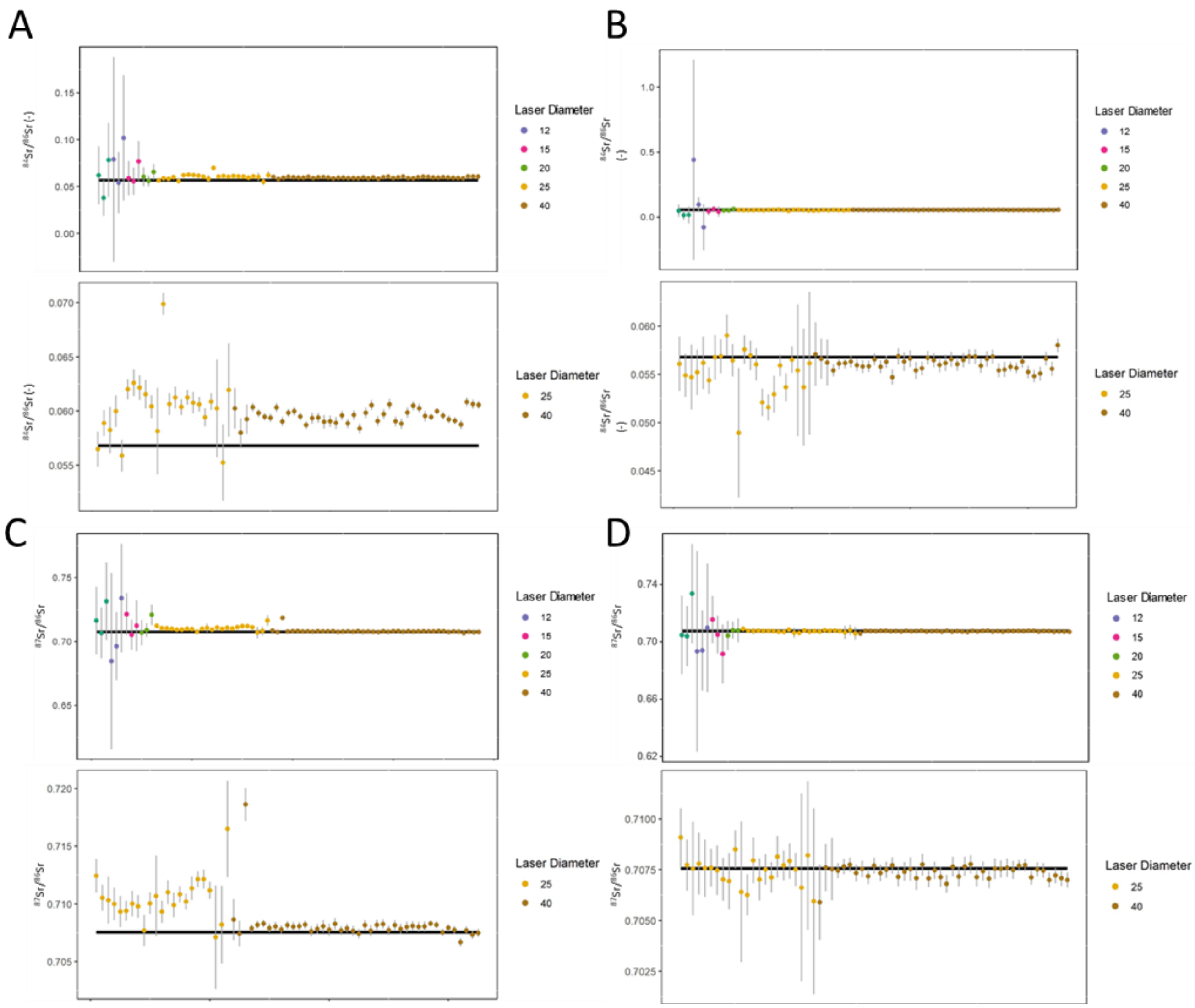

LASS-ICP-MS long-term isotopic data plots for a. $^{84}Sr/^{86}Sr$ uncorrected values b. $^{84}Sr/^{86}Sr$ instrumental corrected values c. $^{87}Sr/^{86}Sr$ uncorrected values d. $^{87}Sr/^{86}Sr$ instrumental corrected values. Closed circle data points indicate the use of nitrogen while open circles indicate no use of nitrogen.

Lau3-5

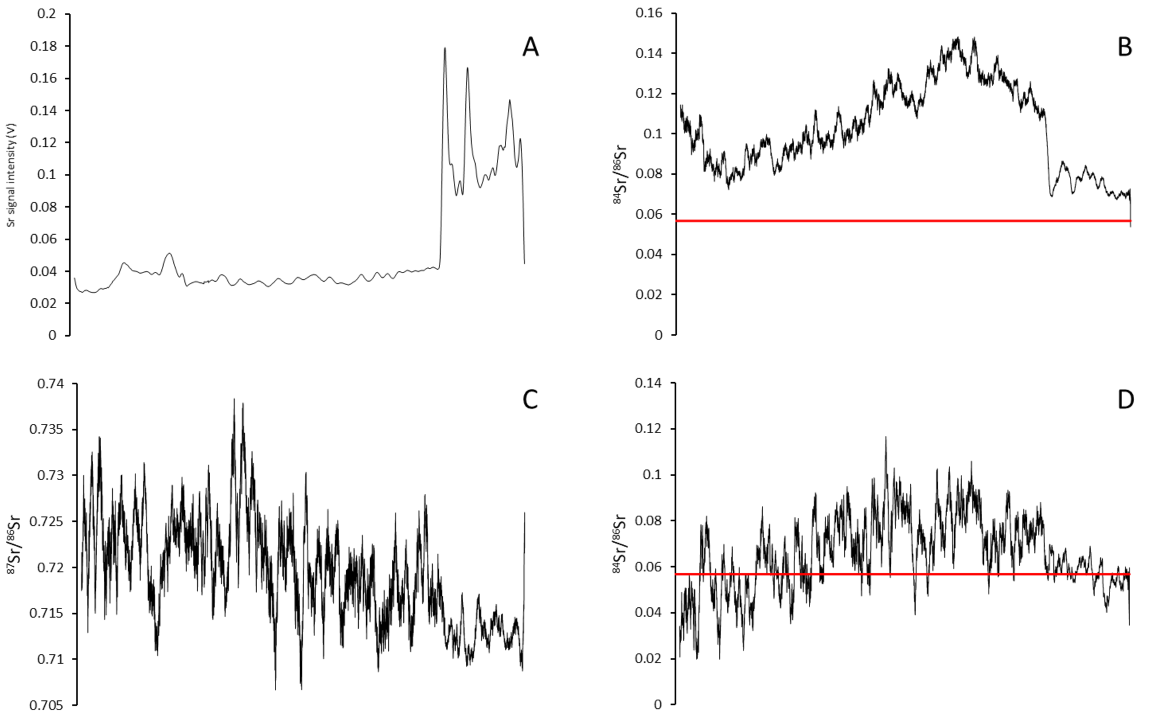

LAU3-5 LASS-ICP-MS isotopic transect data plots for a. Sr signal intensity (V) b. $^{84}Sr/^{86}Sr$ instrumental uncorrected values c. $^{87}Sr/^{86}Sr$ additional standard corrected values d. $^{84}Sr/^{86}Sr$ instrumental corrected values. Horizontal red lines indicate the $^{84}Sr/^{86}Sr$ natural abundance ratio of 0.0568.

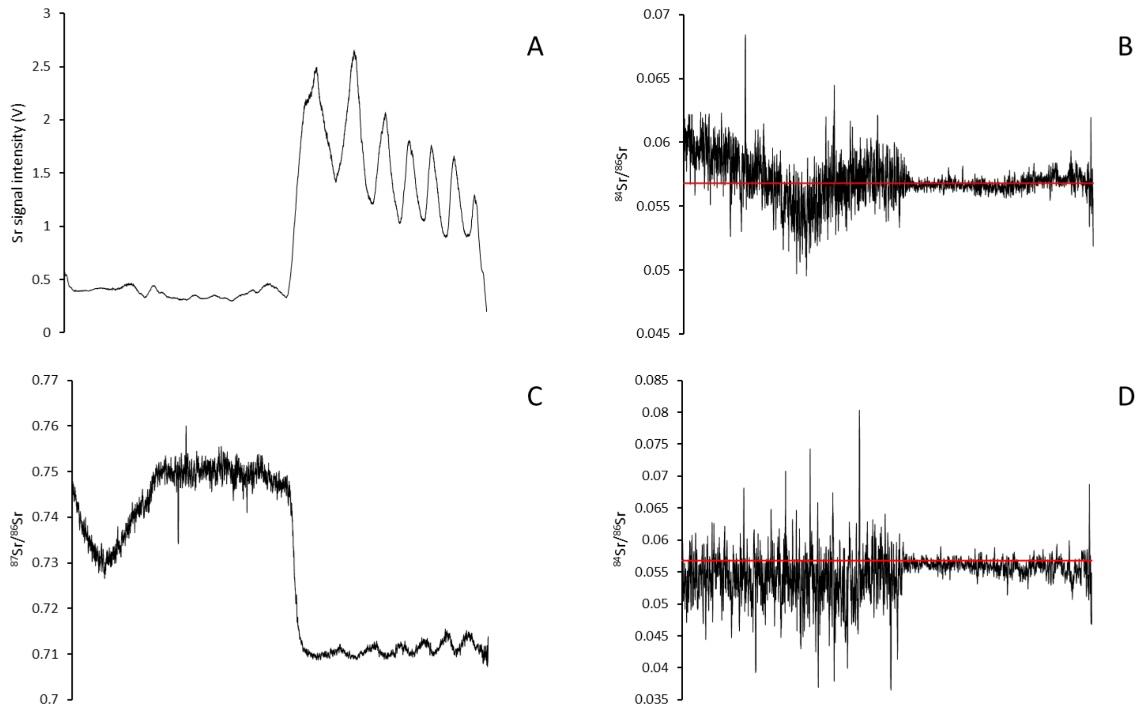

KUG1-1a LASS-ICP-MS isotopic transect data plots for a. Sr signal intensity (V) b. $^{84}Sr/^{86}Sr$ instrumental uncorrected values c. $^{87}Sr/^{86}Sr$ additional standard corrected values d. $^{84}Sr/^{86}Sr$ instrumental corrected values. Horizontal red lines indicate the $^{84}Sr/^{86}Sr$ natural abundance ratio of 0.0568.

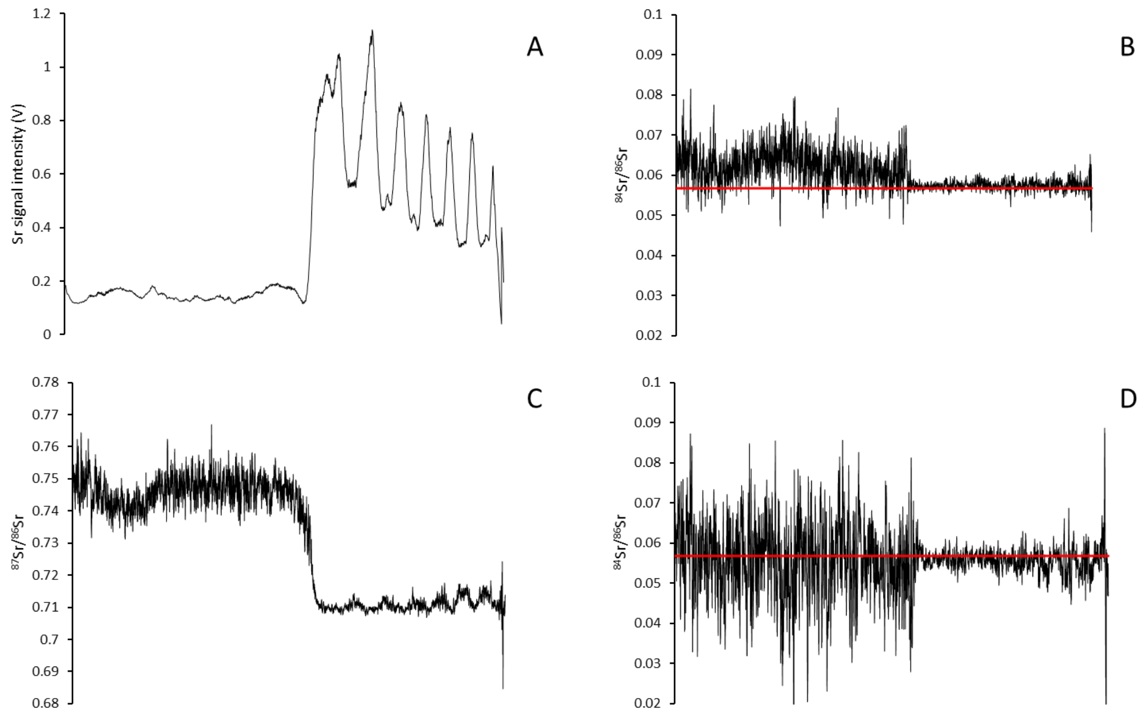

KUG1-1b LASS-ICP-MS isotopic transect data plots for a. Sr signal intensity (V) b. $^{84}Sr/^{86}Sr$ instrumental uncorrected values c. $^{87}Sr/^{86}Sr$ additional standard corrected values d. $^{84}Sr/^{86}Sr$ instrumental corrected values. Horizontal red lines indicate the $^{84}Sr/^{86}Sr$ natural abundance ratio of 0.0568.

Appendix D

Otolith Trace element Data Tables

Mean concentrations, 2SE, and LOD mean values for otolith sample transects (measured in ppm)

	LAU3-5	KUG1-1a	KUG1-1b
Li7 mean	0.02	0.25	0.24
Li7 (2SE)	0.01	0.01	0.01
Li7 LOD	0.04	0.03	0.06
Mg24 mean	21.29	39.88	41.81
Mg24 (2SE)	0.11	0.17	0.22
Mg24 LOD	0.13	0.09	0.22
Al27 mean	2.38	9.03	9.95
Al27 (2SE)	0.23	0.35	0.37
Al27 LOD	0.22	0.12	0.29
P31 mean	63.83	66.61	90.11
P31 (2SE)	1.38	1.30	2.46
P31 LOD	7.68	3.54	8.94
S34 mean	411.41	471.47	690.98
S34 (2SE)	7.36	4.46	10.36
S34 LOD	44.56	28.61	71.72
K39 mean	482.03	839.04	863.68
K39 (2SE)	2.55	3.50	3.73
K39 LOD	0.75	0.33	0.81
Mn55 mean	0.79	5.25	10.31
Mn55 (2SE)	0.04	0.17	0.26
Mn55 LOD	0.28	0.24	0.62
Fe56 mean	0.02	3.98	6.42
Fe56 (2SE)	0.21	0.09	0.22
Fe56 LOD	1.21	0.63	1.57
Cu63 mean	2.38	0.45	0.54
Cu63 (2SE)	0.05	0.02	0.05
Cu63 LOD	0.24	0.14	0.35
Zn66 mean	36.74	50.53	59.30
Zn66 (2SE)	0.65	0.92	1.18
Zn66 LOD	0.24	0.25	0.58
Rb85 mean	0.07	0.15	0.16
Rb85 (2SE)	0.00	0.00	0.01
Rb85 LOD	0.02	0.01	0.03
Sr88 mean	79.83	947.50	916.76
Sr88 (2SE)	1.36	24.42	25.31
Sr88 LOD	0.02	0.01	0.02
Y89 mean	0.00	0.00	-0.01
Y89 (2SE)	0.00	0.00	0.00

Y89 LOD	0.01	0.00	0.01
Zr90 mean	0.01	0.01	0.00
Zr90 (2SE)	0.00	0.00	0.00
Zr90 LOD	0.02	0.01	0.03
Ba137 mean	1.83	15.60	16.25
Ba137 (2SE)	0.04	0.31	0.36
Ba137 LOD	0.05	0.02	0.06
Pb208 mean	0.04	0.05	0.09
Pb208 (2SE)	0.00	0.00	0.01
Pb208 LOD	0.02	0.02	0.05